Thermal Conductivity of Proton Exchange Membrane Fuel Cell Components

Nahla Eid Alhazmi

Supervised by: Prof. M. Pourkashanian, Prof. D. B. Ingham, Dr. L. Ma and Dr. K. Hughes

Submitted in accordance with the requirements for the degree of
Doctor of Philosophy

The University of Leeds
School of Process, Environmental and Materials Engineering (SPEME)

Energy Technology and Innovation Initiative (ETII)

June, 2014

The candidate confirms that the work submitted is her own, except where work which has formed part of jointly-authored publications has been included. The contribution of the candidate and the other authors to this work has been explicitly indicated below. The candidate confirms that appropriate credit has been given within the thesis where reference has been made to the work of others.

The work contained within this thesis is my own primary research. The other authors were my supervisors who acted in an advisory role and gave suggestions regarding the research direction and analysis methods.

Achievements and publications

Intellectual Property (IP)

- A Patent: in the field of improving the performance of fuel cells, A metal-based GDL and the effect of the thermal conductivity of GDL on the performance of PEM fuel cell (Net Scientific Limited), Publication number WO2013/088122. **(Chapters 2&3)**

International conferences

- The 4th European Fuel Cell Conference and Exhibition (December 14-16, 2011, Rome, Italy). **(Chapters 2)**
- The 5th European Fuel Cell Conference and Exhibition (December 11-13, 20013, Rome, Italy). **(Chapters 7)**
- The 4th European PEFC and H2 Forum 2013 (July 2-5, 2013, Lucerne Switzerland). **(Chapters 3)**
- Hydrogen & Fuel Cell Researcher Conference (December 16-18, 2013, Birmingham, UK). **(Chapters 4)**
- The 7th Saudi Students Conference in the UK (February 1-2, 2014, Edinburgh, UK). **(Chapters 1)**

Journal papers

- **Alhazmi N.**; Ismail M. S.; Ingham D. B.; Hughes K. J.; Ma L.; Pourkashanian M., Effect of the anisotropic thermal conductivity of GDL on the performance of PEM fuel cells. International Journal of Hydrogen Energy, 2013, vol. 38, pp.603-611. **(Chapters 2)**
- **Alhazmi N.**; Ismail M. S.; Ingham D. B.; Hughes K. J.; Ma L.; Pourkashanian M., The in-plane thermal conductivity and the contact resistance of the components of the membrane electrode assembly in proton exchange membrane fuel cells. Journal of Power Sources, 2013, vol. 241, pp.136-145. **(Chapters 6)**

- **Alhazmi N.**; Ismail M. S.; Ingham D. B.; Hughes K. J.; Ma L.; Pourkashanian M., The through-plane thermal conductivity and the contact resistance of the components of the membrane electrode assembly in proton exchange membrane fuel cells. Journal of Power Sources, accepted with minor corrections, 30/3/2014. **(Chapters 7)**
- **Alhazmi N.**; Ismail M. S.; Ingham D. B.; Hughes K. J.; Ma L.; Pourkashanian M., Effects of metal-based gas diffusion layer on the temperature and water saturation in proton exchange membrane fuel cells. In preparation. **(Chapters 3)**

Posters

- A poster on " Effect of Metal-based GDLs on The Performance of PEM Fuel Cells" (Energy Building official opening-March 21, 2012, University of Leeds). **(Chapters 3)**
- A poster on "Metal-based gas diffusion layer in proton exchange membrane fuel cells" (The 4th European PEFC and H2 Forum, July, 2-5, 2013, Lucerne Switzerland). **(Chapters 3)**
- A poster on "Effects of the thermal conductivity of the membrane and catalyst layer on the performance of PEM fuel cells" (Hydrogen & Fuel Cell Researcher Conference, December, 16-18, 2013, Birmingham, UK). **(Chapters 4)**
- A poster on "Effect of the flow configuration of the cathode channel on the performance of PEM fuel cells" (The 7th Saudi Students Conference, February, 1-2, 2014, Edinburgh, UK). **(Chapters 1)**

Acknowledgements

In the name of Allah. Prayers and peace Upon Prophet Muhammad, the last messenger for the humanities.

Foremost, I would like to express my deep appreciations to my supervisors Prof. D. B. Ingham and Prof. M. Pourkashanian for their helps and advises. Also, for Dr. L. Ma, Dr. K. Hughes and Dr. M. S. Ismail for the continues support during my PhD.

Furthermore, I appreciate the technical assistances that I have got from Mr Paul Crosby and Mr Gurdev Bhogal in the Energy Technology Innovation Initiative at the University of Leeds. All the experimental works in this thesis could not be done without their help and assistant.

I would like to acknowledge the financial support that I received from the Ministry of Higher Education in Saudi Arabia and King Abdullah scholarship program.

Finally, I extremely appreciate the support that I received from all my family. Words cannot express how grateful I am to my husband Ahmed Almohammadi, my children Farah and Muhannad, my mother, my brothers and sisters.

Abstract

Proton exchange membrane (PEM) fuel cell has the potential to be one of the main energy sources in the future. However, the leading issues when operating the fuel cells are the water and the thermal managements. In this thesis, numerical studies have been developed in order to investigate the sensitivity of the PEM fuel cells performance to the thermal conductivities of the main components in PEM fuel cells, which are the membrane, the gas diffusion layer (GDL) and the catalyst layer. In addition, the effect of the thermal conductivity of these components and the metallic GDL on the temperature distribution and the water saturation was considered conducive to the improvement of the heat and water management in PEM fuel cells.

On the other hand, the experimental work was completed to determine the effects of the thermal conductivity and the thermal contact resistance of the components in PEM fuel cells. The thermal conductivity of the GDL was measured in two directions, namely the in-plane and the through-plane directions taking into account the effect of the main parameters in the GDL which are the mean temperature, the compression pressure, the fibre direction, the micro porous layer (MPL) coating and polytetrafluoroethylene (PTFE) loading. Furthermore, the thermal conductivities of the membrane and the catalyst layer were measured in both directions, the in-plane and the through-plane, with considering the effect of the temperature and the Pt loading in the catalyst layer, and the effect of the water content and temperature on the membrane. This study is a comprehensive study on the thermal conductivity of PEM fuel cells and emphasized the importance of the thermal conductivity of the components in PEM fuel cells.

Table of Contents

List of Tables

List of Figures

Nomenclature

Roman letters

A	Cross-sectional area of the sample (m^{2})
C_{holder}	The thermal conductance of the holder (W·K^{-1})
C_{s}	The thermal conductance of the sample (W·K^{-1})
c_{ph}	The phonon heat capacity (J·g^{-1}·K^{-1})
F	Faraday's constant
I	Current (A)
i^{ref}	Reference current density (A·m^{-2})
J	Reaction rate
k	Thermal conductivity (W·m^{-1}·K^{-1})
k_{air}	Thermal conductivity of air (W·m^{-1}·K^{-1})
k_{cl}	Thermal conductivity of catalyst layer (W·m^{-1}·K^{-1})
k_{GDL}	Thermal conductivity of the GDL (W·m^{-1}·K^{-1})
k_{m}	Thermal conductivity of the standard material (W·m^{-1}·K^{-1})
k_{MEA}	Thermal conductivity of the MEA (W·m^{-1}·K^{-1})
k_{mem}	Thermal conductivity of membrane (W·m^{-1}·K^{-1})
k_{s}	Thermal conductivity of the sample (W·m^{-1}·K^{-1})
k_{water}	Thermal conductivity of water (W·m^{-1}·K^{-1})
L	Length (m)
l_{ph}	The phonon mean free path (m)
L_{s}	Length of the sample (m)
M	Molar mass (kg·mol^{-1})
Q	Heat transfer (W)
q_{low}	Heat transfer through the lower plate (W)
q_{s}	Heat transfer through the sample (W)
q_{up}	Heat transfer through the upper plate (W)
R	Universal gas constant (J·mol^{-1}·K^{-1})
$R_{H\text{-Sample}}$	Thermal contact resistance between two layers of the sample (m^{2}·K·W^{-1})
$R_{\text{Sample-Sample}}$	Thermal contact resistance between two layers of the sample (m^{2}·K·W^{-1})

R_{Total}	Total thermal resistance ($K \cdot W^{-1}$)
R_{CR}	Thermal contact resistance ($m^2 \cdot K \cdot W^{-1}$)
R_S	Sample thermal resistance ($K \cdot W^{-1}$)
R_0	Holder thermal resistance ($K \cdot W^{-1}$)
RH	Relative Humidity
S_e	Energy source term
S_{H2}	Hydrogen source term
S_{H2O}	Water source term
S_{O2}	Oxygen source term
T	Temperature (K)
T_1	Temperatures measured by the first thermocouple (K)
T_3	Temperatures measured by the third thermocouple (K)
T_4	Temperatures measured by the fourth thermocouple (K)
T_6	Temperatures measured by the sixth thermocouple (K)
T_C	Cold plate temperature (K)
T_h	Hot plate temperature (K)
ΔT	Temperature drop (K)
VOC	Voltage Open Circuit (V)
Y	Mass fraction
V	Voltage (V)
v_{cl}	Volume fraction of catalyst
v_{GDL}	Volume fraction of GDL
v_{air}	Volume fraction of air
v_{mem}	Volume fraction of membrane
v_{ph}	The phonon velocity ($m \cdot s^{-1}$)
v_{water}	Volume fraction of water

Greek symbols

ϕ_{mem}	Electrolyte phase potential (V)
ϕ_{sol}	Solid phase potential (V)
ε	Porosity of the porous media
σ_{mem}	The proton conductivity in membrane
σ_{sol}	The electric conductivity of solid

μ	Fluid viscosity (Pa·s)
ρ	Density (kg·m^{-3})

Subscripts

an	Anode
cat	Cathode
CO	Carbon monoxide
CO_2	Carbon dioxide
H_2	Hydrogen
H^+	Proton
H_2O	Water
mem	Membrane
O_2	Oxygen
ref	Reference

Abbreviations

AFC	Alkaline Fuel Cell
CFD	Computational Fluid Dynamics
CL	Catalyst Layer
DMFC	Direct Methanol Fuel Cell
GDL	Gas Diffusion Layer
FVM	Finite Volume Method
MCFC	Molten Carbonate Fuel Cell
MEA	Membrane Electrode Assembly
MPL	Micro Porous Layer
PAFC	Phosphoric Acid Fuel Cell
PEMFC	Proton Exchange Membrane Fuel Cell
PTC	Parallel Thermal Conductance
PTFE	Polytetrafluoroethylene
SEM	Scanning Electron Microscope
SOFC	Solid Oxide Fuel Cell
TPS	Transient Plane Source
TTR	Transient Thermo Reflectance

Chapter 1
Introduction

Over the past few decades, there has been a rapid interest in clean sources of energy, especially after the global warming and climate change issues.

Scientists and researchers are seeking more efficient power generation with as small as possible emissions. Therefore, there has been much development in solar energy, wind energy and fuel cells for power generation [1]. Fuel cell technology holds the promise of high-efficiency and environmentally clean engines with a wide range of applications [2]. Moreover, fuel cells have 80% more efficiency than combustion engines. Therefore, fuel cells have wide applications in portable power stations and transportation [3].

In addition, fuel cells have low, or even zero emissions and estimates indicate that if the hydrogen used to reform in a fuel cell was from natural gas, then the greenhouse gases will be reduced by more than a factor of 2. Moreover, hydrogen can be made from renewable energy sources [3].

In the last few years, there has been much more attention paid by industry on research into fuel cell phenomena and the importance of developing fuel cell processes with a more cost efficient design and better performance [2].

1.1 Fuel Cell History

The first fuel cell was developed in England by Sir William Grove in 1839. He split water into oxygen and hydrogen by using electricity. Sir William believed that the reverse of this process could be used to generate electricity from the reaction of hydrogen with oxygen and this is the basis of how a fuel cell works in principle, as seen in Figure 1.1 [4]. In 1932, Dr. Francis Thomas Bacon developed the first alkaline fuel cell by substituting the platinum electrodes with nickel gauze. After 27 years, Bacon produced a capable fuel cell which generated 5 kW of power. In 1959, Harry Karl in the U.S.A produced the first fuel cell which powered a vehicle by generating 15 kW from a fuel cell stack. In the early 1960s, NASA developed the first proton exchange membrane fuel cell when it was looking for possible ways to power the space flights. In 1955, General Electric scientists developed fuel cells by using a sulphonated polystyrene membrane as the electrolyte and depositing platinum onto this membrane. This technology was used by NASA to develop the fuel cells on the Gemini space project. In the 1970s and 1980s, governments and companies pushed along the research effort to become less dependent on oil. This research effort was helped by the development of materials and the reduction in the cost of fuel cells. In 1993, Ballard (Canadian company) marketed the first fuel cell powered vehicle [4, 5]. During the 1990s, Perny Energy Systems demonstrated fuel cell powered submarines and buses. By the end of the 2000s, almost all the automobile manufacturers tested the fuel cell-powered vehicle [4, 5].

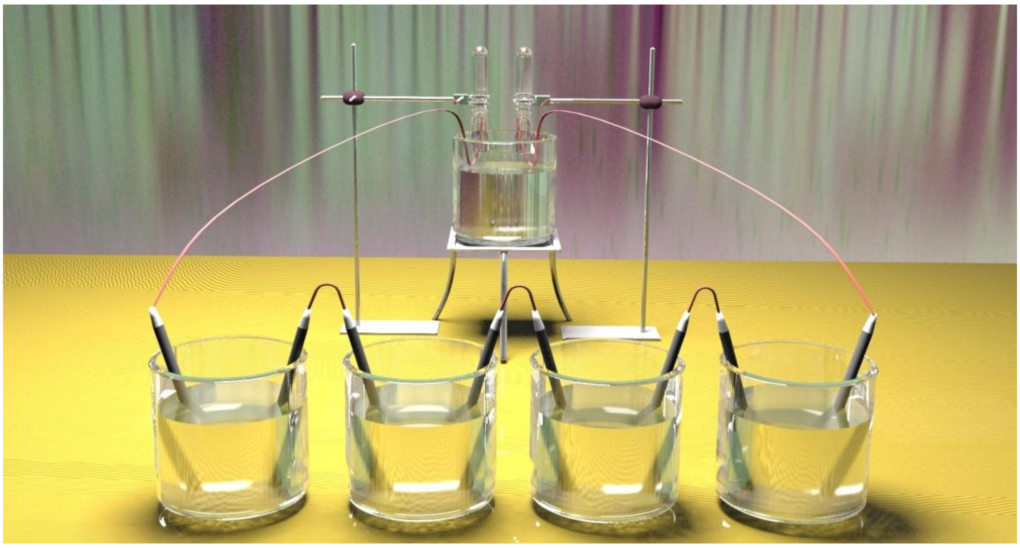

Figure 1.1 Sir William Grove first fuel cell.

1.2 What is a Fuel Cell

In principle, a fuel cell is a device which converts chemical energy into electrical energy, as in the case of batteries. However, the power from fuel cells will be provided as long as the fuel is supplied to the anode and the air to the cathode while the electrical energy is usually stored in batteries [6].

Typically, a fuel cell consists of two electrodes, one positive called the anode and the other is negative called the cathode, and an electrolyte, which carries the reacted particles and the electricity from one electrode to the other, sandwiched between them. The basic structure of a fuel cell is represented in Figure1.2, which consists of an electrolyte sandwiched between the anode side (feed with fuel) and the cathode side (feed with oxidant) [7, 8].

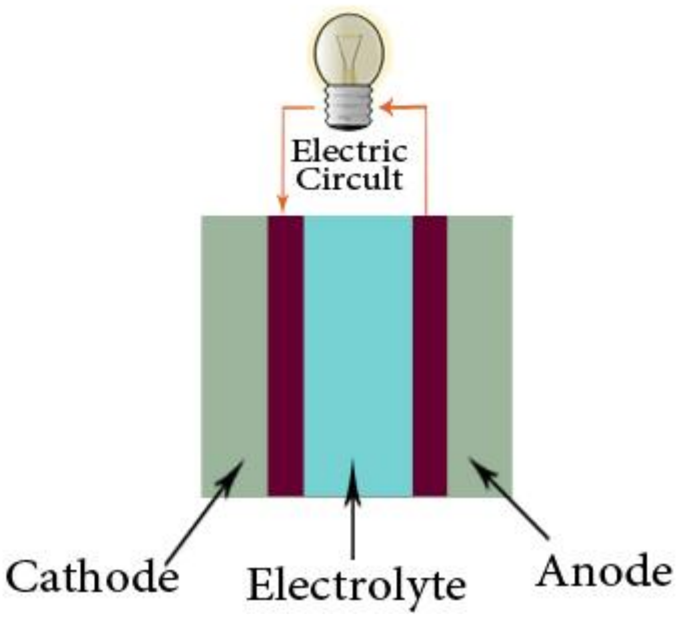

Figure 1.2 The basic structure of a typical fuel cell.

In the fuel cell, hydrogen is supplied at the anode side. Then hydrogen will be oxidized to form positive charge ions and negative charge electrons. Electrons will travel through a wire circuit to generate the electrical current, while ions can pass through the electrolyte to the cathode and react with the oxygen which is supplied at the cathode and the electrons to form water. In general terms, as long as hydrogen and oxygen are supplied to the fuel cell, the fuel cell will generate electricity [9].

1.3 Fuel Cell Advantages

There are several advantages of fuel cells, which leads to many applications. The most significant advantages are as follows:

- The efficiency of the fuel cells, which changes with the operating temperature, pressure and other factors.
- Fuel cells are quiet systems, and this makes them suitable for any environment.
- The fuel cells runtime could be increased by increasing the hydrogen bottles.
- The simplicity of the fuel cell systems. There are very few parts and few need maintenance.
- The extremely low emissions from fuel cells by using hydrogen instead of fuel or batteries which makes fuel cell systems environmentally–friendly.
- The weight of fuel cells is light compared with conventional batteries.
- Fuel cells are safe systems which provide heat and water only as the final products.
- The waste heat from fuel cells can be used to heat space or water.

However, there are some disadvantages of fuel cells and the most notable are its cost [7, 10].

1.4 Fuel Cell Types

In order to achieve great energy efficiency, scientists have designed different sizes and types of fuel cells. These fuel cells use varying materials and the electrodes depend on the kind of electrolyte which is used. Some of the electrolytes are solid, such as the solid oxide and proton exchange membranes. Other electrolytes are liquid such as molten carbonate, phosphoric acid and alkali. The type of fuel which is used in the fuel cell also depends on the kind of the electrolyte. Some of the fuel cells, for example, need a reformer to purify the hydrogen. Other cells need pumps to circulate liquid fuel. Furthermore, the type of electrolyte also dictates the operating temperature for the fuel cell [11]. Therefore, there are five types of fuel cells which depend on the kind of the electrolyte and the mobile ion which have been used, as shown in Table 1.1. However, every type of fuel cell has some advantages and drawbacks which make it suitable for some applications compared to the others and the main types of fuel cells are as follows:

Table 1.1 Summary of the main different types of fuel cell.

Fuel cell Type	Mobile Ion	Operating Temperature
Alkaline AFC	OH^-	50 - 200°C
Proton exchange membrane PEMFC	H^+	50 - 100°C
Phosphoric acid PAFC	H^+	~ 200°C
Molten carbonate MCFC	CO_3^{-2}	~ 650°C
Solid Oxide SOFC	CO_3^{-2}	500 - 1000°C

1.4.1 Proton Exchange Membrane (PEM)

The mobile in this type of fuel cell is the proton and the electrolyte is a solid polymer which gives the advantage of a flexible electrolyte and saves it from leakage or damage. The proton exchange membrane fuel cell is also known as the polymer electrolyte fuel cell. PEM fuel cells run at quite a low temperature, about 60-80 °C. Therefore, PEM is safe to use in homes and cars and it has a wide range of applications (mobiles, portables, vehicles and stationery applications). The reactions in PEM fuel cells start quickly due to the low operating temperature and this allows the fuel cell to have a better durability. This type of fuel cell normally requires humidified gases, hydrogen and oxygen. The electrochemical reactions in PEM fuel cells are as follows:

Anode $$H_2 \rightarrow 2H^+ + 2e^- \tag{1.1}$$

Cathode $$O_2 + 4H^+ + 4e^- \rightarrow 2H_2O \tag{1.2}$$

The proton Exchange Membrane (PEM) efficiency is about 50%, and the output power is from 50 to 250 kW. The main disadvantage is that it uses platinum as the catalyst which increases the cost of the PEM fuel cell [11-13]. The basic structure of the PEMFC is shown in Figure 1.3.

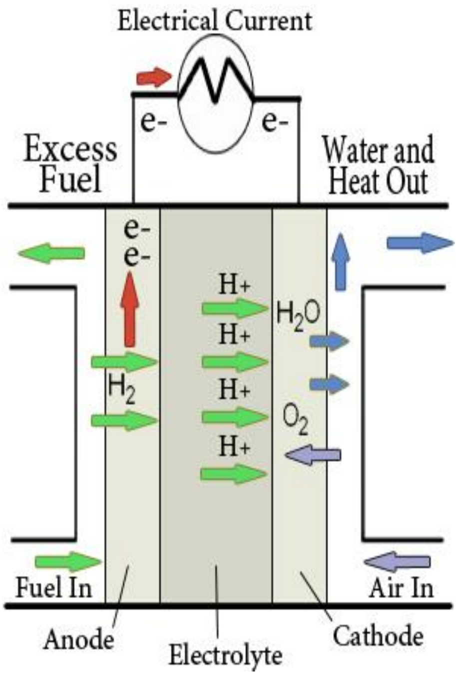

Figure 1.3 The basic structure of a PEM.

1.4.2 Alkaline Fuel Cells (AFC)

Alkaline Fuel Cells use a solution of potassium KOH, or sodium hydroxide NaOH in water, as the electrolyte as seen in Figure 1.4, The activation losses from alkaline fuel cells are less than from other kinds of fuel cells and the electrolyte is considerably cheaper. This type of fuel cell runs at a high operating pressure and it has been used in both the Apollo space craft and in the Shuttle space craft to provide the electricity and the drinking water. However, this kind of fuel cell usually has a short life time due to the leak of the liquid electrolyte [14]. The electrochemical reactions at the anode and cathode in the AFC are as follows:

Anode $$H_2 + 2OH^- \rightarrow 2H_2O + 2e^- \tag{1.3}$$

Cathode $$O_2 + 2H_2O + 4e^- \rightarrow 4OH^- \tag{1.4}$$

This type of fuel cell uses catalysts, such as silver and nickel [12]. The efficiency of AFC is about 60% and the operating temperature is 150 to 250 °C. The output power for the AFC is between 300 W and 5 kW. However, this kind of fuel cell is easily poisoned by carbon dioxide and this effects the fuel cell life time and makes it necessary to purify the hydrogen and oxygen in the cell from carbon dioxide [12].

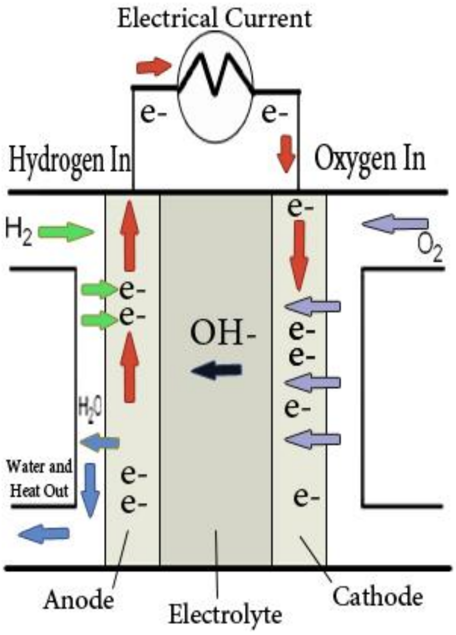

Figure 1.4 The basic structure of the AFC.

1.4.3 Phosphoric Acid Fuel Cells (PAFC)

This type of fuel cell uses phosphoric acid as the electrolyte and the operating temperature is between 150 and 200 °C. The basic structure of the PAFC is shown in Figure 1.5.

The PAFC is usually used in stationary power plants due to its long life time [11, 15]. The rate-determining step for the oxygen reduction in platinum is given by:

$$M + O_2 + H^+ + e^- \rightarrow MHO_2 \qquad (1.5)$$

In general, the output power from this type of fuel cells is about 200 kW. Phosphoric acid fuel cells are typically used for stationary power generation and large vehicles. Phosphoric Acid Fuel Cells are expensive because of the use of a platinum catalyst. The efficiency of this type of fuel cell, when it used to generate electricity, is about 37%. In order to increase the efficiency of the PAFC, the platinum catalyst is usually bonded with carbon monoxide. However, this may be poisoned by carbon monoxide [15].

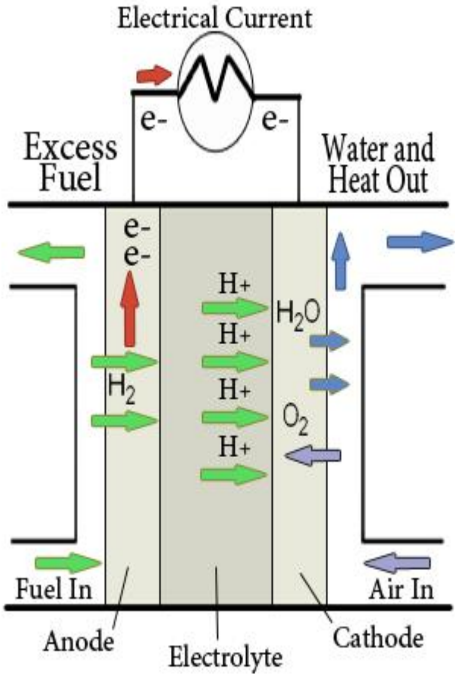

Figure 1.5 The basic structure of the PAFC.

1.4.4 Molten Carbonate Fuel Cell (MCFC)

Molten Carbonate Fuel Cells use alkali (Li, Na, K) carbonates as the electrolyte, see Figure 1.6.

The operating temperature of this type of fuel cell is between 600 and 700°C and the output power is about 2 MW which make them suitable for electrical utility, neutral gas power plants and military applications [12, 15]. Hydrocarbon fuel reforms with water to give hydrogen and carbon monoxide which is oxidized by the carbonate ions to produce H_2O and CO_2. At the cathode, CO_2, O_2 and the electrons react to supply carbonate ions. In MCFC, a molten alkali carbonate mixture is retained in a porous lithium aluminate and this is used as the electrolyte. At the cathode:

$$\frac{1}{2}O_2 + CO_2 + 2e^- \rightarrow CO_3^{2-} \tag{1.6}$$

Then, the ionic current through the electrolyte matrix is carried to the anode ions:

$$H_2 + CO_3^{2-} \rightarrow H_2O + CO_2 + 2e^- \tag{1.7}$$

The efficiency of the MCFC is about 65% and in order to increase the MCFC efficiency, the waste heat could be captured and recycled by coupling the fuel cell with a turbine. The high operating temperature of the MCFC allows the fuel to convert to hydrogen by the internal reforming without the need for an external reformer. Moreover, the MCFC is not carbon dioxide poisoned and it is resistant to impurities. However, the main disadvantage of the MCFC is its durability because of the corrosion and breakdown components due to the high operating temperatures. Currently, scientists are trying to explore corrosion–resistance materials in order to increase the molten carbonate fuel cells life time [15].

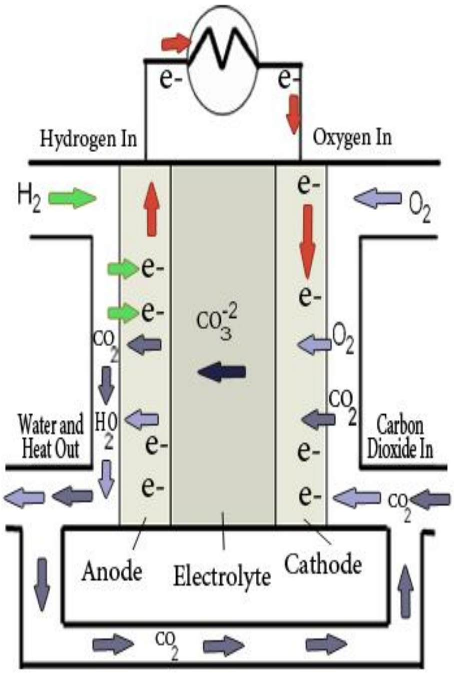

Figure 1.6 The basic structure of the MCFC.

1.4.5 Solid Oxide Fuel Cell (SOFC)

Solid oxide fuel cells use a non-porous solid metal oxide as the electrolyte. The operating temperature of a solid oxide fuel cell is higher than all the other types of fuel cells (between 500°C and 1000°C) and the electrolyte is usually ceramic-based. This type of fuel cell has a high output and a long life time [12, 15]. The operating principles of a SOFC are given by:

Cathode $$\frac{1}{2}O_2 + 2e^- \rightarrow O^{2-} \tag{1.8}$$

Anode $$H_2 + O^{2-} \rightarrow H_2O + 2e^- \tag{1.9}$$

Solid oxide fuel cells use a solid ceramic, such as calcium or zirconium oxides as the electrolyte. The basic structure of the SOFC is shown in Figure 1.7.

The efficiency for this kind of fuel cell is about 50-60%. The output power is about 100 kW. The SOFC can use gases made from coal because it is not poisoned by the carbon monoxide and it is the most sulfur resistant type of fuel cell.

The high operating temperature for the solid oxide fuel cell results in a slow start up and the use of high durability materials which are the main disadvantages for this type of fuel cell. Scientists are trying to develop a lower operating temperature SOFC with low cost materials which are the major challenges facing researches in SOFC [15].

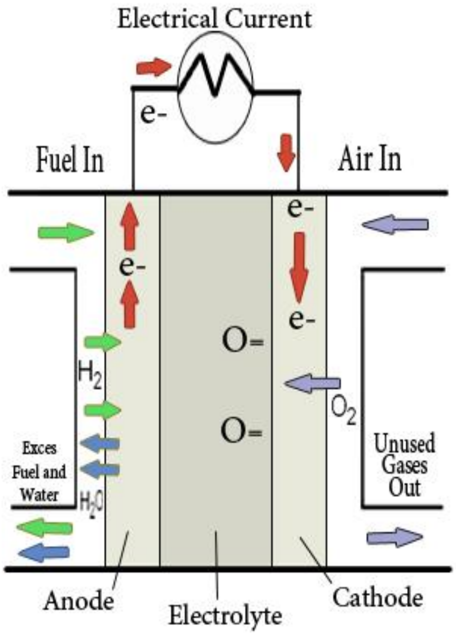

Figure 1.7 The basic structure of the SOFC.

1.4.6 Direct Methanol Fuel Cell (DMFC)

The electrochemical reactions at the anode and cathode in the DMFC are as follows:

Cathode $CH_3OH + H_2O \rightarrow CO_2 + 6H^+ + 6e^-$ (1.10)

Anode $\frac{3}{2}O_2 + 6H^+ + 6e^- \rightarrow 3H_2O$ (1.11)

DMFC is suitable for portable applications due to the low operating temperature (about 60°C) and there is no need for a reformer for the fuel. The efficiency is about 25-30%. However, this type of fuel cell requires a high amount of expensive platinum as a catalyst which is similar to the PEM fuel cell [15].

1.5 Fuel Cell Applications

Fuel cells have a wide range of applications in many systems handling many watts and megawatts, as shown in Table 1.2. Some of these applications are associated with the power supply of electronic equipment, such as mobile phones or computers. Other fuel cells have been used in space crafts, such as the Apollo and other space shuttles. Also, fuel cells have been used by the transport industry for their vehicles [6]. Fuel cells have several applications which may be summarized as the following fields:

- The lighting of roads.
- The power supply for environmental monitoring stations in remote locations.

- Replace power cords in mobile telephones, vacuum cleaners and various cleaning machines, etc.
- Auxiliary power for electricity in camping, boats and other vehicles [16].
- The power generation for many commercial vehicles such as buses, vans and general motor vehicles.
- Blood alcohol measurement which senses the alcohol in the breath.
- To generate electrical and heat energy in buildings.
- In space crafts, such as the Apollo and shuttle spacecraft [17].

Table 1.2 Some applications of the different types of fuel cells.

Applications	Power In watts	Types of fuel
Portable electronics equipments	1W – 100W	PEMFC
Cars, Boats and domestic CHP	100W – 100kW	PEMFC, AFC, SOFC
Distributed power generation and buses	100kW -10 MW	SOFC, MCFC, PAFC

1.6 Fuel Cell Actual Voltage

There are some differences between the voltage we expected from a typical fuel cell and the real voltage we obtained and this is illustrated in Figure 1.8. The theoretical fuel cell voltage is about 1.23V and the voltage drop in fuel cells are shown in four different regions (the activation losses, the fuel crossover, the ohmic losses and the mass transport losses).

Some electro-chemists have used the over potential of the cell to describe this difference or the polarization. Other scientists have described this difference between the voltage that is obtained from fuel cells and the theoretical cell voltage as the voltage drop or the irreversibility [18]. The main causes for the voltage drop are discussed in the following subsections:

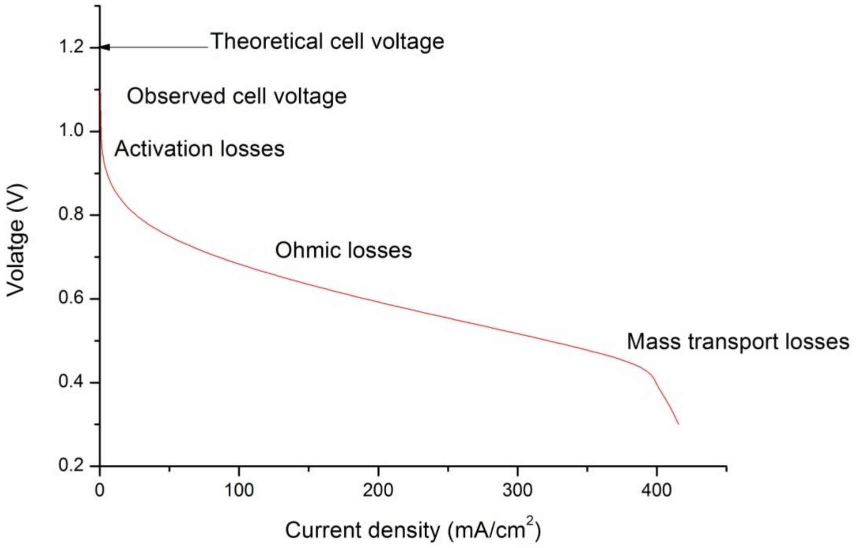

Figure 1.8 A typical polarization curve for a PEM fuel cell.

1.6.1 Activation losses

The experimental results have show that the reactions need time to take place on the surface of the electrode and this causes the differences between the experimental and theoretical considerations. This voltage drop can be calculated from the current density as follows:

$$V = A\ln(\frac{i}{b}) \tag{1.12}$$

where *i* is the current density, and *A* and b are constants dependent on the cell operating conditions and the electrode.

The activation losses can be reduced by increasing the temperature of the cell, or the operating pressure. Also, by raising the real surface area of the electrode, by increasing the roughness of the electrodes, or by using oxygen instead of air in the cathode channel [19, 20].

1.6.2 Fuel crossover

This loss in the cell voltage is due to the loss of fuel when it passes through the electrolyte. In the theoretical consideration, the electrolyte should only transport protons through the cell. However, in reality there will be some amount of the fuel transported as well. This is not a significant effect but it is important to be taken into consideration in low temperature fuel cells [19].

1.6.3 Ohmic losses

This voltage drop is caused by the electrical resistance of the electrodes. There are some ways to reduce the Ohmic losses, such as decreasing the thickness of the electrolyte or using a suitable material for the bipolar plates and using a high conductivity electrode. This voltage drop can be calculated as follows:

$$V = IR \tag{1.13}$$

where I is the current density, R is the electrical resistance and V is the Ohmic loss [19].

1.6.4 Mass transport losses

This voltage loss is due to the change in concentration of the materials at the electrodes. The voltage drop can be calculated as follows:

$$V = -B\ln(1-\frac{i}{I}) \tag{1.14}$$

where V is the mass transport loss, B is a constant dependent on the fuel cell operating conditions, i is the current density and I is the limiting current density when the fuel supply is at maximum speed [18].

1.7 PEM Fuel Cells

The PEM fuel cell is an electrochemical cell that is fed hydrogen at the anode and oxygen at the cathode side. In principle, the PEM fuel cell separates the oxidation of hydrogen fuel into the catalysts, which are on the two sides of the electrolyte membrane. The final products from the PEM fuel cell are water vapour, heat and electric potential. The PEM fuel cell is the most popular type of fuel cell due to its low operating temperature and it has been used in Gemini space craft. The proton exchange membrane fuel cell is also referred to as a polymer electrolyte membrane fuel cell [21]. Furthermore, PEM fuel cells have almost zero emissions and this makes them an environmentally friendly system and it is also a quiet system which makes them suitable for use anywhere. However, the PEM fuel cell system needs to be improved and developed because it needs a pure hydrogen supply which makes it an expensive system [6, 21]. Moreover, the complexity of the thermal and water management needs to be taken into account when designing PEM fuel cells. To solve these problems, many researchers have used a computational fluid dynamic technique to model the fuel cell water and thermal distributions in order to increase the efficiency of the PEM fuel cells [9]. On the other hand, hydrogen can be supplied to the PEM fuel cells from methane, or from fossil fuels as biomass gasification [6]. In the PEM fuel cell, hydrogen is oxidized at the anode side to produce protons. The protons are conducted through the membrane and that will release electrons which travel on an external circuit so that an electrical current will be generated [11].

The typical electrochemical reactions in PEM fuel cells are illustrated in Figure 1.9.

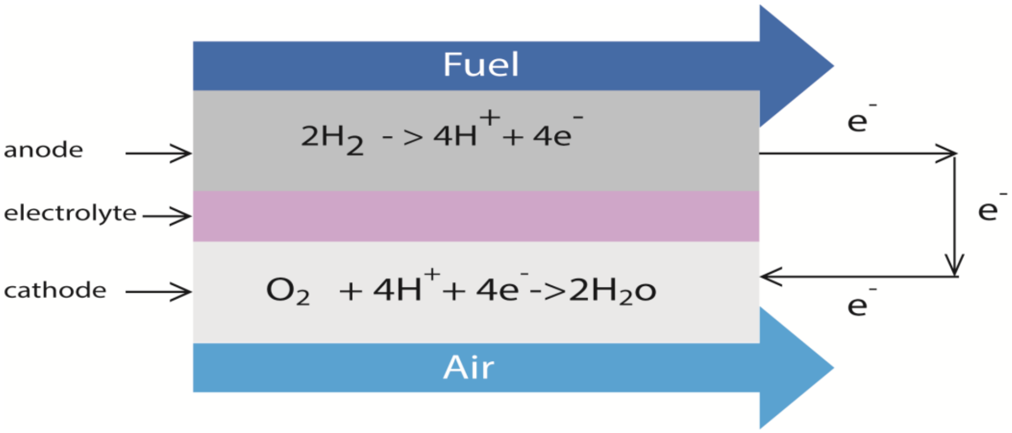

Figure 1.9 The typical electrochemical reactions in a PEM fuel cell.

The main components in PEM fuel cells are shown in Figure 1.10 and they are as follow:

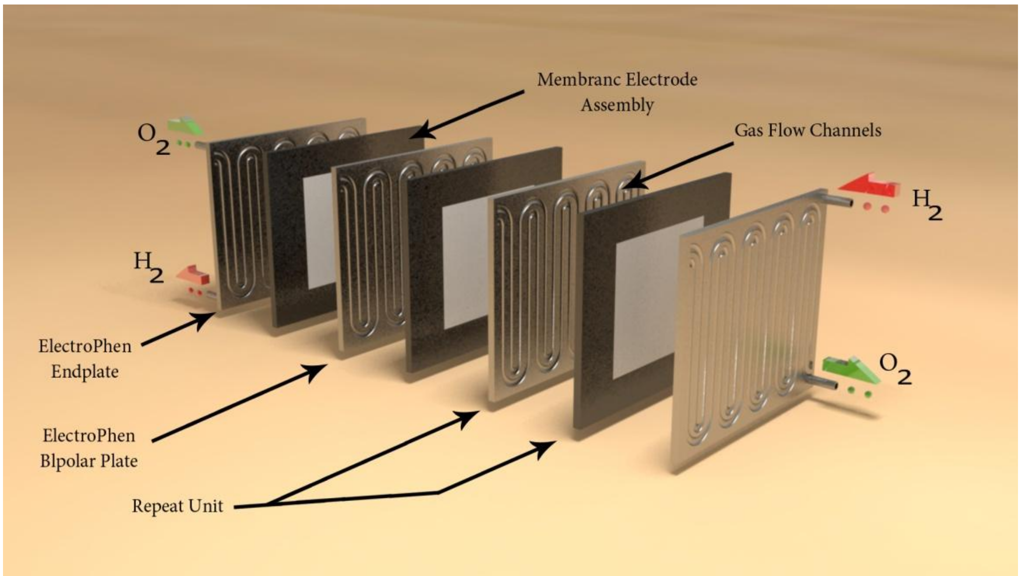

Figure 1.10 The basic structure of a PEM fuel cell.

1.7.1 Membrane

The most common material produced using the polymer electrolyte membrane is sulphonated fluoroethylene, which is known as Nafion®. This material is used in the electrodes of PEM fuel cells because of its high resistance and hydrophobic nature which helps to remove the product water out of the electrode.

The basic polymer polytetrafluoroethylene is modified by substituting fluorine for the hydrogen in the polyethylene.

The polytetrafluoroethylene (PTFE) structure is shown in Figure 1.11.

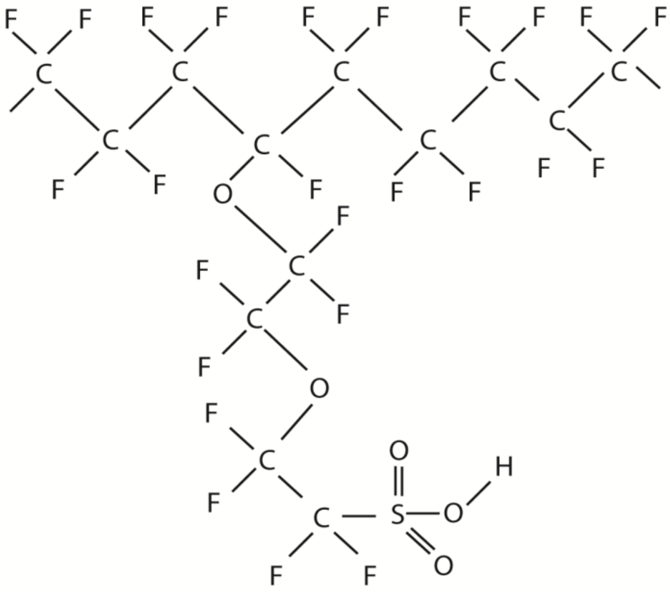

Figure 1.11 The chemical structure of polytetrafluoroethylene (PTFE).

In order to provide protonic conductivity and strong mechanical structure to PEM fuel cells, a composite membrane made up of a Teflon-like material was employed. The Nafion® membranes have been manufactured in several thicknesses and different sizes.

Furthermore, the membrane structure and the water content inside the membrane are one of the main factors which affect the protonic conductivity of the membrane [21].

The amount of water in the membrane depends on the water state. Membranes may contain liquid water molecules more than vapour water molecules. The Nafion® membrane changes its dimensions with different water content by an order of magnitude of about 10%. Therefore, this swelling in the membrane should be taken into account in the PEM fuel cell design [22].

1.7.2 The electrodes

In PEM fuel cells, there is a layer between the porous media and the membrane. This layer is called the catalyst layer where the electrochemical reactions take place. The reactions of the three species gases, electrons and protons travel through the catalyst. Also, the catalyst is coated with ionomer to allow the protons to travel through it. In addition, electrodes are made of porous media to allow gases to travel to the reaction region [22].

The most well known catalyst in PEM fuel cells is platinum. Platinum was used in PEM fuel cells in large amounts during the early days of PEM fuel cell development. However, later it was discovered that the only important parameter in the platinum is its surface area. So, it is important to have small particles of platinum and a large surface area. The catalyst layer should be as thin as possible in order to minimize the potential losses because of the rate of gas and proton transport and reactant through the catalyst layer. Furthermore, the catalyst layer should be loaded with higher amounts of Pt which assist in producing more voltage. However, it should be taken into account that the current density is calculated per area of catalyst, which means there will not be any significant difference in the cell performance. To increase the surface active area of the Pt catalyst, the Pt is usually painted with an alcohol and a water mixture to include ionone in the surface of the catalyst [23].

By using carbon powders on the surface of the catalysts to support the platinum particles, and a porous conductive material, such as carbon paper or carbon cloth, the electrode is fixed at each side to include a porous layer. The catalyst layer is attached to the membrane by depositing the catalyst to the gas diffusion layer, which is usually carbon paper or carbon cloth, then hot-press these two layers to the membrane. The membrane, gas diffusion layer and catalyst layer are called the membrane electrode assembly, which is also referred to as the MEA [23].

1.7.3 Gas diffusion layer

Between the catalyst layer and the bipolar plates, there is a diffusion current collector layer, which is called the gas diffusion layer (GDL). This layer has many important functions in PEM fuel cells as follows:

- It allows the gases to travel from the channels to the catalyst layers where the reactions take place.
- It provides a pathway to allow the produced water to flow from the catalyst to the channels.
- It allows the electrons to travel from the catalyst layers to the bipolar plates.

- It removes the heat which is generated from the electrochemical reactions in the catalyst to the bipolar plate.
- It provides the mechanical support to the PEM fuel cell.

Moreover, the gas diffusion layer should be a porous material and the porosity of the GDL should be taken into account, both in the in-plane and the through-plane directions. Also, the anisotropy of the thermal and electrical conductivity of the gas diffusion layer should be taken into account for both the in-plane and the through-plane directions [24].

Typically, the gas diffusion layer is made of a carbon fibre paper or a carbon cloth, as illustrated in Figure 1.12, which is treated by a different range of PTFE from 5% to 30%. In addition, the porosity of the gas diffusion layer is between 70% and 80% [25].

The bulk and contact resistance should both be included for the thermal and electrical conductivity of the gas diffusion layer.

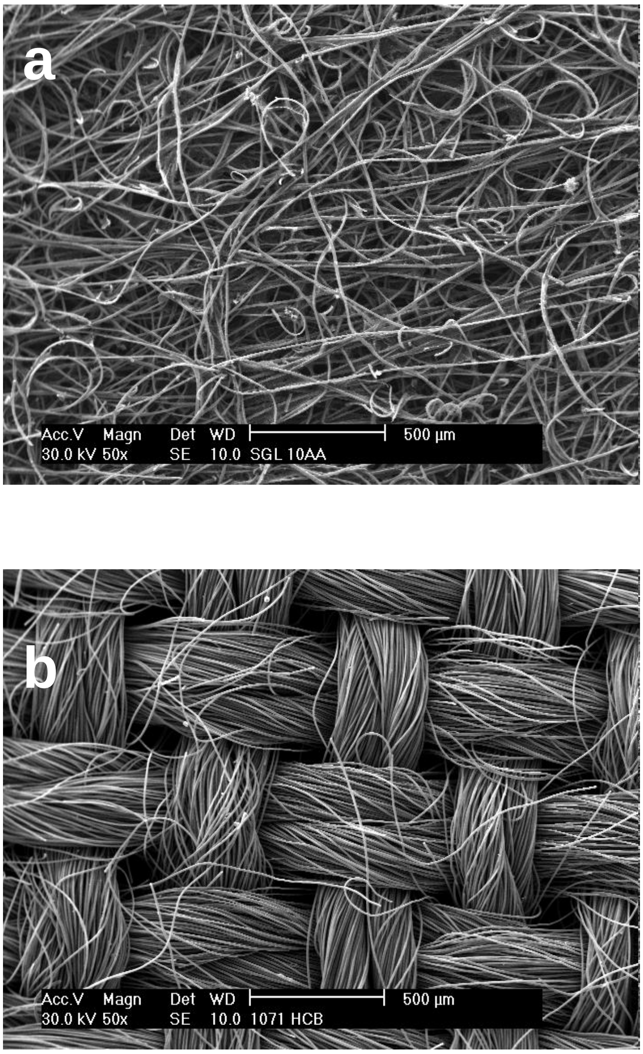

Figure 1.12 Scanning Electron Microscope at 50× magnification of the material of a GDL: (a) carbon paper, and (b) carbon cloth.

1.7.4 The bipolar plates or the current collectors

One of the essential layers in the PEM fuel cell is the bipolar plates which are known also as the current collectors. Bipolar plates connect the anode to the cathode sides electrically in series and help to collect the current from the anode to the cathode, which means that the bipolar plates should be electrically conductive. The bipolar plates also assist in spreading the reactant gases and cool the fuel cell using the cooling fluid channels [26]. Moreover, the bipolar plates must be made of a strong material in order to provide a support to the fuel cell stack. Typically, bipolar plates contain the flow field channels and the cooling channels, so they must thermally conduct the heat from the MEA to the cooling channels. The most commonly used material for the bipolar plates is graphite. The advantages which make it suitable for the fuel cell are the low density of the graphite which is less than any other suitable metals, and it has a higher conductivity. Some metallic bipolar plates are used for PEM fuel cells, such as aluminium, steel, titanium and nickel [27].

Bipolar plates cost about 30% of the total cost of a PEM fuel cell and it accounts for more than 60% of the weight of a PEM fuel cell.

There are different flow-field designs which have been used in PEM fuel cells, such as the parallel flow field, serpentine, planner and interdigitated flow field [28, 29]. These different flow field designs are shown in Figure 1.13.

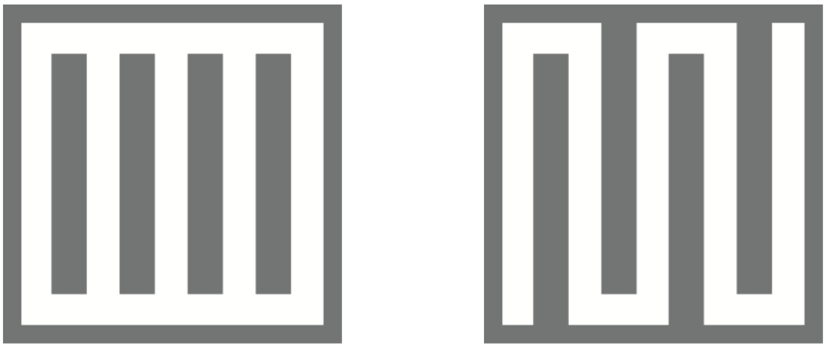

Parallel flow field

Serpentine flow field

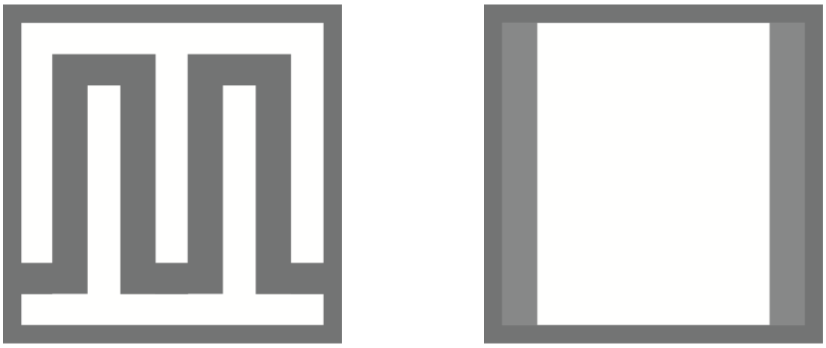

Interdigitated flow field

Planner flow field

Figure 1.13 Typical PEM fuel cell flow fields.

1.8 PEM Fuel Cell Challenges

Despite the fact that PEM fuel cells have wide applications and several advantages over the other fuel cell types, there are some issues which need to be taken into consideration in PEM fuel cells, such as the water and thermal management which are the major technical challenges in fuel cells.

On the other hand, the cost and durability are the main challenges to the commercialization of fuel cells. Therefore, the key challenges of PEM fuel cells are as follows:

1.8.1 Water management in PEM fuel cells

In PEM fuel cells, there should be a sufficient amount of water in the electrolyte to ensure that the polymer electrolyte has good conductivity. However, if there is too much water in the electrodes then it may block the gas diffusion layer and flood the electrolyte [30].

There are some complications relating to the balance of water in the electrolyte because when protons are moving from the anode to the cathode, they will carry some water molecules with them. This process is called the electro-osmotic drag. Furthermore, there is a risk from the drying effects when the cell reaches a high temperature. To solve these problems, the air is usually humidified before it is pumped into the channels of the fuel cell [31].

Another complication is that there are some differences in the amounts of water in the electrolyte. In practice, some parts of the cell may be dry and others may be flooded while the air is moving through the electrodes. So, the amount of water in the PEM fuel cell should be well balanced and controlled [32]. Since the high humidity inside the PEM fuel cell could block the gas diffusion layer and also block the gas transportation and reactant. This is indicated by a sudden voltage drop in the polarisation curve. Therefore, advanced water management should be achieved to control the water in the PEM fuel cell [33].

1.8.2 Thermal management of the PEM fuel cell

There are some differences between the actual cell voltage and the voltage which is presented from the fuel cell. These differences are produced as heat in the PEM fuel cell.

There are several ways of removing this heat from the fuel cell. One common way is to provide a cool air flow which assists in the evaporation of the water. This method is used for PEM fuel cell systems of approximately 2 kW power. Another method is to use cool water which is suitable for some applications, such as in combustion engines. The cooling air can maximize the size of the PEM fuel cell. However, the effect of the cooling water is greater than the effect of the cooling air in PEM fuel cells. Usually PEM fuel cells, which are more than 10 kW use water cooling [32].

In these two methods of cooling PEM fuel cells, the cooling channels are produced in a bipolar plate [32].

1.8.3 PEM fuel cell cost and durability

One of the biggest challenges which face PEM fuel cell technology is their cost and durability. The polarisation curve can indicate that a low current density implies less operating cost (mainly hydrogen and temperature) and a higher capital cost (mainly membrane material and catalyst layer) and the opposite is observed at a high current density [34]. The cost target for fuel cells by 2015 is $30/kW and it was $45/kW by 2010 and the durability is about 5000 hours [35].

Almost half of the fuel cell cost comes from the cost of platinum and the catalyst ink. In addition, the membrane is the major cost for the fuel cells with low production volumes. The price of manufacturing fuel cells, between 2004-2008, decreased by about 73% and it is expected that the price of manufacturing fuel cells will fall at the same rate over the next two decades. These cost reductions are driven by an improvement in the system design and production methods [36]. Furthermore, there are some costs which must be taken into consideration as price of distribute the hydrogen [37].

1.9 Fuel Cells Systems

The fuel cells systems are a complex system and are varying depend on the applications and the amount of output power which is needed.

However, fuel cell systems usually consist of: fuel cell stack, fuel processor, current conditioners, current inverters and the heat management system, water management systems, see Figure 1.14 [26, 32].

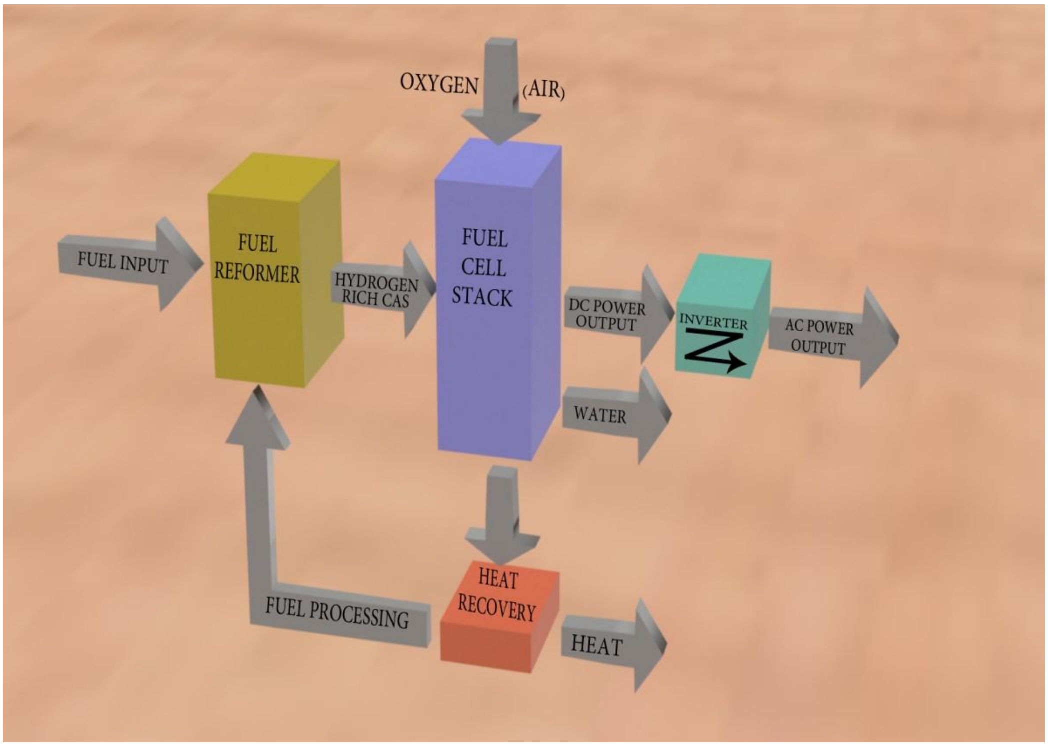

Figure 1.14 Schematic of the fuel system.

1.9.1 Fuel cell stack

The output power of a single fuel cell is very low and this makes them suitable for only small applications. Therefore, the fuel cell is usually combined in series to form the fuel cell stack. Typically, a fuel cell stack consists of hundreds of fuel cells to produce an applicable amount of power [21, 26].

1.9.2 Fuel processor

Typically, the fuel reformer is used to convert the fuel, such as gasoline, methanol, and diesel, to hydrogen and impurities, such as carbon dioxide and sulphur, are removed from the system to avoid poisoning the fuel cell catalyst and as a consequence the effect on the fuel cell life time. The same types of fuel cell, such as the molten carbonate and solid oxide, do not need to convert the fuel to hydrogen due to the high operating temperature which allows the fuel to be reformed itself without a reformer. This procedure is ultimately known as internal reforming [26, 32].

1.9.3 Current conditioners

The power in the fuel cell systems need to be controlled by the control of the current flow, frequency and the voltage in order to make the electrical characteristics suitable for the applications [32].

1.9.4 Current inverters

The fuel cell stack generates the electricity from the chemical reactions inside the fuel cells to direct current which needs to be converted to an alternating current in order for it to be used in many applications [32].

1.9.5 The heat management system

The waste heat from the fuel cell systems is recycled in the high operating temperature fuel cells, such as the molten carbonate fuel cells and solid oxide fuel cells, by a turbine to increase the efficiency of the fuel cell system [26, 32].

1.9.6 The water management system

Most of the fuel cell systems contain a humidity control system and waste water control system [26, 32].

1.10 Research Aims and Objectives

Although one of the most important parameters to understand the heat transfer in fuel cells is the thermal conductivity, to the best of the knowledge of the author there is not enough research on the thermal conductivity of the membrane electrode assembly (MEA) and no results are available for the in-plane thermal conductivity of the MEA. In addition, the effect of many parameters are ignored and not reported in the previous studies on the through-plane thermal conductivity measurements.

In this thesis, a computational fluid dynamic technique (CFD) is used to predict and visualize the water distribution and the thermal distribution in PEM fuel cells by using the commercial CFD software Fluent®, and the effect of the thermal conductivity of the main components in PEM fuel cells, namely the membrane, the catalyst layer and the GDL, is investigated. Following this, the experimental measurement of the thermal conductivity and the contact resistance of the MEA components are reported. This provides a comprehensive study on the thermal conductivity and the thermal contact resistance of the components in the MEA.

The aims of the present study are as follows:

- To numerically investigate the effect of the thermal conductivity of the gas diffusion layer (GDL) on the temperature distribution, water saturation and the overall performance of the PEM fuel cells.

- To numerically investigate the effect of the metallic-based GDL on the performance of PEM fuel cells.

- To numerically investigate the effect of the thermal conductivity of the MEA on the temperature distribution, water saturation and overall performance of the PEM fuel cells.

- To experimentally determine the effect of the in-plane and through-plane thermal conductivity on different types of GDLs in PEM fuel cells.

- To experimentally determine the effect of many GDL properties on the thermal conductivity of the GDL as follows:

i. The effect of the PTFE content on the thermal conductivity of the GDL.

ii. The effect of the mean temperature on the thermal conductivity of the GDL.

iii. The effect of the micro porous layer (MPL) on the thermal conductivity of the GDL.

iv. The effect of the fibre direction on the thermal conductivity of the GDL.

v. The effect of compression load on the thermal conductivity of the GDL.

- To experimentally measure the thermal conductivity of the catalyst layer and the membrane in the in-plane and through-plane directions while taking into account the most important parameters in the membrane and the catalyst in PEM fuel cells as follows:

vi. The effect of temperature and water content on the thermal conductivity of the membrane.

vii. The effect of temperature and Pt loading on the thermal conductivity of the catalyst layer.

1.11 Structure of the Thesis

The thesis consists of eight chapters. Chapter 1 describes the basic structure of fuel cells, fuel cell types and the advantages of fuel cells and their applications, as well as the challenges which are faced in the performance of fuel cells. Chapter 2 examines the effect of the anisotropic thermal conductivity of gas diffusion layers on the performance of PEM fuel cells, which is investigated by using Fluent®. The fundamentals of the CFD modelling of fuel cells is also described. In addition, the metallic-based GDL are modelled and discussed in Chapter 3. In Chapter 4, the effect of the thermal conductivity of the catalyst layer and the membrane on the performance of the PEM fuel cell is illustrated and investigated by using the fuel cell module in Fluent®.

Chapter 5 consists of a literature review on the experimental techniques of measuring thermal conductivity. In Chapter 6, the experimental technique for measuring the thermal conductivity in the in-plane direction is developed and the results obtained for the effects of temperature and polytetrafluoroethylene (PTFE) loadings, Micro Porous Layer (MPL) coatings and fibre direction on the in-plane thermal conductivity of the gas diffusion layer. In addition, the in-plane thermal conductivities of the membrane and catalyst layer are reported with the effect of temperature and water content on the in-plane thermal conductivity of the membrane taken into account, as well as the effect of Pt loading and temperature on in-plane thermal conductivity of the catalyst layer.

In Chapter 7, the thermal conductivity of the MEA is measured experimentally with the effect of the GDL compression, PTFE loadings, MPL coatings and temperature on the through-plane thermal conductivity of the GDL taken into account. Additionally, the through-plane thermal conductivity of the membrane is reported as a function of temperature and the through-plane thermal conductivity of the catalyst layer is reported as a function of temperature and Pt loading. Chapter 8 contains the conclusions of all the major results of the thesis and the recommendations for possible future work.

Chapter 2
Effect of the Anisotropic Gas Diffusion Layer on the Performance of PEM Fuel Cells

2.1 Introduction

Recently, researchers have shown an increased interest in the effect of the anisotropic properties of GDLs on the performance of PEM fuel cells. Knowing the thermal conductivity is essential for the water and thermal management of PEM fuel cells [38].

A number of researchers have employed the computational fluid dynamic technique to predict the performance of PEM fuel cells because it assists in reducing the cost and time of experimental work. However, as yet, CFD modelling cannot capture the realistic temperature distribution and the real liquid distribution in the fuel cells. The difference between the experimental results and the modelling results may be due to the failure to obtain accurate estimates of all the governing parameters [38]. One of these parameters is the thermal conductivity of the GDL, which is usually assumed for simplicity to be an isotropic material and this is because there is no available data for the in-plane thermal conductivity of GDLs and there are very limited data for the through-plane thermal conductivity [39-42]. Many numerical investigations have been performed to investigate the effect of the thermal conductivity of the GDL. However, most PEM fuel cell models assume that the GDLs are comprised of an isotropic material. Pharoah and Burheim [43] developed two-dimensional models to investigate the temperature distribution in PEM fuel cells. The effect of the thermal conductivity of the GDL and the change in the water phase leads to higher temperatures in the cathode side than in the anode side. Zamel et al. [44] numerically estimated the in-plane and through-plane thermal conductivity of carbon paper, which is typically used as a gas diffusion layer in PEM fuel cells. The thermal conductivity of the GDL was sensitive to the porosity of the carbon paper. The thermal conductivity of the carbon paper was found to increase with a decrease in the porosity of the carbon paper, and the in-plane thermal conductivity was much higher than the through-plane thermal conductivity of the carbon paper. Burlatsky et al. [45] developed a mathematical model to investigate the scenario of water removal in PEM fuel cells. The water transport was dependent on the thermal conductivity of the GDL and the water diffusion coefficients. He et al. [46] investigated the effect of the thermal conductivity of the GDL on the temperature distribution in PEM fuel cells. Their results indicated that the anisotropic thermal conductivity of the GDL results in higher temperature gradients than for an isotropic GDL, which led to a decrease in the water saturation in the anisotropic case. However, so far, no researchers have validated their model results with experimental data. In the present study, the effects of anisotropic GDLs on the temperature distribution, water saturation, and current density are assessed using a CFD model, and the results were validated with the experimental data obtained using an in-house PEM fuel cell. The current model takes into account the anisotropic properties of the GDL, such as the electrical conductivity, thermal conductivity, and permeability; this will definitely enhance the prediction of the numerical model.

2.2 Modelling Three-dimensional PEM Fuel Cells

For fuel cells, as for other equipments, collaboration between experimental work and modelling is required in order to develop the fuel cell processes. Models provide some estimates of the critical parameters, which could be the subject of experimental work and material development. In turn, experimental measurements can be used as a guide which allows the experimental parameters to be used in the CFD models. On the other hand, models sometimes cannot capture the real situation because of the difficulty of accurately capturing the balance of the temperature and liquid water transport through the multi-phases in fuel cells [47].

Fuel cell models require the following:

- Mass transport of species:

In PEM fuel cells, the water, electrons, protons and gas mobility should be considered through PEM fuel cells [47].

- Two phase flow models through the porous media: Hydrophobicity and capillary forces, combined with porosity and permeability, are parameters of the GDL layers [47].

- Unit cell modelling:

  Mathematical models can be as simple as a 1-dimensional transport through the membrane electrode assembly and this avoids the time consuming computational fluid dynamic calculations due to the simplified geometry [47].

2.2.1 Governing equations

Basically, the steady fluid flow in the fuel cell is governed by the following equations [39, 48]:

Conservation of mass:

$$\nabla \cdot \left(\varepsilon \rho \vec{u} \right) = 0 \qquad (2.1)$$

Conservation of momentum:

$$\nabla\left(\varepsilon\rho \vec{u}\vec{u}\right) = -\varepsilon\nabla \mathrm{P} + \nabla\cdot\left(\mu\nabla\varepsilon \vec{u}\right) + \frac{\varepsilon\mu}{\tau} \quad (2.2)$$

Conservation of species:

$$\nabla\left(\varepsilon\rho \vec{u} Y_k\right) = \nabla\cdot\left(\rho D_k^{eff}\nabla Y_k\right) + S_k \quad (2.3)$$

where ρ is the fluid density, $\vec{u}$ is the fluid velocity vector, *P* is the fluid pressure, μ is the mixture viscosity, Y_k is the mass fraction for gas species *k*, ε is the porosity of the porous media, τ is the permeability of the porous media, S_k is the source or sink term for species *k*, and D_k^{eff} is the diffusion coefficient of species *k* and it can be calculated as follows:

$$D_k^{eff} = \varepsilon^{\xi} D_k \tag{2.4}$$

where ξ is the tortuosity of the porous media and D is the ordinary diffusion coefficient.

Conservation of charge:

$$\nabla \cdot \left(\sigma_{sol} \nabla \phi_{sol}\right) = \begin{cases} -J_a \\ -J_c \end{cases} \tag{2.5}$$

$$\nabla \cdot \left(\sigma_{mem} \nabla \phi_{mem}\right) = \begin{cases} J_a \\ J_c \end{cases} \tag{2.6}$$

where σ_{sol} is the electric conductivity of solid, σ_{mem} is the proton conductivity in membrane, ϕ_{sol} is the potential of solid phase, ϕ_{mem} is the potential of membrane phase, J_a is anode catalyst reaction rate and J_c is cathode catalyst reaction rate.

Conservation of liquid water formation:

$$\nabla \cdot \left(\rho_L V_L S\right) = r_w \tag{2.7}$$

where S is the liquid water saturation, L is the liquid water and r_w is the mass transfer rate between the gas and liquid.

Conservation of energy:

$$\left(\rho c_P\right)_{eff} \left(V \cdot \nabla T\right) = \nabla \cdot \left(k_{eff} \nabla T\right) + S_e \tag{2.8}$$

where c_P is the specific heat capacity of the gas mixture, T is the temperature, S_e is the energy source term and k_{eff} is the effective thermal conductivity of the gas mixture which is defined as the follows:

$$k_{eff} = 2k_s + \left(\frac{\varepsilon}{2k_s + k_F} + \frac{1-\varepsilon}{3k_s}\right)^{-1} \tag{2.9}$$

where k_s and k_F are the thermal conductivities of the solid and fluid regions, respectively.

All the source terms in the above equations are listed in Table 2.1.

Table 2.1 Source terms in the governing CFD equations.

Source terms	Defining equation
Species volumetric source terms	$S_{H_2} = -\frac{M_{W,H_2}}{2F}$ $S_{O_2} = -\frac{M_{W,O_2}}{4F}$ $S_{H_2O} = \frac{M_{W,H_2O}}{2F}$
Energy source term	$S_e = h_{react} - R_{an,cat}\eta_{an,cat} + I^2 R_{ohm} + h_I$
Cathode catalyst reaction rate	$J_C = J_c^{ref}\left(\frac{\gamma_{o_2}}{\gamma_{o_2}^{ref}}\right)\left[\exp\left(\frac{-\alpha_a}{RT}(\phi_{mem} + \phi_{sol} - VOC)\right) - \exp\left(\frac{-\alpha_c}{RT}(\phi_{mem} + \phi_{sol} - VOC)\right)\right]$
Anode catalyst reaction rate	$J_a = J_a^{ref}\left(\frac{\gamma_{H_2}}{\gamma_{H_2}^{ref}}\right)\left[\exp\left(\frac{\alpha_C}{RT}(\phi_{SOL} - \phi_{mem})\right) - \exp\left(\frac{-\alpha_c}{RT}(\phi_{sol} - \phi_{mem})\right)\right]$
Mass transfer rate between gas and liquid	$r_w = I^2 R_{ohm} + \eta_{an,cat} J_{an,cat} + r_w h_L$

* See the nomenclature for the definitions of all the symbols.

2.2.2 Computational domain

The performance of PEM fuel cells is usually investigated by using polarisation curves, which are mainly the current density versus the cell potential plots [49]. In this chapter, the polarisation curves for PEM fuel cells with an anisotropic GDL are investigated and the results are compared with the experimental data obtained from the University of Leeds PEM fuel cell which was developed by Ismail et al. [50]. This fuel cell takes into account the anisotropic permeability and electrical conductivity of the GDL, but not the thermal conductivity [50]. The parameters of the anisotropic GDL were obtained and they are used as input parameters for the CFD model, which was developed by using the Fluent® software. The results obtained from different thermal conductivities are compared in terms of the temperature distribution, water content and the electrical conductivity. In this investigation, the whole PEM fuel cell, this cell consists of 11 channels with a serpentine flow field. A schematic of the 11-channel serpentine flow field of the PEM fuel cell is shown in Figure 2.1. The PEM fuel cell dimensions were 32× 10.81 × 32 mm in the x, y and z directions, respectively. The 3-D model consisted of nine zones which are: cathode current collector, cathode channel, cathode gas diffusion layer, cathode catalyst layer, membrane, anode catalyst layer, anode gas diffusion layer, anode channel, and anode current collector, the fuel cell dimensions are listed in Table 2.2.

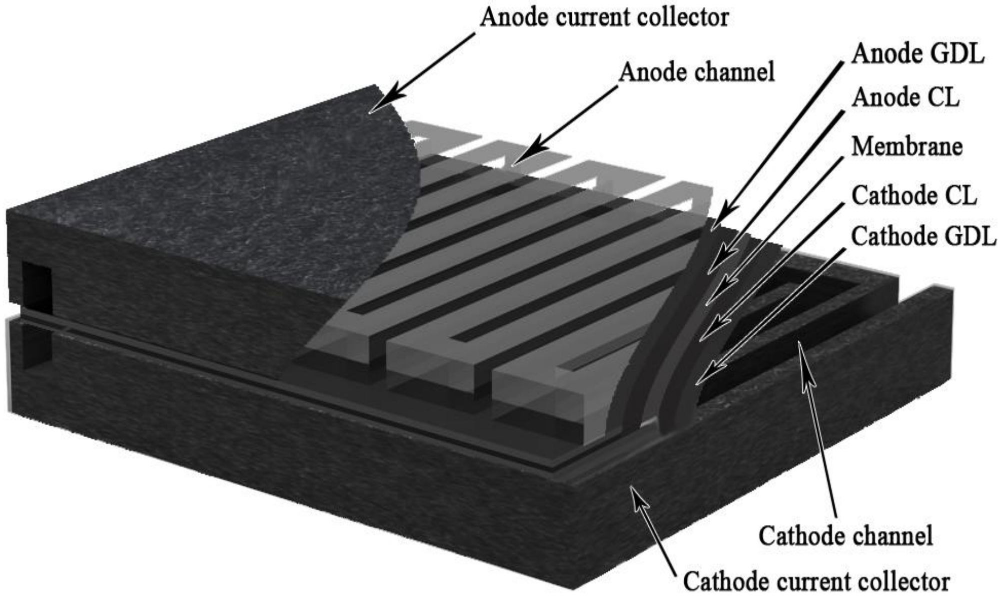

Figure 2.1 Schematic of the PEM fuel cell computational domain.

Table 2.2 The CFD investigated PEM fuel cell dimensions.

Dimension	Value
Channel length (m)	11× (2.8 × 10^{-2})
Channel height (m)	2.0 × 10^{-3}
Channel width (m)	2.0 × 10^{-3}
GDL thickness (m)	3.0 × 10^{-4}
Catalyst layer thickness (m)	3.0 × 10^{-5}
Membrane thickness (m)	1.5 × 10^{-4}

For simplicity, and to reduce the calculation time, the model assumed that the fluid flow to be laminar, as the inlet velocity was low; the reactions were under steady state conditions; and the reaction gases were assumed to be ideal gases.

2.2.3 Boundary conditions

The fluid flow in the PEM fuel cell was generated under steady state conditions and all of the governing parameters, at the same values as the experimental parameters, are listed in Table 2.3. The velocity at the anode side was set to be 0.42 m/s with fully humidified hydrogen, while the velocity at the cathode channel was 1.06 m/s with humidified air, as shown in Figure 2.2. Isothermal constant temperature wall boundaries were defined for the cell sides and the current collectors. The operating temperatures were 303K, 313K, 323K, and 333K, respectively. The gauge pressure was set to be 2.5 bar at both the anode and cathode sides. The physical and operational parameters are listed in Table 2.3.

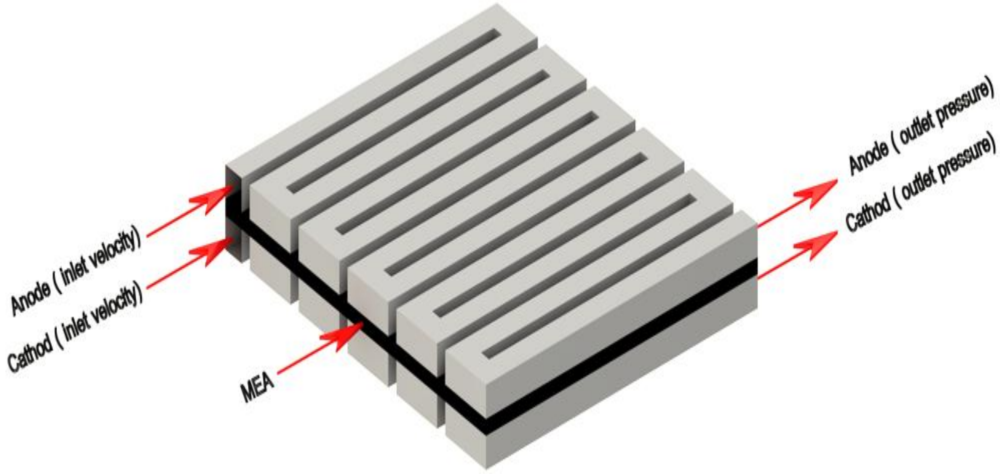

Figure 02.2 Schematic of the eleven-serpentine channels and the boundary conditions.

Table 2.3 Operational parameters for the PEM fuel cell base case.

Parameter	**Value**
Operating temperature (K)	303
Gauge pressure at anode (bar)	2.5
Gauge pressure at cathode (bar)	2.5
Porosity of catalyst layer	0.4 [51]
Porosity of GDL	0.7 [52]
Through-plane permeability of GDL (m^2)	4.97×10^{-13}[53]
In-plane permeability of GDL (m^2)	1.87×10^{-12}[53]
Through-plane inertial coefficient of GDL (m^{-1})	4.22×10^{7}[53]
In-plane inertial coefficient of GDL (m^{-1})	4.05×10^{6}[53]
Through-plane electrical conductivity of GDL (S/m)	48[54]
In-plane electrical conductivity of GDL (S/m)	4000 [54]
Permeability of catalyst layer (m^2)	1×10^{-13} [55]
Electrical conductivity of catalyst layers (S/m)	300 [55]
Permeability of membrane (m^2)	1.8×10^{-18}
Density of current collectors (kg/m^3)	1860[56]
Specific heat capacity of current collectors (J/(kg.K))	865 [56]
Electrical conductivity of current collectors (S/m)	3200 [56]
Anode inlet gas velocity (m/s)	0.42
Cathode inlet gas velocity (m/s)	1.06
Inlet mass fraction of hydrogen (Anode)	0.37
Inlet mass fraction of water (Anode)	0.63
Inlet mass fraction of oxygen (Cathode)	0.22
Inlet mass fraction of nitrogen (Cathode)	0.72
Inlet mass fraction of water (Cathode)	0.06
Transfer coefficients for cathode reaction	0.512 [57]
Reference exchange current density at cathode (A/m^2)	193 [57]
Transfer coefficients for anode reaction	0.5 [57]

2.2.4 Check for mesh independency

The conservation of mass, momentum, electrochemical reactions and energy equations were solved using the finite volume method [58].

In order to check that the solution of the conservation equations do not change significantly with the number of cells, and to ensure the solution accuracy, 5 different meshes were built with different numbers of cells, as shown in Table 2.4.

Table 2.4 The number of the cells in the five meshes investigated.

	Number of cells									Total number of cells
Mesh number	**membrane**	**Anode catalyst**	**Cathode catalyst**	**Anode gas diffusion**	**Cathode gas diffusion**	**Anode channel**	**Cathode channel**	**Anode current collector**	**Cathode current collector**	
Mesh1	67500	45000	45000	157500	157500	64440	64440	250560	250560	876990
Mesh2	112500	90000	90000	180000	180000	85920	85920	296580	296580	1064680
Mesh3	157500	135000	135000	202500	202500	107400	107400	387600	387600	1822500
Mesh4	202500	180000	180000	250000	250000	128880	128880	478620	478620	2277500
Mesh5	225000	202500	202500	285000	285000	150360	150360	569640	569640	2640000

The average current density at 0.65 V was calculated for these 5 meshes as shown in Table 2.5. It was found that the current density increased with increasing the number of cells until the current density reaches almost a constant value which was about 105.75 $mA{\cdot}cm^{-2}$. It is clear from Table 2.5 that there is no significant difference between the results obtained for the mesh numbers 3, 4 and 5. As a result, mesh number 3, which has about 1,800,000 control volumes, was used in order to save the calculation times and the computing memory, to investigate the effect of the anisotropy thermal conductivity of the GDL on the performance of a PEM fuel cell.

Table 2.5 The average current density at 0.65V for the different meshes.

Mesh Number	Average Current Density at 0.65V(with a current collector in the end side)
Mesh 1	89.44 ($mA{\cdot}cm^{-2}$)
Mesh 2	96.13 ($mA{\cdot}cm^{-2}$)
Mesh 3	105.75 ($mA{\cdot}cm^{-2}$)
Mesh 4	105.89 ($mA{\cdot}cm^{-2}$)
Mesh 5	106.21 ($mA{\cdot}cm^{-2}$)

2.2.5 Results and discussion

The current density of the fuel cell model was plotted for different voltages. The polarisation curve was generated by plotting the current density at these different voltages while keeping all the parameters to be the same as those given in Table 2.3. On comparing the modelling results with the experimental data [50], Figure 2.3 shows that the modelling results are in good agreement with the experimental data.

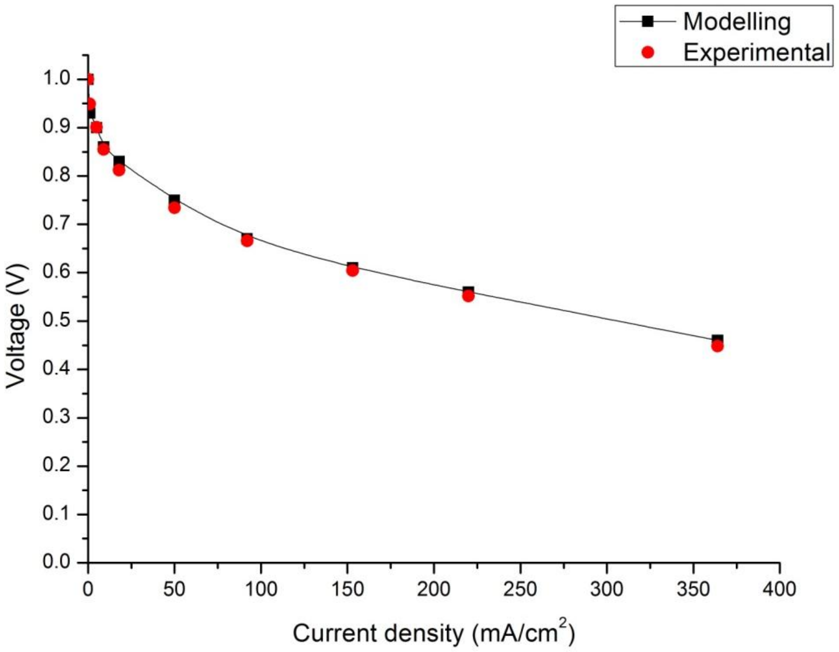

Figure 2.3 The polarization curves for the PEM fuel cell with a current collector on the end side compared with the experimental data of Ismail et al. [50].

2.3 Effect of Anisotropic GDL on the Thermal Conductivity

In order to investigate the effect of the anisotropic thermal conductivity of the GDL in PEM fuel cells, six different cases have been developed. The first three cases investigated the effect of the in-plane thermal conductivity, while the last three investigated the effect of the through-plane thermal conductivity. The first three cases are listed in Table 2.6.

Table 2.6 List of the different cases investigated for investigating the effect of the in-plane thermal conductivity.

Case Number	Through-plane thermal conductivity of GDL ($W \cdot m^{-1} \cdot K^{-1}$)	In-plane thermal conductivity of GDL ($W \cdot m^{-1} \cdot K^{-1}$)
I	1	1
II	1	10
III	1	100

The in-plane thermal conductivity of the GDL was increased from 1 to 10 to 100 $W \cdot m^{-1} \cdot K^{-1}$. The in-plane thermal conductivity has been reported to be between 10-15 $W \cdot m^{-1} \cdot K^{-1}$ and based on this it has been decided to increase and decrease this value by a factor of 10. The through-plane thermal conductivity of the GDL was retained at a constant value of 1 W·m^{-1}·K^{-1}, namely the reported experimental value [40-44]. The polarisation curves were generated for the different cases and compared with the experimental data for the in-house PEM fuel cell, as seen in Figure 2.4.

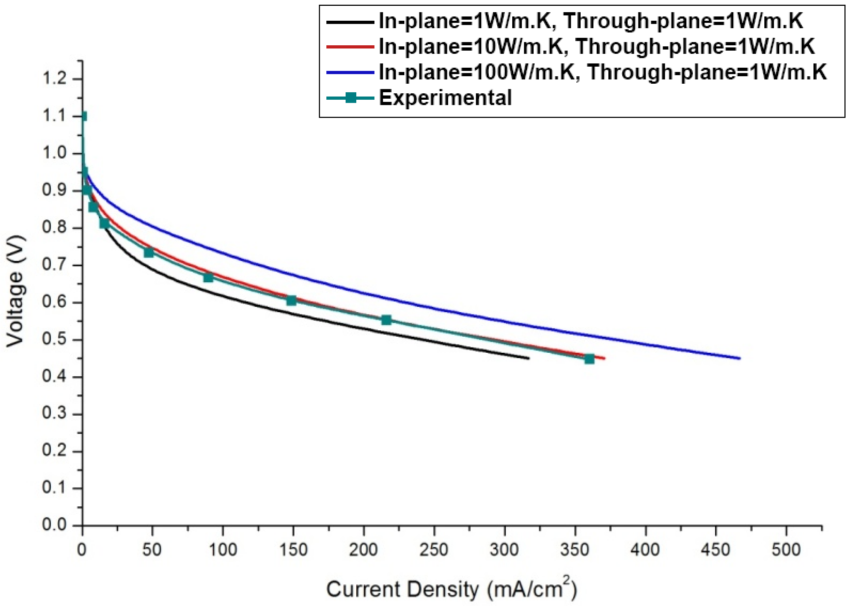

Figure 2.4 Polarisation curves for the different in-plane thermal conductivities of the GDL compared with the experimental data.

We observe that the numerical results show good agreement between the experimental data and the case II, where the in-plane thermal conductivity was 10 W·m^{-1}·K^{-1}and the through-plane thermal conductivity was 1 W·m^{-1}·K^{-1} as mentioned earlier, this is most likely to be the thermal conductivity values in the experimental investigations. The power density of the PEM fuel cell at 0.55 V, which is one of the normal operating voltages of PEM fuel cells, is illustrated in Figure 2.5, and it is clear that as the in-plane thermal conductivity of the GDL increases from 1 to 10 to 100 W·m^{-1}·K^{-1}, the power density of the PEM fuel cell increases from 84.2 to 109.5 to 152.1 mA·cm^{-2}, respectively. A similar, though less pronounced effect was found at the higher operating temperatures of the PEM fuel cell of 313 K, 323 K and 333 K.

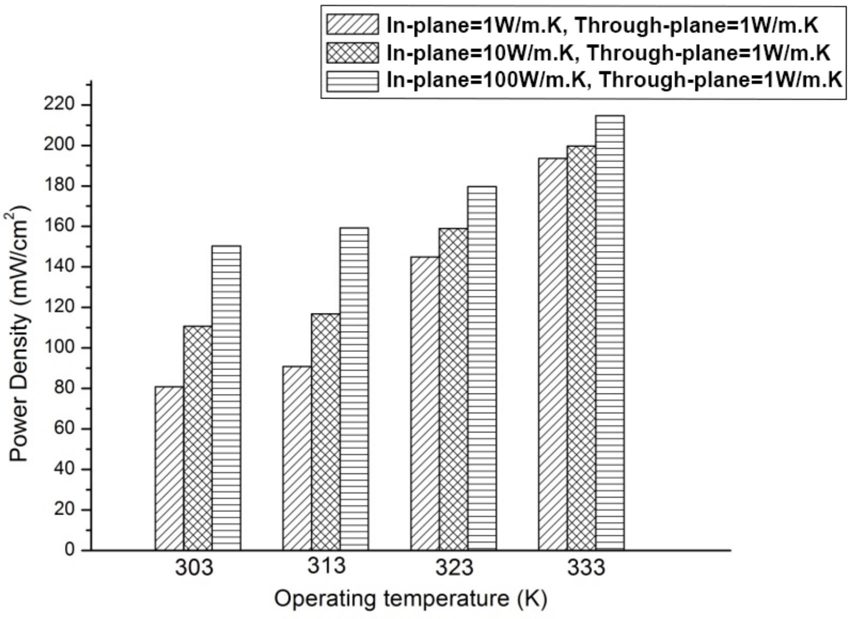

Figure 2.5 The effect of the in-plane thermal conductivities of the GDL on the power density (mW·cm^{-2}) of the PEM fuel cell.

The effect of the thermal conductivity of the GDL on the power density was because of the decrease in the electrical resistance when the temperature decreases as a result of increasing the thermal conductivity [59]. Furthermore, the increased overall thermal conduction of the GDL assists in dissipating the heat from the MEA and consequently these results in a more uniform temperature distribution and having more liquid water to humidify the membrane, which enhances the ionic conductivity, and subsequently improves the performance of the cell [60].

The temperature distribution through the GDL is presented in Figure 2.6. The results show that as the in-plane thermal conductivity of the GDL increases, the difference in the temperatures decreases and the temperature in the GDL became more uniform. The maximum temperature was found to be 313.6K when the in-plane thermal conductivity of the GDL was 1 $W \cdot m^{-1} \cdot K^{-1}$ and the difference in the temperatures was 10K. Then the maximum temperature decreases to 308.5K when the in-plane thermal conductivity of the GDL increases to 10 $W \cdot m^{-1} \cdot K^{-1}$and the difference in the temperatures was 5.5K.

Finally, the maximum temperature became 306.1K when the in-plane thermal conductivity was 100 $W \cdot m^{-1} \cdot K^{-1}$ and the temperature becomes more uniform along the GDL.

The low in-plane thermal conductivity causes regions of the fuel cell to remain relatively cold, thus increasing the likelihood of the formation of water pockets which may block the channels in the PEM fuel cell.

It can be seen from Figure 2.7 that the maximum water saturation was 0.367 when the in-plane thermal conductivity was at its maximum value, namely 100 W/mk. This high water saturation means that more liquid water remains in the cathode because of the low temperature which is caused by the high in-plane thermal conductivity of the GDL [45, 60]. This leads to less water, which is produced by the electrochemical reactions in the cell, to vaporize than in the low in-plane thermal conductivity cases [61].

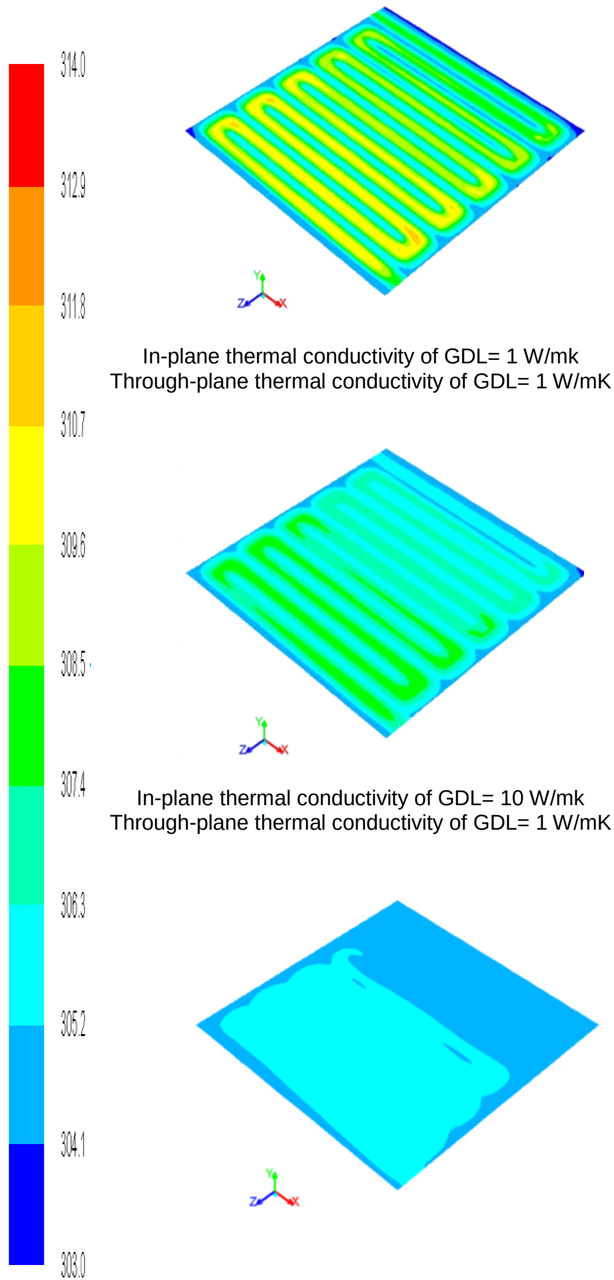

In-plane thermal conductivity of GDL= 1 W/mk
Through-plane thermal conductivity of GDL= 1 W/mK

In-plane thermal conductivity of GDL= 10 W/mk
Through-plane thermal conductivity of GDL= 1 W/mK

In-plane thermal conductivity of GDL= 100 W/mk
Through-plane thermal conductivity of GDL= 1 W/mK

Figure 2.6 The effect of the in-plane thermal conductivities of the GDL on the temperature (K) distribution within the cathode GDL.

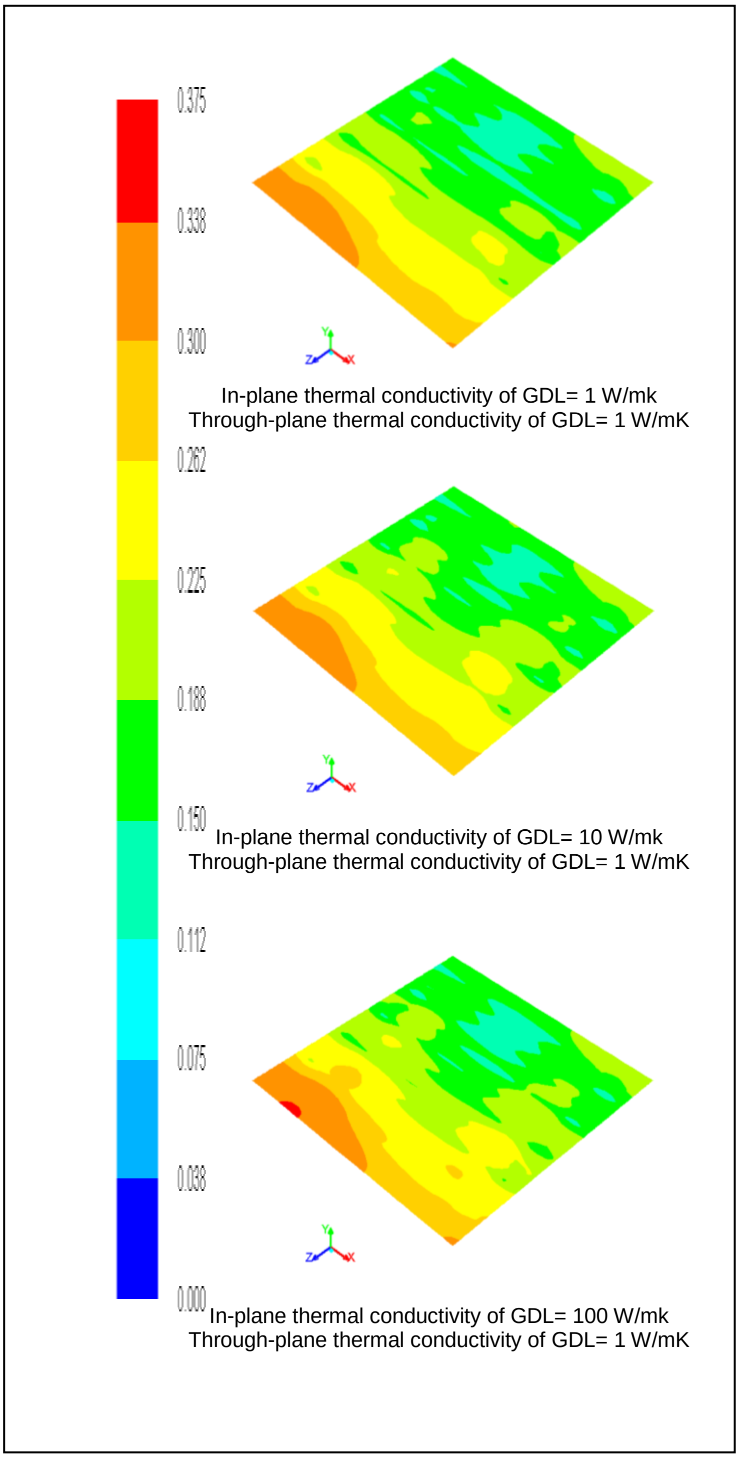

In-plane thermal conductivity of GDL= 1 W/mk
Through-plane thermal conductivity of GDL= 1 W/mK

In-plane thermal conductivity of GDL= 10 W/mk
Through-plane thermal conductivity of GDL= 1 W/mK

In-plane thermal conductivity of GDL= 100 W/mk
Through-plane thermal conductivity of GDL= 1 W/mK

Figure 2.7 The effect of the in-plane thermal conductivities of the GDL on the water saturation at the interface between the cathode GDL and catalyst layer.

The effect of the through-plane thermal conductivity was then investigated, in particular for the cases listed in Table 2.7. The through-plane thermal conductivity of the GDL increases from 0.1 to 1 to 10 $W \cdot m^{-1} \cdot K^{-1}$, while the in-plane thermal conductivity of GDL was kept constant at 10 $W \cdot m^{-1} \cdot K^{-1}$. The through-plane thermal conductivity was reported to be between 0.1-1 $W \cdot m^{-1} \cdot K^{-1}$ [40, 44] and based on this it has been decided to increase and decrease this value by a factor of 10.

Table 2.7 List of the different cases investigated for the effect of the through-plane thermal conductivity.

Case Number	Through-plane thermal conductivity of GDL ($W \cdot m^{-1} \cdot K^{-1}$)	In-plane thermal conductivity of GDL ($W \cdot m^{-1} \cdot K^{-1}$)
IV	0.1	10
V	1	10
VI	10	10

The polarisation curves obtained from the CFD model were compared with the experimental data for the in-house PEM fuel cell, as seen in Figure 2.8. The results show good agreement between the experimental data and case V, which is literally Case II in Table 2.6.

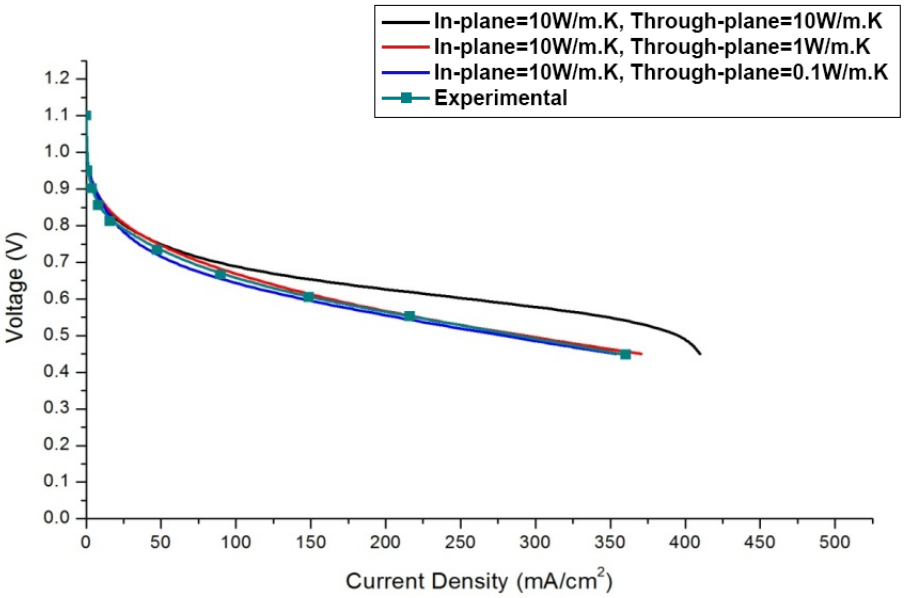

Figure 2.8 Polarisation curves for the different in-plane thermal conductivities of the GDL compared with the experimental data.

The power density of the PEM fuel cell at 0.55 V, one of the typical operating voltages of PEM fuel cells, is illustrated in Figure 2.9, and as the in-plane thermal conductivity of the GDL increases from 0.1 to 1 to 10 W·m^{-1}·K^{-1}, the power density of the PEM fuel cell increases from 84.1 to 109.5 to 119.2 mA·cm^{-2}, respectively. This behaviour is the same as that we observed when the operating temperature of the PEM fuel cell increases from 313K to 323K to 333K. The increased through-plane thermal conductivity assists in decreasing the difference in the temperatures and subsequently less liquid water is evaporated and this improves the performance of the PEM fuel cell.

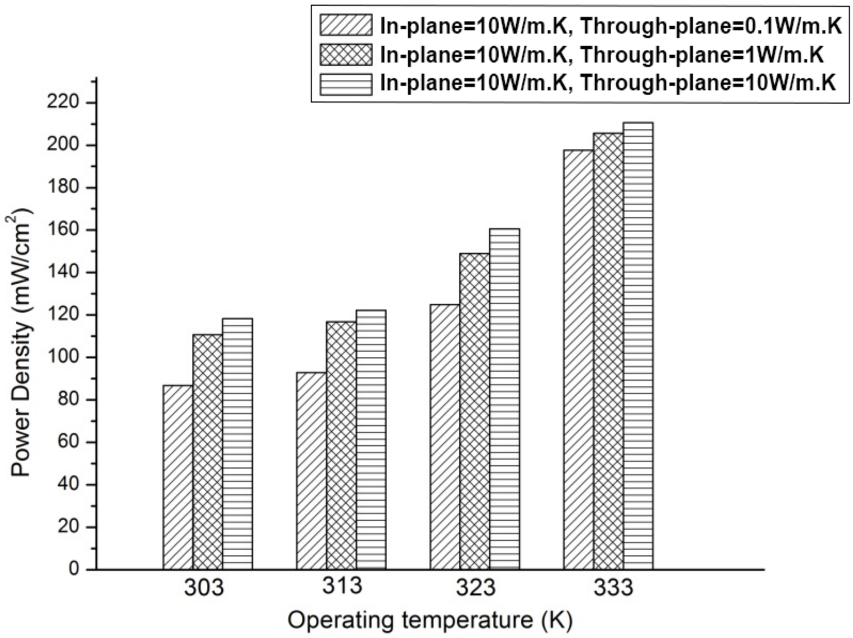

Figure 2.9 The effect of the through-plane thermal conductivity of the GDL on the power density (mW·cm^{-2}) of the PEM.

The effect of the through-plane thermal conductivities of the GDL on the temperature distribution in the PEM fuel cell is illustrated in Figure 2.10. The maximum temperature was found to be 312.4 K when the through-plane thermal conductivity of the GDL was 0.1 W·m^{-1}·K^{-1} and the maximum difference in the temperatures was

9.4 K. Then the maximum temperature reduces to 308.5K when the through-plane thermal conductivity of the GDL increases to 1 $W{\cdot}m^{-1}{\cdot}K^{-1}$ and the maximum difference in the temperatures was 5.5 K.

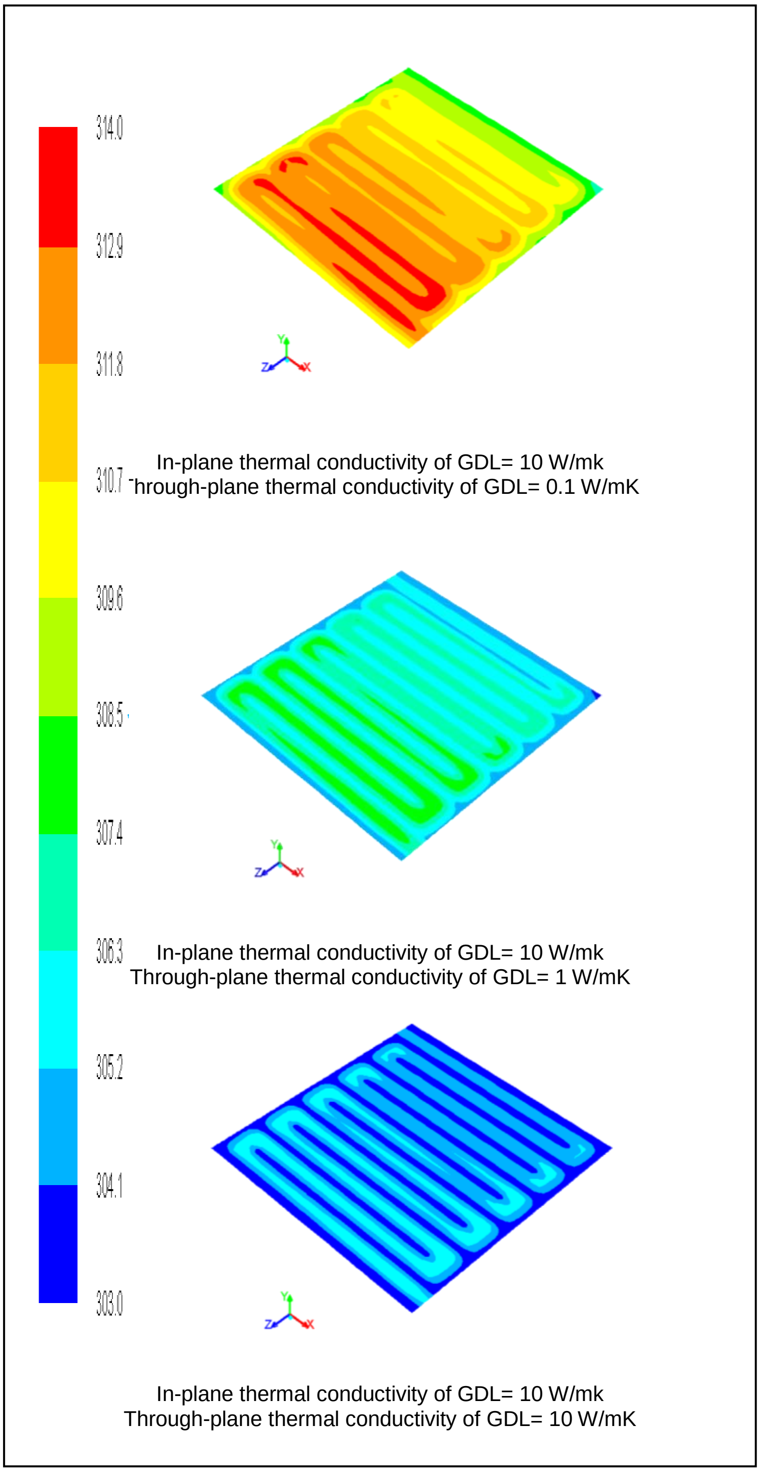

In-plane thermal conductivity of GDL= 10 W/mk
Through-plane thermal conductivity of GDL= 0.1 W/mK

In-plane thermal conductivity of GDL= 10 W/mk
Through-plane thermal conductivity of GDL= 1 W/mK

In-plane thermal conductivity of GDL= 10 W/mk
Through-plane thermal conductivity of GDL= 10 W/mK

Figure 2.10 The effect of the through-plane thermal conductivities of the GDL on the temperature (K) distribution within the cathode GDL.

Finally, the maximum temperature became 305.9K when the in-plane thermal conductivity was 10 W·m^{-1}·K^{-1}, the temperature became more uniform along the GDL, and the difference in the temperatures was no more than 2.9 K. This is because the increase in the heat removal within the GDL assists in producing a more uniform temperature distribution [60].

It can be seen from Figure 2.11 that the maximum water saturation was 0.371 when the through-plane thermal conductivity was a maximum, namely 10 W·m^{-1}·K^{-1}.

This high water saturation means that more liquid water remains in the cathode because of the low temperature which is caused by the high in-plane thermal conductivity of the GDL. This water saturation reduces to 0.355 when the through-plane thermal conductivity of the GDL was reduced to 0.1 W·m^{-1}·K^{-1}.

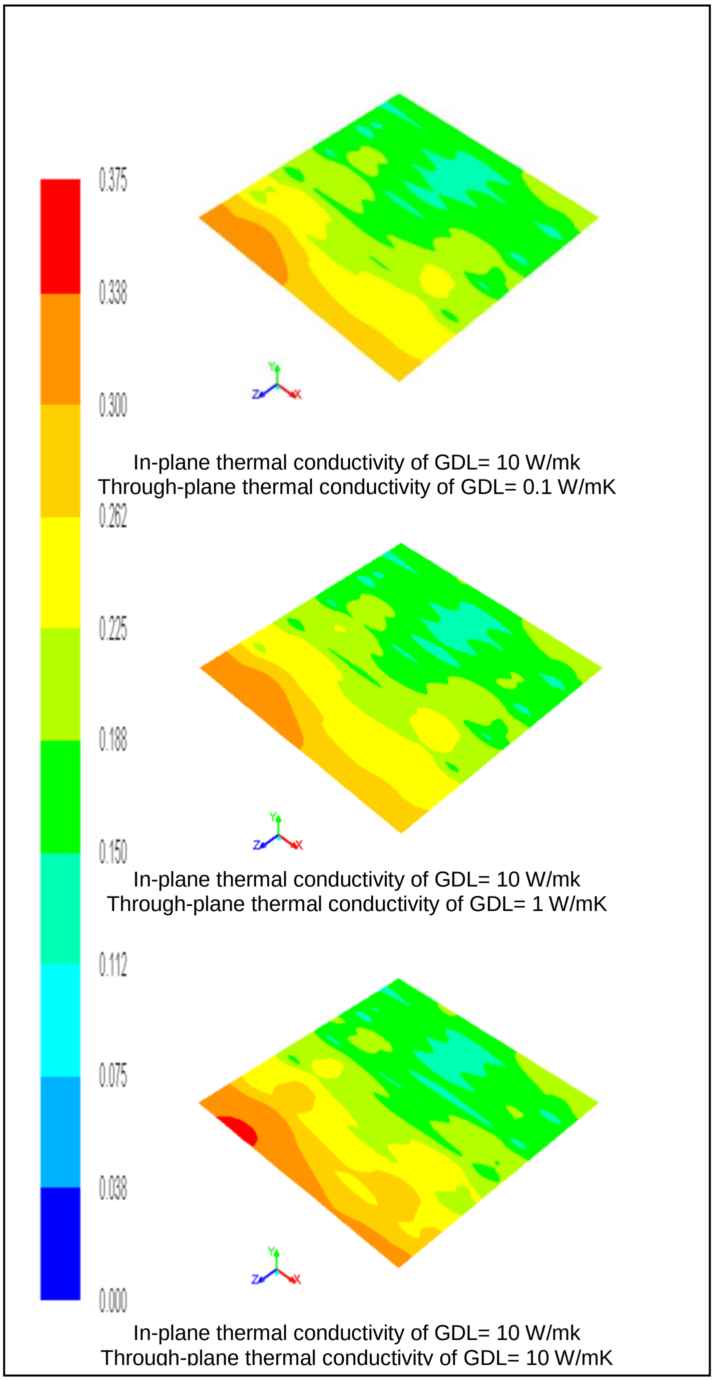

In-plane thermal conductivity of GDL= 10 W/mk
Through-plane thermal conductivity of GDL= 0.1 W/mK

In-plane thermal conductivity of GDL= 10 W/mk
Through-plane thermal conductivity of GDL= 1 W/mK

In-plane thermal conductivity of GDL= 10 W/mk
Through-plane thermal conductivity of GDL= 10 W/mK

Figure 2.11 The effect of the through-plane thermal conductivities of the GDL on the water saturation at the interface between the cathode GDL and cathode catalyst layer.

2.4 Conclusions

A 3-D multiphase model has been developed to investigate the effect of the anisotropic thermal conductivity of the GDL on the performance of PEM fuel cells, and the results have been validated with an in-house PEM fuel cell for different operating temperatures (303K, 313K, 323K, and 333K).

The main conclusions of this study are as follows:

- It has been found that the maximum temperature in the PEM fuel cell decreases when the thermal conductivity increases under the operating conditions investigated.

- The temperature gradient decreases when increasing the in-plane and through-plane thermal conductivities due to dissipating the heat from the membrane electrode assembly which results in a more uniform temperature distribution within the fuel cell components.

- The results show an increase in the current density of PEM fuel cells with an increase in the thermal conductivity of the GDL in both directions, namely the in-plane and the through-plane. Increasing the current density of the fuel cell results from decreasing the electrical resistance in the fuel cell when the temperature decreases after increasing the thermal conductivity of the gas diffusion layer.

- Increasing the thermal conductivity of the GDL increases the liquid water saturation as the maximum temperature decreases which was the result from the uniform temperature distribution which caused by the increase in the thermal conductivity of gas diffusion layer. This lead to more liquid water to be humidify in the membrane.

This study has highlighted the need to accurately determine the thermal conductivity of the GDL. As a result of this study, it is clear that it is important to obtain the thermal conductivity of the GDL for both directions, in-plane and through-plane directions as they have a significant effect on the PEM fuel cell performance.

It is essential to improve the accuracy of the CFD model of the PEM fuel cells and to provide a good prediction of the temperature distribution which helps the thermal management in PEM fuel cells. This will decrease the difference between the results obtained from CFD models and the experimental results as it will take into account the anisotropy of the membrane electrode assembly.

In future studies, the experimental work will be completed and the thermal behaviour and the water transport in a PEM fuel cell will be modelled using the Fluent® software.

Chapter 3
Metal-based GDL

3.1 Introduction

As mentioned in Section 1.7.3, the gas diffusion layer (GDL) is one of the key components that have a significant role in the performance of a PEM fuel cell stack. The gas diffusion layer offers a physical support for the catalyst layer and allows gas to be transported to the catalyst layer. Also it helps increase the ionic conductivity of the membrane by allowing water vapour to reach the membrane, while assisting the liquid water produced by the chemical reaction to leave the catalyst and membrane interface. Therefore, the GDL should be designed and made from a material which balances the hydrophobicity and hydrophilicity properties [62]. These properties have to be balanced carefully in order to guarantee that the fuel cell system works efficiently without drying off or flooding. Typically, the gas diffusion layer is made from carbon paper, or carbon cloth, which is treated with polytetrafluoroethylene (PTFE) [63]. In addition, the pore size distribution of the GDL is optimised in order to allow water to be transported from the cathode catalyst to the flow channel through the GDL. However, it is difficult to make the GDL with an optimized porosity from the carbon fibre, or the carbon cloth, especially with the compression stress which may decrease the porosity [64]. Moreover, the gas diffusion layer should be good electrical conductor and heat dissipater [65]. Therefore, the GDL should be made from a high thermal conductive and a high electrical conductive material with a uniform and optimized pore size. The conventional carbon fibre GDLs meets most of these requirements. However, the currently-used GDLs have far less electrical and thermal conductivities compared to metallic GDLs [65]. In addition, metals have the promise to be appropriate material for the GDL and have advantages of low manufacturing cost and high electrical and thermal conductivities [66]. Many metallic gas diffusion layers have been employed in the direct methanol fuel cells, such as the titanium mesh [67, 68], stainless steel wire cloth [69], gold-plated nickel mesh [70] and the nickel-chromium [71]. All the results have shown improvement in the fuel cell performance and an enhancement in the water management in the direct methanol fuel cells by using the metallic GDL [71]. Zhang et al. [72] fabricated a metal gas diffusion layer, which was 125 µm thick and made of foil copper using photolithography. This copper based GDL enhances the water management of the fuel cell and improves the fuel cell performance at low flow rates. In this chapter, the effect of the metallic GDL on the thermal management of PEM fuel cell is numerically investigated by using a copper and aluminium based GDL. In addition, the temperature distribution and the water saturation is compared between the metallic GDL and the conventional carbon fibre GDL.

3.2 Physical and Operational Parameters

All the parameters have been chosen to be those used in the experimental investigation of the in-house PEM fuel cell with the conventional carbon fibre-based GDL. The PEM fuel cell channel was 2.0×10^{-3} m in both height and width and the thickness of the GDL, catalyst layer and membrane were 3.0×10^{-4}, 3.0×10^{-5} and 1.5×10^{-4} m, respectively. All the operational parameters are kept the same as listed in Table 2.3.

In order to investigate the effect of the metallic GDL on the performance of PEM fuel cells, three different cases have been simulated: Case I, in which the GDL is made from the conventional carbon fibres; Case II, in which the GDL is made from aluminium; and Case III, in which the GDL is made from copper. These cases were run using commercial Computational Fluid Dynamic (CFD) software, Fluent®, and the polarization curves were generated for these three cases. In the computations, we change some of the properties of the materials, namely the in-plane and the through-plane thermal and electrical conductivity of the GDL in order to change from one case to another. The changes made in these key properties indicates the change of the material of the GDL, which is about 0.4 $W \cdot m^{-1} \cdot K^{-1}$, and the in-plane thermal conductivity, which is of the order of 12.15 $W \cdot m^{-1} \cdot K^{-1}$, while the electrical conductivity of the conventional GDL is about 4000 S/m and 48 S/m for the in-plane and through-plane directions, respectively.

In the second and third cases, the conventional GDL has been assumed to be replaced with a metallic foil of aluminium or copper, which is 300 µm thick and has the same porosity as a typical GDL, namely 0.7, and all the other parameters are kept the same as those listed in Table 2.3.

As listed in Table 3.1, the electrical and the thermal conductivities of the copper and the aluminium based GDLs are higher than those of the conventional GDL by at least four and two orders of magnitudes, respectively. The electrical conductivity of copper based GDL was set to be 5.96 × 107 S/m, which is at least four orders of magnitude higher than the electrical conductivity of a typical GDL and the thermal conductivity is 386 $W \cdot m^{-1} \cdot K^{-1}$ [73], which is at least two orders of magnitude higher than the thermal conductivity of the typical carbon fibre GDL. In addition, the thermal conductivity of the aluminium based GDL is 235 $W \cdot m^{-1} \cdot K^{-1}$, which is at least two orders of magnitude higher than that of the conventional GDL and the electrical conductivity is 3.5×10^{7} S/m, which is at least four orders of magnitude higher than a typical GDL [74], as listed in Table 3.1. It is worth noting that the thermal conductivity and electrical conductivity for the metallic based GDL is isotropic and homogenous [75].

Table 3.1 List of the electrical and thermal conductivities of the investigated GDLs.

Parameter	Carbon-based GDL	Aluminium-based GDL	Copper-based GDL
Through-plane electrical conductivity of GDL (S/m)	48[54]	3.5×10^7 [74]	5.96×10^7 [73]
In-plane electrical conductivity of GDL (S/m)	4000[54].	3.5×10^7 [74]	5.96×10^7 [73]
Through-plane thermal conductivity of GDL ($W\cdot m^{-1}\cdot K^{-1}$)	0.4[40]	235[74]	386 [73]
In-plane thermal conductivity of GDL ($W\cdot m^{-1}\cdot K^{-1}$)	12.15[76]	235 [74]	386 [73]

3.3 Results and Discussions

The current density of the PEM fuel cell at 0.55 V, which is one of the typical operating voltages of PEM fuel cells, is illustrated for all the cases studied in Figure 3.1, (note that the entire predicted polarisation curve for the carbon-fibre GDL case has been previously validated against some experimental data [50] in Figure 2.3. The results obtained show that the current density of the fuel cell increases by about 32% when the aluminium based GDL is used and by about 40% when the copper based GDL is used.

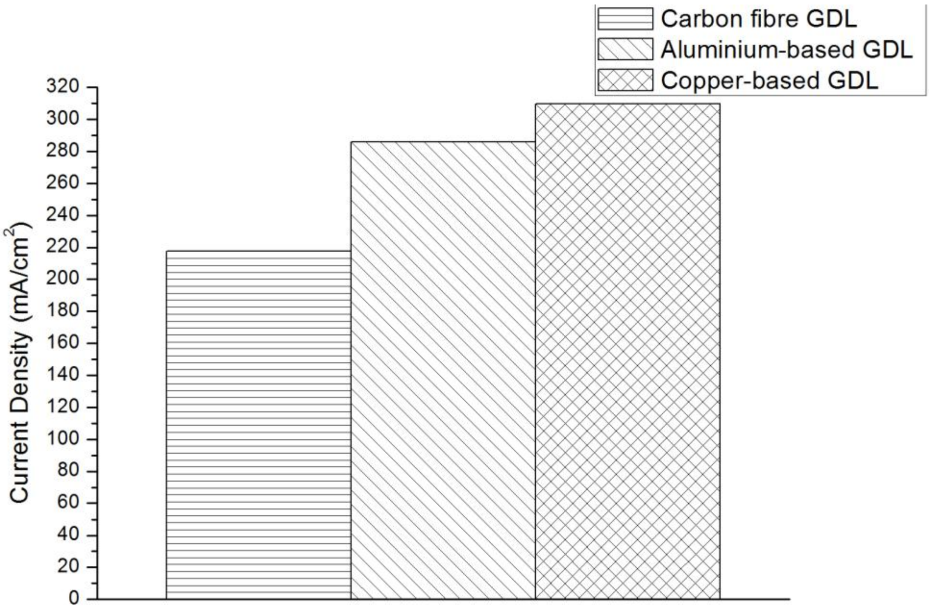

Figure 3.1 The effect of the metal-based GDLs on the current density (mA·cm^{-2}) of the PEM fuel cell.

The effect of the metallic GDL on the temperature distribution is illustrated in Figure 3.2 and it is clear that the temperature is more uniform within the fuel cell when the metallic GDL is used. Further, the temperature gradient decreases, and the temperature does not change by more than about 1 K within the GDL when the metallic based GDL was employed.

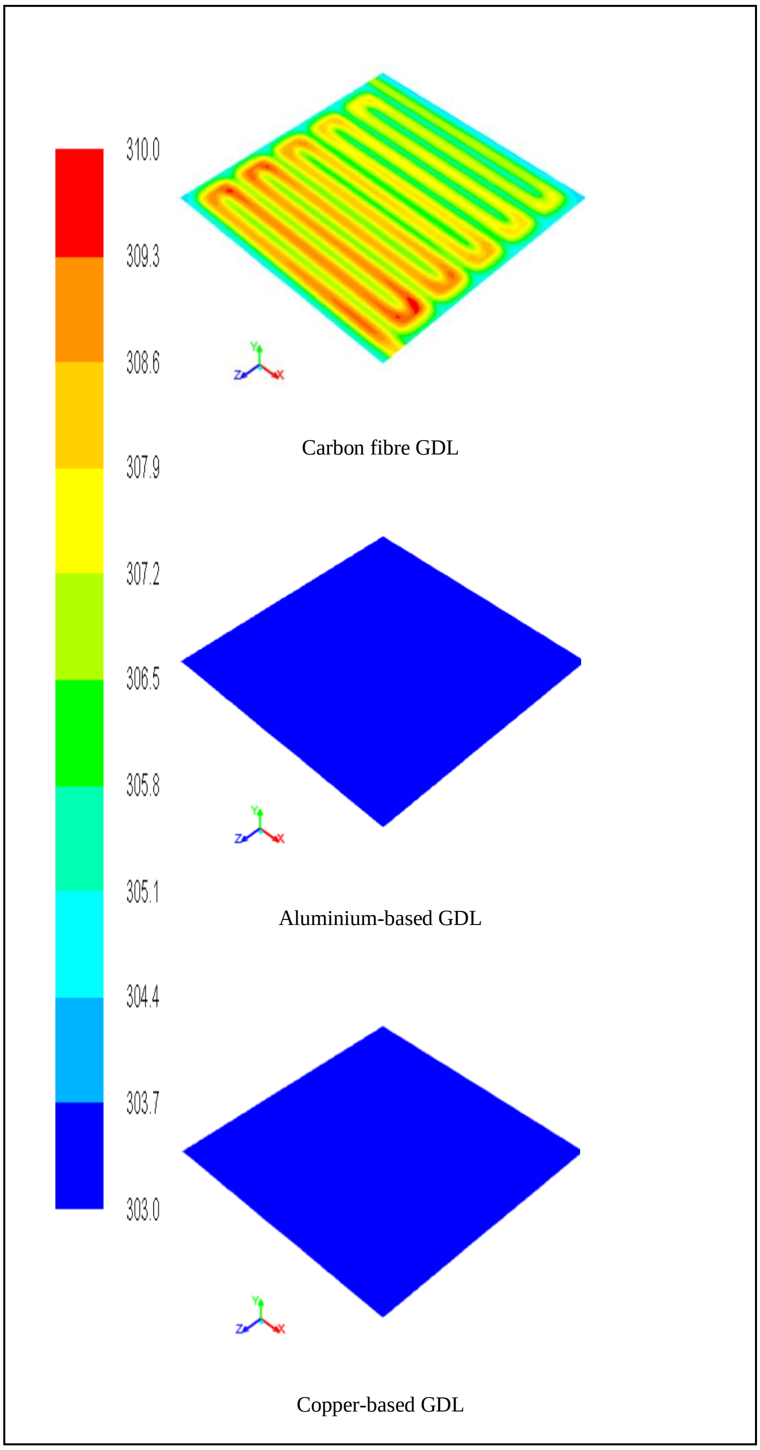

Figure 3.2 The effect of the metal-based GDL on the temperature distribution (K) at the mid-thickness of the GDL in the PEM fuel cell.

The maximum temperature obtained was about 309.6 K when the carbon based GDL is used, while the maximum temperature was about 303.9 K and 303.6 K when the aluminium and copper based GDLs are used, respectively. The metallic based gas diffusion layers have a higher thermal conductivity compared to the conventional carbon fibre GDL, and this results in the dissipation of more heat from the membrane electrode assembly and this leads to a more uniform temperature within the fuel cell.

The effect of the metallic gas diffusion layer on the water saturation in the PEM fuel cell is shown in Figure 3.3. The maximum water saturation within the GDL was 0.378 when the carbon based GDL is used and this value increases to 0.381 and 0.393 when the aluminium and copper based GDLs are employed, respectively. More water saturation means more liquid water available for the humidification of the membrane. Owing to high thermal conductivity of the metallic GDLs, this is clearly due to low temperatures which result in low saturation pressures.

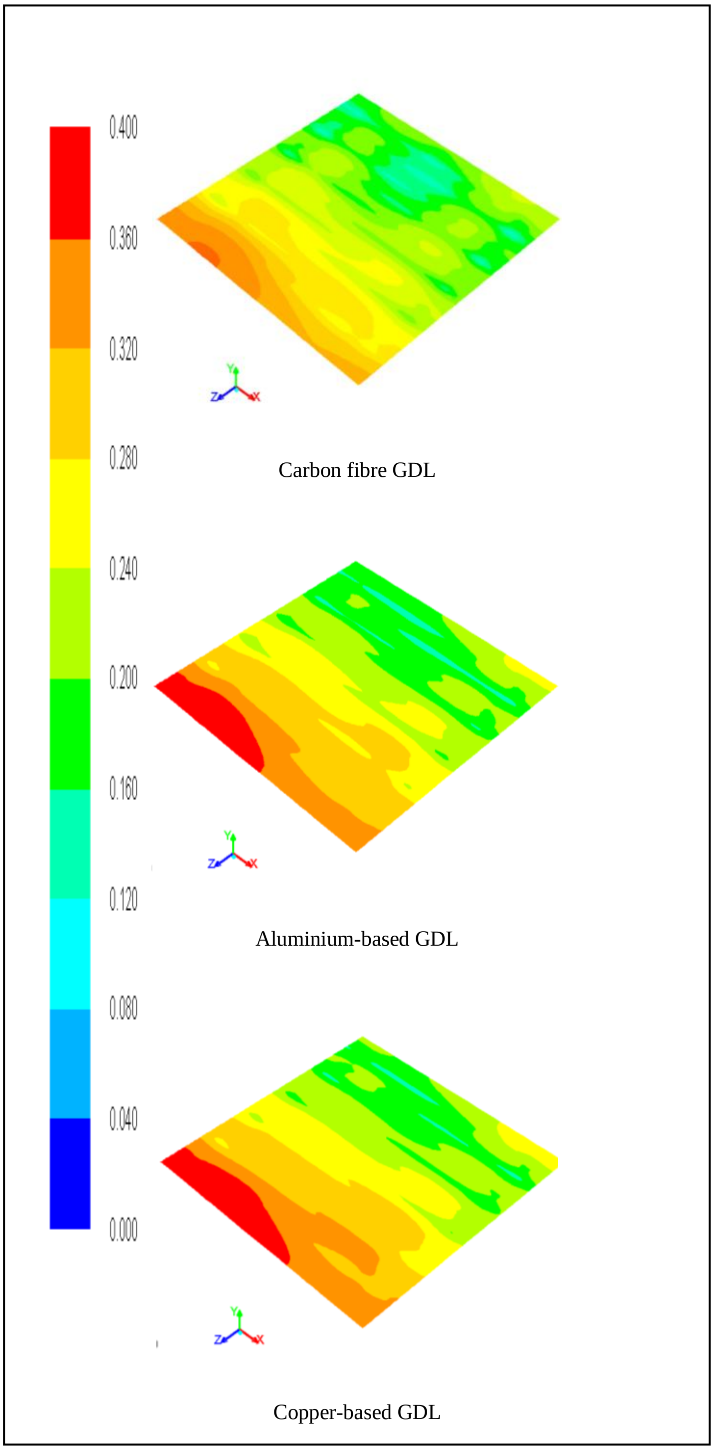

Figure 3.3 The effect of the metal-based GDL on the water saturation in the PEM fuel cell.

3.4 Challenges of Using the Metallic GDL

Metal-based GDLs, such as metal mesh, metal foam, and micro machined metal substrate should be useful to PEM fuel cells due to high thermal and electrical conductivities and mechanical strength. The major challenges regarding using a metallic GDL are to decrease the contact resistance and to increase the corrosion resistance [77]. In this chapter, the contact resistances of the metallic GDLs have been assumed to be negligible, which is a major issue that needs to be properly tackled. However, by coating the GDL layer with a low resistance oxide layer, such as tungsten oxide [78], or depositing the GDL layer with protective coatings the corrosion resistance of the metallic GDL will be increased significantly [79].

3.5 Conclusions

A 3-D multiphase model has been developed to investigate the effect of a metallic based GDL on the thermal management of PEM fuel cells. The temperature distribution and the water saturation of PEM fuel cells operating with the copper based and aluminium based GDL have been compared with that operating with the conventional GDL. The main conclusions of this study are as follows:

- There is an increase in the power density of the PEM fuel cells when a metallic based gas diffusion layer is used. The results show that, at a typical cell potential, the power density of the fuel cells increases by about 40% when the copper based GDL is used, and by about 32% when the aluminium based GDL is used. The increased power density of the fuel cell operating with the metallic GDL results from the decreased electrical resistance (due to significantly higher electrical conductivity of the metallic GDLs) and the better heat dissipation (due to significantly higher thermal conductivity of the metallic GDLs).

- The maximum temperature in the PEM fuel cell decreases when the metallic based GDLs have been used and the temperature gradient decreases due to good dissipation of the heat from the membrane electrode assembly. This results in a more uniform temperature distribution within the fuel cell components.

- The use of the metallic based GDL increases the liquid water saturation, which is beneficial for the humidification of the membrane. This is because of the high thermal conductivity of the metallic GDL, leading to good heat dissipation, lower temperatures and consequently lower saturation pressures.

This study has highlighted the need to increase the thermal conductivity and the electrical conductivity of the GDL, which will enhance the PEM fuel cell performance and improve the thermal and the water management within the fuel cell.

Chapter 4

Effect of the Thermal Conductivity of the Membrane and the Catalyst Layer on the Performance of PEM Fuel Cells

4.1 Introduction

A detailed knowledge of the thermal conductivity of the MEA is crucial for the PEM fuel cell development. However, it was difficult to measure the thermal conductivity of the MEA directly due to the structure of the MEA and the micro scale size of these components. Several studies have been reported on the thermal conductivity of the membrane and the catalyst layer. Vie and Kjelstrup [80] used the temperature profile of a single PEM fuel cell to calculate the thermal conductivity of the PEM fuel cell components by inserting many thermocouples at different locations inside a single fuel cell. The temperature in the channels was about 3 °C lower than the temperature between the catalyst and the membrane and temperature gradient through the gas diffusion layer was about 2 °C. In addition, the thermal conductivity of the gas diffusion layer and the catalyst was estimated to be 0.19±0.05 $W \cdot m^{-1} \cdot K^{-1}$. However, this value was not accurate due to the high uncertainty in the thermocouple locations in the fuel cell. Maggio et al. [81] reported the thermal conductivity of the membrane to be 0.21 $W \cdot m^{-1} \cdot K^{-1}$, while Yan et al. [82] reported it to be 0.14 $W \cdot m^{-1} \cdot K^{-1}$. Khandelwal and Mench [40] measured the thermal conductivity of Nafion® membrane to be 0.16±0.03 W·m^{-1}·K^{-1} under a compression of 20 bar. They used the steady state method of measuring the thermal conductivity of the sample after sandwiching the sample between 2 aluminium bronze plates. However, the thickness of the sample was assumed to be constant under different pressures. Burhem et al. [83] used the steady state method to measure the thermal conductivity of a wet and dry Nafion® but without taken into account the differences in the thicknesses under different pressures to eliminate the thermal contact resistance. The thermal conductivity of the dry membrane was predicted to be 0.177±0.008 W·m^{-1}·K^{-1}, while the thermal conductivity of the wet membrane was 0.254±0.018 W·m^{-1}·K^{-1}.

In this chapter, the effects of the thermal conductivity of the membrane and catalyst layers have been investigated numerically using the Fluent® software. In this investigation, a three-dimension (3-D) multiphase model was developed to investigate the effect of the thermal conductivity of the membrane electrode assembly on the performance of the PEM fuel cell in two stages. In the first stage the thermal conductivity of the catalyst layer has been investigated and in the second stage the thermal conductivity of the membrane has been investigated.

4.2 Modelling the Effect of the Thermal Conductivity of the Catalyst Layer

4.2.1 Boundary conditions

In order to investigate the effect of the thermal conductivity of the catalyst layers on the performance of PEM fuel cells, three different cases have been developed. In the first case the thermal conductivity of the catalyst layer was 1 $W \cdot m^{-1} \cdot K^{-1}$.

Then the thermal conductivity of the catalyst layer was increased one order of magnitude to be 10 $W \cdot m^{-1} \cdot K^{-1}$ and it is increased again in the third case to be 100 $W \cdot m^{-1} \cdot K^{-1}$ while all the other fuel cell parameters were kept the same as these listed in Table 2.3. These three cases are listed in Table 4.1 and they have been performed by using the fuel cell module in Fluent® software.

Table 4.1 List of the different cases investigated for the effect of the thermal conductivity of the catalyst layer.

Case Number	thermal conductivity of the catalyst layer ($W \cdot m^{-1} \cdot K^{-1}$)
I	1
II	10
III	100

It is worth noting that the default value for the thermal conductivity of the catalyst layer in Fluent® was 10 W·m^{-1}·K^{-1}.

4.2.2 Results and discussions

The power densities of the PEM fuel cells for these three cases have been compared at 0.55 V, which is a typical operating voltage for the fuel cell.

As it can be seen form Figure 4.1, there is no significant difference between the power density of the fuel cells and the power density remains almost constant with increasing the thermal conductivity of the catalyst layer. However, the power density of the fuel cell in the third case, where the thermal conductivity of the catalyst was at its maximum value 100 W·m^{-1}·K^{-1} was slightly higher and it was about 112.9 mW·cm^{-2}, while the power density was 109.4 and 108.5 mW·cm^{-2} when the thermal conductivity of the catalyst were 10 and 1 W·m^{-1}·K^{-1}, respectively.

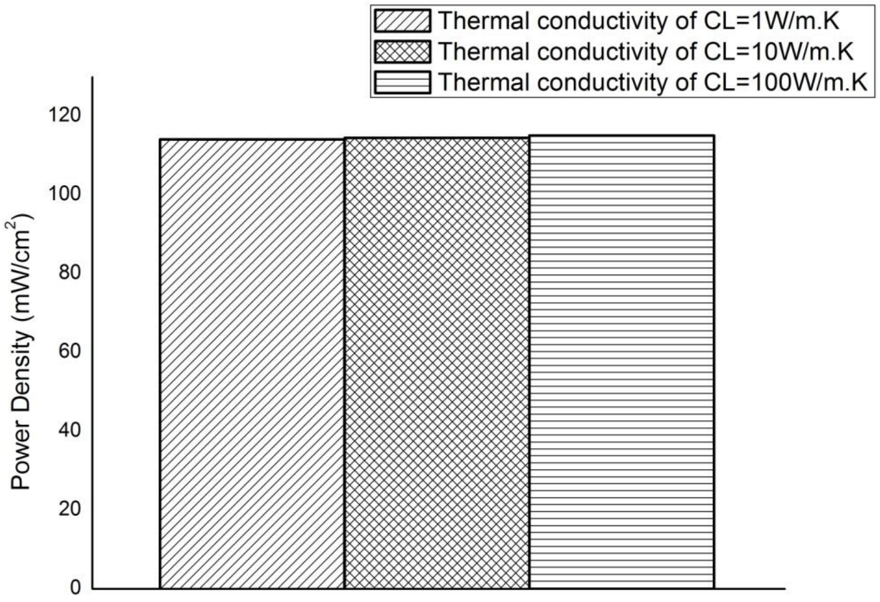

Figure 4.1 The effect of the thermal conductivity of the CL on the power density (mW·cm^{-2}) of the PEM.

The effects of the thermal conductivity on the temperature distribution have been investigated, as shown in Figure 4.2. It is clear from the figure that the maximum temperature in the catalyst layer was 306.6 K when the thermal conductivity of the catalyst layer was at the minimum value investigated, namely 1 W·m^{-1}·K^{-1}. This value is reduced to 305.3 and 305.1 K when the thermal conductivities of the catalyst were 10 and 100 W·m^{-1}·K^{-1}, respectively.

The increase in the thermal conductivity of the catalyst layer assists in more heat being dissipating from attaining the MEA and consequently a uniform temperature distribution within the fuel cell.

Moreover, the effects of the thermal conductivity of the catalyst layer on the water saturation have been investigated, as shown in Figure 4.3. It is clear from the figure that the water saturation was 0.334 when the thermal conductivity of the catalyst was at the minimum value investigated, namely 1 $W \cdot m^{-1} \cdot K^{-1}$. Furthermore, the water saturation is increased to 0.340 and 0.347 when the thermal conductivity of the catalyst increased to 10 and 100 $W \cdot m^{-1} \cdot K^{-1}$, respectively.

This is most likely due to the decrease in the temperature gradient in the fuel cell when the thermal conductivity of the catalyst layers increases and this enhances the dissipation of the heat from the membrane electrode assembly which results in a uniform temperature through the PEM fuel cell and more liquid water in the membrane and more water saturation.

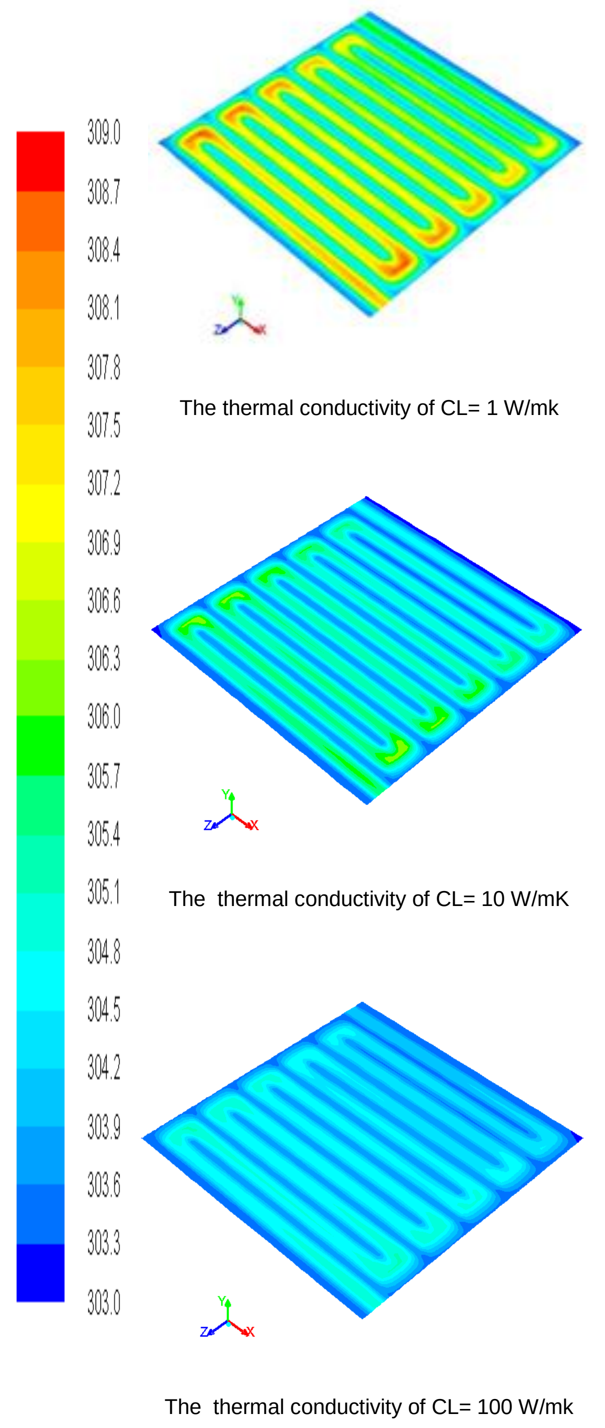

The thermal conductivity of CL= 1 W/mk

The thermal conductivity of CL= 10 W/mK

The thermal conductivity of CL= 100 W/mk

Figure 4.2 The effect of the thermal conductivity of the CL on the temperature distribution (K) in the PEM.

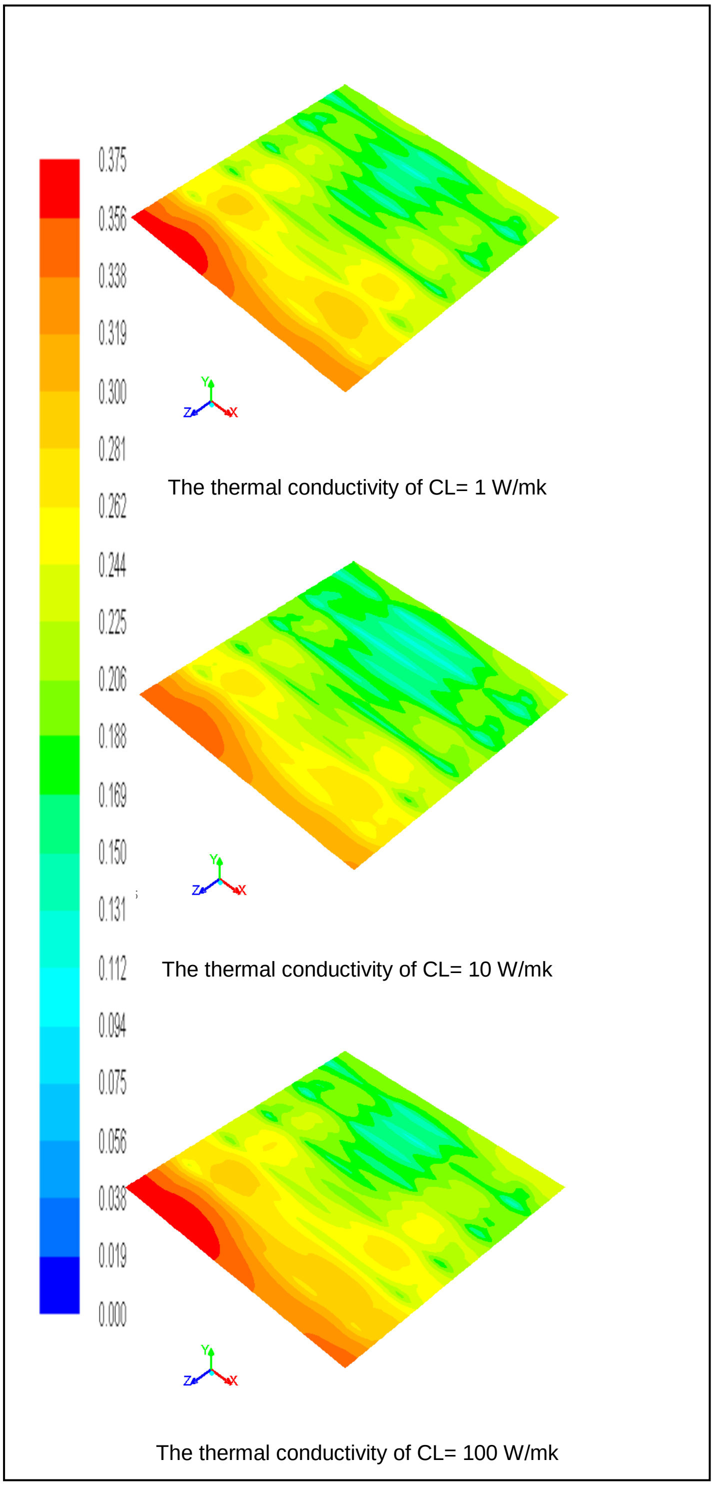

The thermal conductivity of CL= 1 W/mk

The thermal conductivity of CL= 10 W/mk

The thermal conductivity of CL= 100 W/mk

Figure 4.3 The effect of the thermal conductivity of the CL on the water saturation in the PEM.

4.3 Modelling the Effect of the Thermal Conductivity of the Membrane

4.3.1 Boundary conditions

In order to investigate the effect of the thermal conductivity of the membrane on the performance of the PEM fuel cell, three different cases have been investigated. In the first case, the thermal conductivity of the membrane was set to be 1 $W{\cdot}m^{-1}{\cdot}K^{-1}$. Then it is increased by one order of magnitude to be 10 and 100 $W{\cdot}m^{-1}{\cdot}K^{-1}$ in the second and the third cases investigated, respectively. See Table 4.2.

Table 4.2 List of the different cases investigated for the effect of the thermal conductivity of the membrane.

Case Number	thermal conductivity of the membrane ($W{\cdot}m^{-1}{\cdot}K^{-1}$)
IV	1
V	10
VI	100

All the other parameters were kept at the same values as listed in Table 2.4. These cases have been performed in the fuel cell module in the Fluent® software and the default value for the thermal conductivity of the membrane was 10 $W \cdot m^{-1} \cdot K^{-1}$.

4.3.2 Results and discussions

The power densities have been calculated at an average voltage of 0.55 V. As seen in Figure 4.4, there is no significant difference between the power density in all the three cases investigated but the power density of the fuel cell increased very slightly on increasing the thermal conductivity of the membrane, namely these values were taken to be 111.5, 109.4 and 108.1 $mW \cdot cm^{-2}$ when the thermal conductivity of the membrane increased from 1 to 10 to 100 $W \cdot m^{-1} \cdot K^{-1}$, respectively.

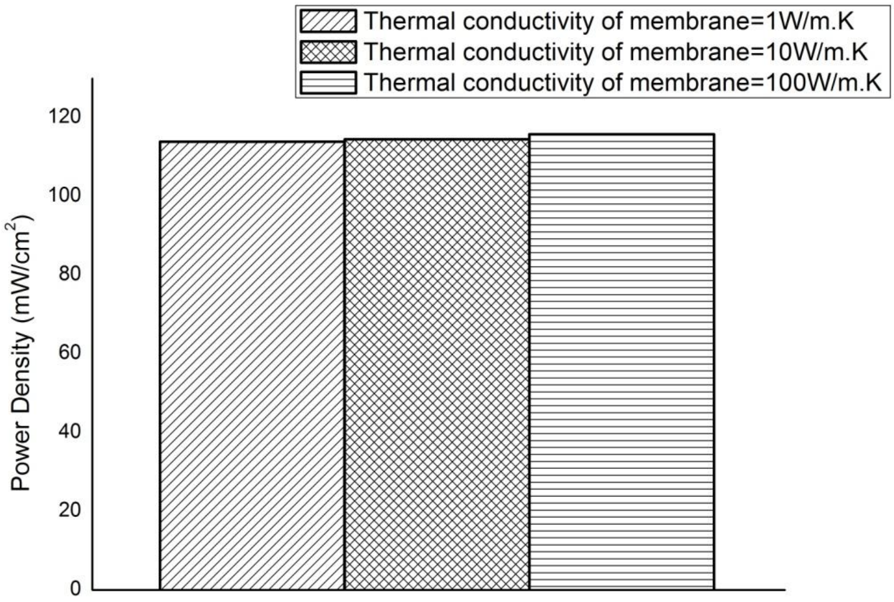

Figure 4.4 The effect of the thermal conductivity of the membrane on the power density (mW·cm^{-2}) of the PEM fuel cell.

The effect of the thermal conductivity of the membrane on the temperature distribution of PEM fuel cell is clear in Figure 4.5 and the maximum temperature was 306.8 K when the thermal conductivity of the membrane was at its minimum value of 1 W·m^{-1}·K^{-1}. The temperature becomes more uniform along the membrane and the temperature gradient does not change by more than 2K when the thermal conductivity of the membrane was at its maximum value of 100 W·m^{-1}·K^{-1}. This is due to the dissipation of more heat from the MEA when the thermal conductivity increases which is a result of a more uniform temperature along the membrane and more liquid water being humidified and more water saturation, as clearly seen in Figure 4.6. The maximum water saturation was 0.347 when the thermal conductivity of the membrane was at its maximum value of 100 $W \cdot m^{-1} \cdot K^{-1}$. This value reduces to 0.340 and 0.334 when the thermal conductivity of the membrane decreases to 10 and 1 $W \cdot m^{-1} \cdot K^{-1}$, respectively.

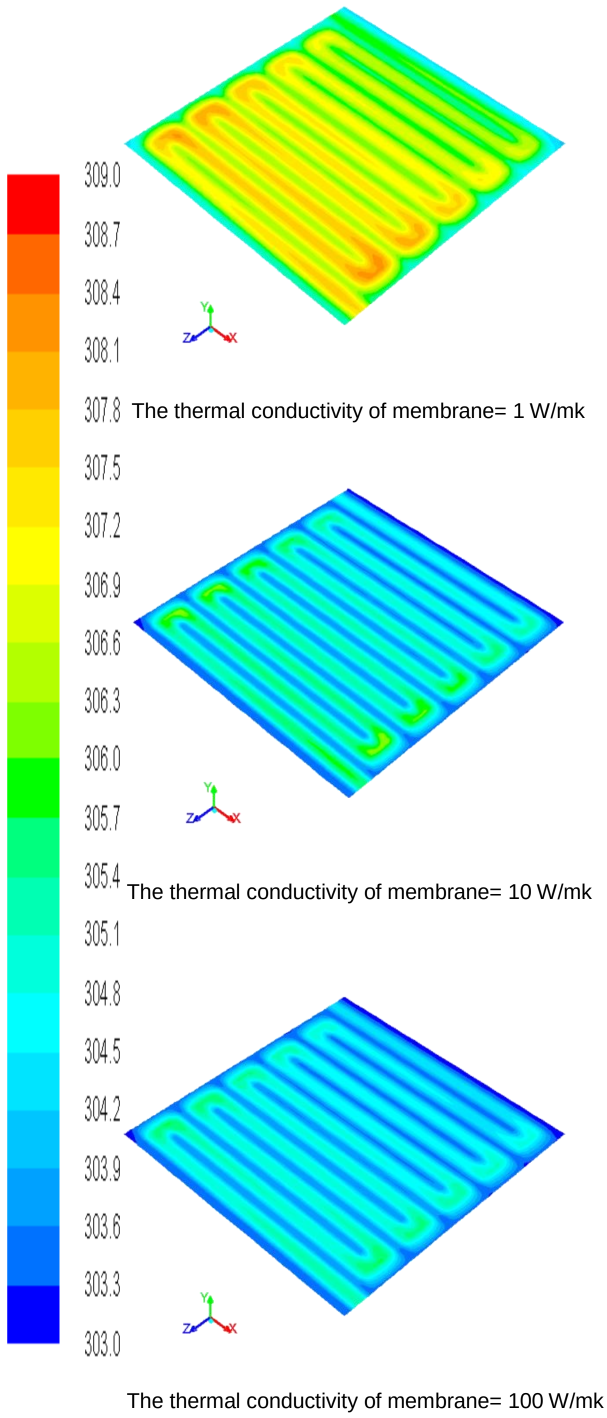

The thermal conductivity of membrane= 1 W/mk

The thermal conductivity of membrane= 10 W/mk

The thermal conductivity of membrane= 100 W/mk

Figure 4.5 The effect of the thermal conductivity of the membrane on the temperature distribution (K) in the PEM.

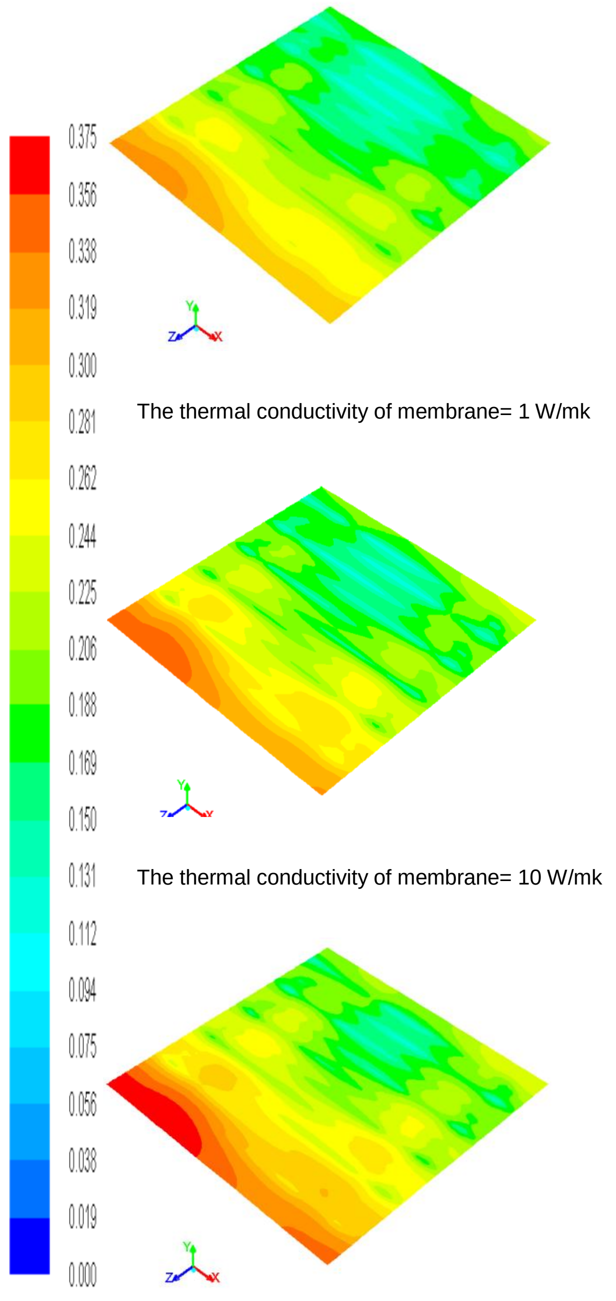

The thermal conductivity of membrane= 1 W/mk

The thermal conductivity of membrane= 10 W/mk

The thermal conductivity of membrane= 100 W/mk

Figure 4.6 The effect of the thermal conductivity of the membrane on the water saturation in the PEM.

4.4 Conclusions

A 3-D multiphase model has been developed to investigate the effect of the thermal conductivity of the membrane and the catalyst layer on the performance of PEM fuel cells.

The main conclusions from this study are as follows:

- There are no significant differences in the power density of the fuel cell when the thermal conductivities of the membrane or the catalyst layer increase.

- The temperatures gradient decreases when the thermal conductivity of the catalyst layer and membrane increase in the PEM fuel cells due to the dissipation of the heat from the membrane electrode assembly, which results in a more uniform temperature distribution within the fuel cell components. It is observed that the maximum temperature in the PEM fuel cell decreases when the thermal conductivity of the catalyst and the membrane increases.

- Increasing the thermal conductivity of the membrane and the catalyst layer increases the liquid water saturation as the maximum temperature decreases, which is a result of the uniform temperature distribution which causes the increase in the thermal conductivity of the membrane and the catalyst layer.

This study has highlighted the need to accurately determine the thermal conductivity of the catalyst layer and the membrane, despite the fact that there is no significant effect on the fuel cell power density by increasing the thermal conductivity of the catalyst and the membrane, they have a significant effect on the temperature distribution and the water saturation.

Chapter 5
Methods for Measuring Thermal Conductivity

5.1 Introduction

The knowledge of the thermal properties of the materials is one of the key parameters to the understanding of the heat transfer phenomena. There are many experimental and numerical methods which could be used to estimate the thermal conductivity of the material [59]. In this chapter, the main numerical models, such as the parallel, series, Krischer, Maxwell Eucken and effective medium theory model are discussed and employed to calculate the thermal conductivity of the GDL and these provide an approximate estimation of the effective thermal conductivity of the components of the membrane electrode assembly (MEA) [84-89]. In addition, the most common experimental technique which is used to calculate the thermal conductivity and the thermal contact resistance is investigated in order to develop an appropriate technique to measure the thermal conductivity and the contact resistance of the components of the MEA in proton exchange membrane (PEM) fuel cells.

5.2 Calculating the Effective Thermal Conductivity

The effective thermal conductivity of a gas diffusion layer may be calculated theoretically based on the thermal conductivity of carbon and air, and the porosity of the GDL. The effective thermal conductivity of a GDL may be written as follows:

$$k_{eff} = (k_{Carbon}, k_{air}, \varepsilon) \tag{5.1}$$

where k_{eff} is the effective thermal conductivity of the GDL, k_{carbon} and k_{air} are the effective thermal conductivity of carbon and air, respectively, and ε is the porosity of the GDL [84-89].

The gas diffusion layer consists of a solid phase and a fluid phase. The solid phase contains carbon composite binders and the PTFE which is added in order to increase the hydrophobicity of the GDL. The fluid phase contains the gases, such as oxygen, nitrogen, water vapour and hydrogen [44, 90]. In addition, liquid water is present in the GDL due to the electrochemical reactions in the fuel cell. Furthermore, the gas diffusion layer is highly anisotropic due to the non uniform distribution of the fibres in the layer [44, 90]. Much theoretical estimations have been reported for the gas diffusion layer effective thermal conductivity. The maximum reported effective thermal conductivity was 65 $W \cdot m^{-1} \cdot K^{-1}$ and the minimum effective thermal conductivity is reported to be 0.15 $W \cdot m^{-1} \cdot K^{-1}$ [44]. There are many theoretical models that may be used to estimate the effective thermal conductivity of the GDL based on the thermal conductivity of carbon and air and their volume fractions without taking into account the effect of the structure of the GDL on the thermal conductivity [86-89]. The maximum thermal conductivity can be calculated using the parallel model which predicts the upper bound for the effective thermal conductivity [84, 85]. The parallel thermal conductivity estimation for the effective thermal conductivity may be written as follows:

$$k_{eff} = \varepsilon k_{air} + (1 - \varepsilon) k_{Carbon} \tag{5.2}$$

The minimum effective thermal conductivity of the gas diffusion layer can be estimated using the series model which predicts the lowest bound for the effective thermal conductivity [84, 85]. The series model may be written as follows:

$$k_{eff} = \frac{1}{\frac{\varepsilon}{k_{air}} + \frac{(1-\varepsilon)}{k_{Carbon}}} \tag{5.3}$$

A combination of the series and the parallel models can predict the effective thermal conductivity of the heterogeneous material. This model is known as the Krischer model and may be written as follows:

$$k_{eff} = \frac{1}{\frac{f}{k_{ser}} + \frac{1-f}{k_{parallel}}} \tag{5.4}$$

where f= 0, gives the parallel model.

f=1, gives the series model.

K_{ser} is the series effective thermal conductivity, and $k_{parallel}$ is the parallel effective thermal conductivity

The Maxwell Eucken models assume that the material is composed of small spheres in a continuous matrix [86-89]. There are two cases: the first case, which assumes that the carbon is the continuous phase and the air is the dispersed phase, may be written as follows:

$$k_{eff} = \frac{k_{carbon}(1-\varepsilon) + k_{air}\varepsilon \dfrac{3k_{Carbon}}{2k_{Carbon} + k_{air}}}{(1-\varepsilon) + \varepsilon \dfrac{3k_{Carbon}}{2k_{carbon} + k_{air}}} \qquad (5.5)$$

The second case assumes that the carbon is the dispersed phase and the air is the continuous phase and may be written as follows:

$$k_{eff} = \frac{k_{air}\varepsilon + k_{carbon}(1-\varepsilon) \dfrac{3k_{air}}{2k_{air} + k_{Carbon}}}{\varepsilon + (1-\varepsilon) \dfrac{3k_{air}}{2k_{air} + k_{Carbon}}} \qquad (5.6)$$

The last model for the effective thermal conductivity is the effective medium theory model, where it is assumed that the material is distributed randomly [86-89] and may be written as follows:

$$(1-\varepsilon)\frac{k_{Carbon}-k_{eff}}{k_{Carbon}+2k_{eff}}+\varepsilon\frac{k_{air}-k_{eff}}{k_{air}+2k_{eff}}=0 \tag{5.7}$$

A schematic of the structure of these models is shown in Figure 5.1.

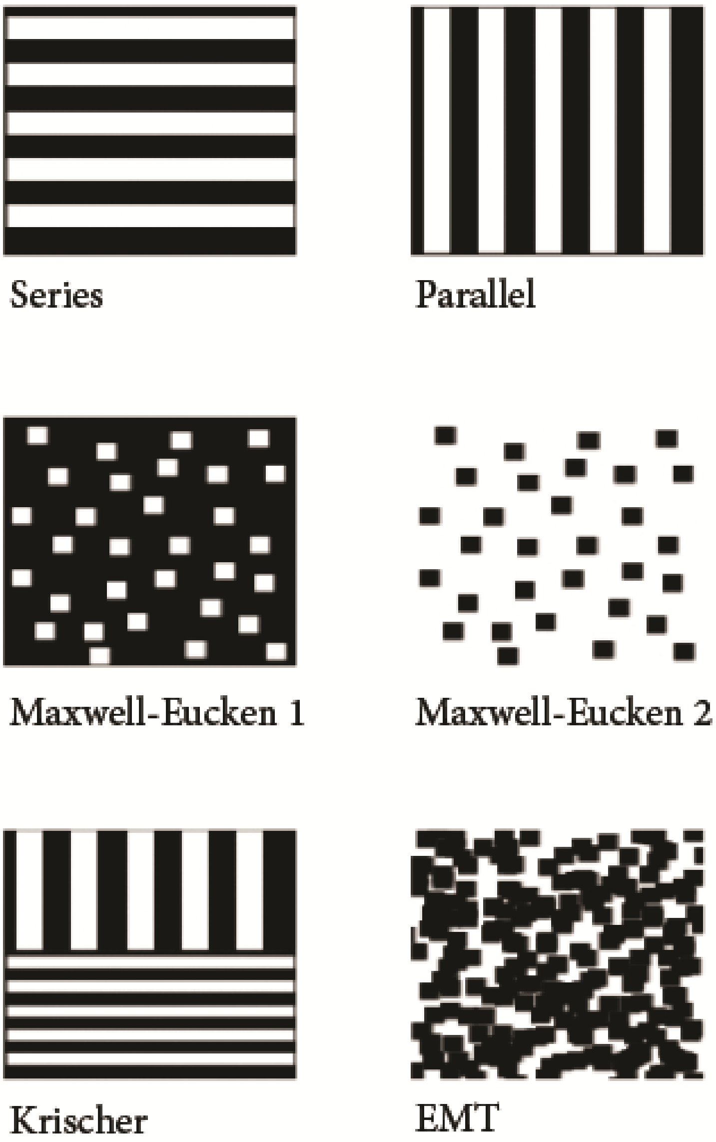

Figure 5.1 Schematic of the structure of the thermal conductivity models (assuming the heat transfer in the vertical direction).

The effective thermal conductivity of these models are calculated and plotted as a function of the GDL porosity, see Figure 5.2.

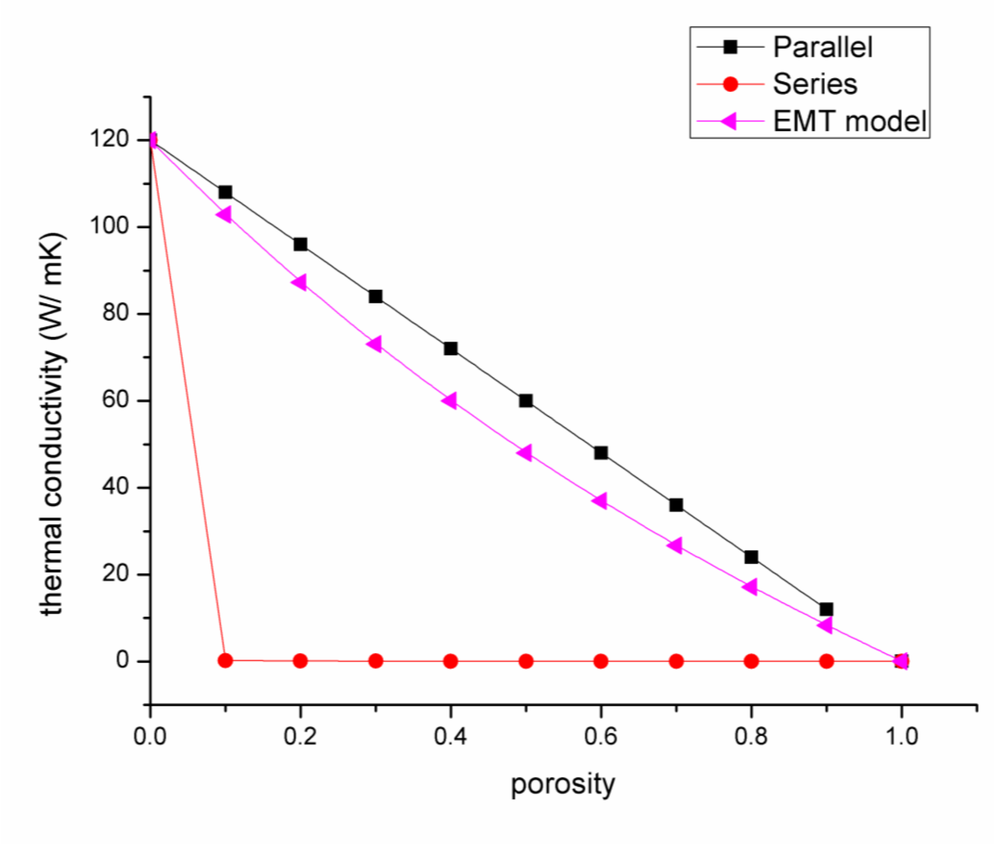

Figure 5.2 The calculated effective thermal conductivity of a GDL as a function of the porosity.

It is clear from Figure 5.2 that the maximum thermal conductivity of the GDL, which has the porosity of 0.77, and is the value used in a typical PEM fuel cell, was no more than 20 $W \cdot m^{-1} \cdot K^{-1}$ and the minimum effective thermal conductivity of the GDL was not less than 0.02 $W \cdot m^{-1} \cdot K^{-1}$. The in-plane thermal conductivity of the GDL should be closer to the parallel model, while the through-plane thermal conductivity of the GDL should be closer to the series model.

5.3 Methods of Measurement of The thermal Conductivity

The thermal conductivity is the ability of the material to transfer heat and it is appears in the Fourier law. Many parameters could affect the thermal conductivity, such as the chemical and physical structure, the temperature and the compression [59].

Typically, there are two ways to measure the thermal conductivity, namely the steady state method and the transient method.

5.3.1 Transient method

In the transient method, the thermal conductivity is determined by measuring the temperature increase in the sample as a function of time after applying a steady heat flux from a line or a plane heat source [59]. This technique has different types as follows:

5.3.1.1 Three ω method

The procedure for determining the thermal conductivity by the three ω method is to apply a steady heat flux from a line heat source. This method uses an electrical wire as a heat source and a heat sensor. In this method, the current, which is supplied to the line heat source at a frequency of ω, generates joule heating in the sample at a frequency of 2ω. The voltage drop across the line heat source and the corresponding temperature drop across the sample are recorded to determine the thermal conductivity of the sample as follows:

$$V_{3\omega} = \frac{I_{\circ} R_{\circ} \alpha_T \Delta T}{2} \tag{5.8}$$

where $V_{3\omega}$ is the output voltage, I_o is the current which is supplied, α_T is the temperature coefficient, R_o is resistance between the pads. ΔT is the temperature drop across the sample which is used to determine the thermal conductivity of the sample as follows:

$$k = \frac{pL}{2b\Delta T} \tag{5.9}$$

where *k* is the thermal conductivity of the sample, *b* is the half length of the line heat source, *P* is the power which is supplied and *L* is the sample thickness [91].

5.3.1.2 Transient plane source method

In the transient plane source method, which is also known as the TPS method, the heat source is a plane which also acts as a sensor for the temperature drop across the sample. The transient plane source, as illustrated in Figure 5.3, is basically a two nickel double spiral sandwiched between kapton sheets [59, 91]. Then this plane is sandwiched between two samples from the same material and the temperature gradient is measured after applying an electric power to the transient plane. The temperature gradient is calculated at a specific time as follows:

$$\Delta T(t) = \frac{1}{\alpha}\left(\frac{R(t)}{R_{\circ}} - 1\right) \tag{5.10}$$

where R_o is the inner resistance, $R(t)$ is the resistance at time t, α is the coefficient of the thermal expansion.

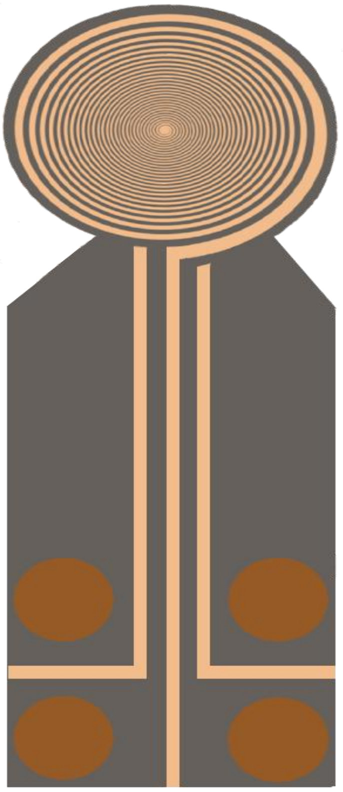

Figure 5.3 The transient plane thermal conductivity source.

5.3.1.3 Transient thermo reflectance method

The transient thermo-reflectance method is also known as the TTR method. In this method a laser irradiation is used to heat the sample to a specific temperature. Then, the corresponding changes in the sample surface are recorded by an oscilloscope. The thermal conductivity of the sample is extracted by fitting the transient temperature response as a function of time. This method is the most frequently employed transient method and there is no corrosion in the sample because there is no contact between the heat source and the sample, such as the transient plane method or the 3-ω method [59, 92].

5.3.2 The steady state method to measure thermal conductivity

There are many ways to use the steady state methods, such as the unidirectional steady heat flow through the sample, which called the guarded hot plate method [93]. The thermal conductivity is measure from the temperature gradient by placing two identical samples on either side of the main heater and guard heater, as shown in Figure 5.4.

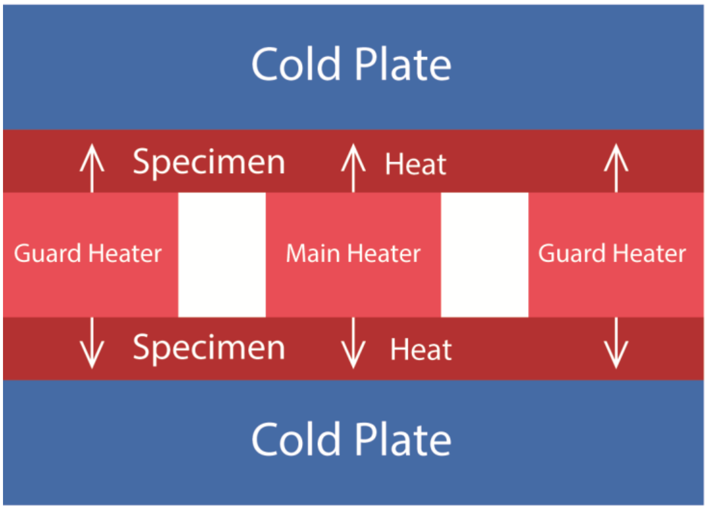

Figure 5.4 A schematic of the guarded hot plate method.

The stack of the two samples and the heaters is placed between two cold plates at a fixed temperature. Then the thermal conductivity of the sample is calculated by using the Fourier law as follows:

$$Q = 2AK\frac{\Delta T}{L} \tag{5.11}$$

The factor 2 that appears in this equation is because the heat flux in this method is divided between the two samples. The other steady state method is to sandwich the sample between two standard materials whose thermal conductivity is known. In this thermal conductivity measurement technique, a uniform heat flux is applied through the sample via a hot plate (heat source) to a cold plate (heat sink). After achieving a steady state temperature, the temperature drop across the sample is measured by the use of thermocouples [59], as presented Figure 5.5.

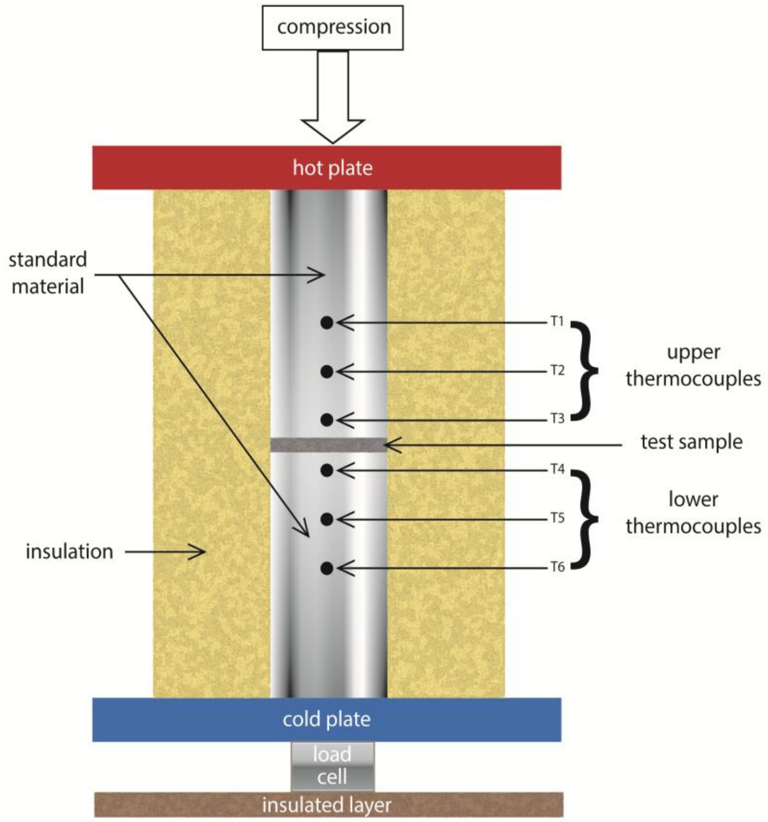

Figure 5.5 A schematic of the experimental apparatus used to measure the thermal conductivity.

It should be noted that some researchers have used the steady state method to measure the through-plane thermal conductivity of the GDL in a PEM fuel cell [40-42], which will be discussed in details in Chapter 7.

5.3.3 Description of the Parallel Thermal Conductance technique (PTC)

Based on the thermal resistance measurements using a steady state method to measure the thermal conductivity, the parallel thermal conductance technique (PTC) has been used to measure the thermal conductivity [93]. The parallel thermal conductance technique (PTC) was developed to conduct the steady state method of measuring the thermal conductivity of very small samples with very low thermal conductivity of single crystals and carbon fibres [93]. The parallel thermal conductance technique (PTC) is suitable for measuring the thermal conductivity of the GDL because it can measure the thermal conductivity of very thin films and small diameter samples. Furthermore, the PTC is a suitable technique to measure the low thermal conductivity directly based on the output power and the temperature drop through the sample [93].

The parallel resistance circuit is used to measure the thermal conductivity of a sample, as shown in Figure 5.6. This circuit consists of an aluminium holder which has two branches. The first branch is attached to a heat source and the other to a heat sink. A material, with a low thermal conductivity should be attached in the heat flow path between the heat source and the heat sink in order to ensure that the magnitude of the thermal conductance of the sample is at least 10% of the thermal conductance of the sample holder. This is because this will assist in ensuring that the thermal conductivity of the sample is more than the error range of the measurement procedure.

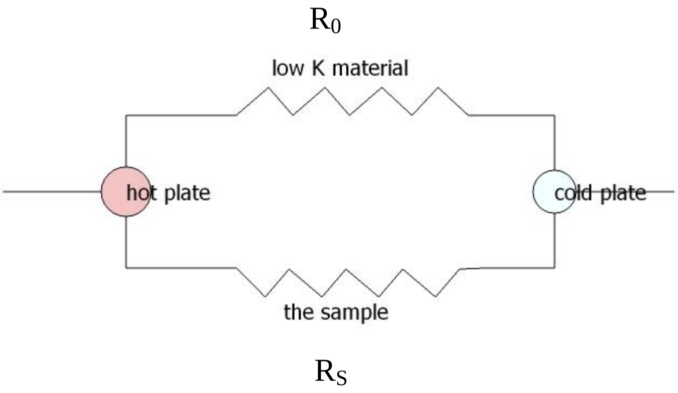

Figure 5.6 Schematic of the parallel thermal conductance circuit.

The parallel thermal method is more accurate and more flexible for measuring the thermal conductivity of very small samples because there is no effect on the stress which may affect the measurement of the thermal conductivity, or damage the material properties with the compression pressure [93, 94]. On the contrary, the steady state method requires that the sample should be strong enough to sustain the thermal stress during the measurement [93, 94].

The parallel thermal conductance technique was developed by Zawilski et al. [93] and they successfully measured the in-plane thermal conductivity of pentatellurides and single carbon fibres. The sample holder developed to measure the thermal conductivity of very small cross sectional samples. As shown in Figure 5.7, the sample holder consists of two copper plates, the first one attached to a heater and it works as a heat source and the second one as a heat sink. A supporting post is placed between theses plates and the thermal conductivity is calculated twice in the absence of the sample and after attaching the sample. Then, by subtraction, the thermal conductivity of the sample is calculated [93].

The in-plane thermal conductivity of very small sized crystals, such as NaxCO2O4, was reported by Tang et al. [95] by using a parallel thermal conductance technique and it was found to be about 5 $W \cdot m^{-1} \cdot K^{-1}$.

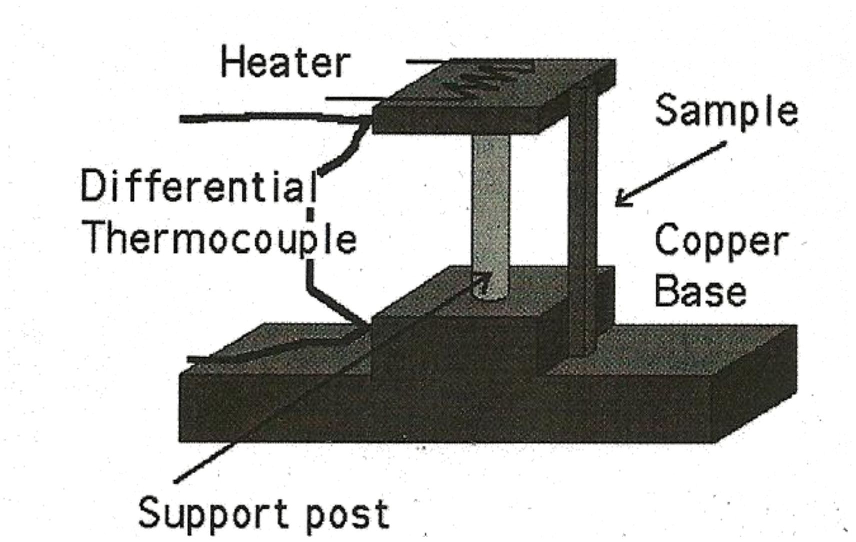

Figure 5.7 Schematic of the parallel thermal conductance technique as developed by Zawilski et al. [93].

5.4 Conclusions

Many methods have been employed to measure the thermal conductivity of unknown material.

- The first method is based on applying steady heat to the sample under investigation. Then the temperature difference across the sample is measured over a specific time. This method is known as the transient method and it has many types that depend on the heat source which is used and they are: the three ω method, the transient plane source method and the transient thermo reflectance method.

- The second method is based on sandwiching the sample between a heat source and a heat sink. Then the temperature difference is measured at different locations and this is known as the steady state method.

- The third method is the parallel thermal conductance technique, which is based on the thermal resistance measurement in the circuit. Then calculate the thermal conductivity from the thermal resistance.

The transient method is difficult to be used to measure the thermal conductivity of PEM fuel cell components due to the micro scale length of the fuel cell components and the structure of the materials in the PEM fuel cells. Furthermore, the transient method requires information about the heat capacity of the fuel cell materials which are not available. Therefore, the thermal conductivity of the fuel cell components is measured by the parallel thermal conductance technique which is developed from the steady state thermal conductivity. The sample holder, which used in the parallel thermal conductance technique, is developed to measure the thermal conductivity of the fuel cell components in the in-plane direction.

Chapter 6

Measurement of the in-plane thermal conductivity and the contact resistance of the components of the membrane electrode assembly in proton exchange membrane fuel cells

6.1 Introduction

As a result of the numerical studies which carried out in Chapters 2-5, and in order to understand the heat transfer through a PEM fuel cell, the thermal properties of the PEM fuel cell elements, such as the membrane electrode assembly (MEA), are required to be known in both directions, namely in-plane and the through-plane directions [97, 98]. However, very limited studies have been focused on the in-plane thermal conductivity.

Teertstra et al. [95] measured the in-plane thermal conductivity of a GDL at a mean temperature of 70 °C. The maximum thermal conductivity for Toray paper with 30% PTFE loading is found to be 15.1 $W \cdot m^{-1} \cdot K^{-1}$. However, they did not calculate the contact resistance and the effects of the mean temperature have not been taken into account.

Sadeghi et al. [99] developed a test bed to measure the in-plane thermal conductivity of a GDL as a function of the PTFE loading. They found that the thermal conductivity of a stack of Toray papers is approximately constant with PTFE loading and it is about 17.5 W·m^{-1}·K^{-1} at a mean temperature of 65 °C. Furthermore, they assumed that the contact resistance between the GDL layers is negligible. However, the effect of the temperature on the in-plane thermal conductivity of the MEA is not taken into account.

In the present study, the parallel thermal conductance (PTC) technique, which developed by Zawilski et al. [94] to measure the in-plane thermal conductivity of single carbon fibres, was employed to measure the in-plane thermal conductivity of several components of MEA at different operating temperatures. The thermal conductivities measured by the PTC were compared with those measured by the conventional steady-state method. Furthermore, the effects of water content and temperature on the thermal conductivity of the membrane, and the effects of PTFE loading, fibre direction and micro porous layer coating on the in-plane thermal conductivity of GDL were investigated. The effect of platinum loading on the thermal conductivity of the catalyst layer was accurately investigated. These measurements provide a database for the in-plane thermal conductivity of a membrane, GDL and the catalyst layer required to accurately determine the temperature distribution within the MEA.

6.2 Materials and Procedures

6.2.1 Test apparatus

An experimental apparatus was developed to measure the in-plane thermal conductivity of the MEA and is shown in Figure 6.1. This apparatus consisted of two parts. The first part was fixed and called the hot plate since it was electrically heated. The second part was the cold plate and was adjustable. This enables one to measure the thermal resistance of various lengths of the sample so that the thermal contact resistance can be determined. The PTC technique was developed to accurately measure the thermal conductivity of the GDL and the MEA in a PEM fuel cell by measuring at steady state the temperature drop and the voltage and current of the electric heater, from which the thermal conductivity of the sample was calculated based on the thermal resistance. This method is more accurate and more flexible than the conventional steady state method for measuring the thermal conductivity of very small samples because there is no dependence on the stress which may affect the measurement of the thermal conductivity, or even change the material properties with the compression pressure [96]. The conventional steady state method requires that the sample should be strong enough to sustain the thermal stress during the measurement.

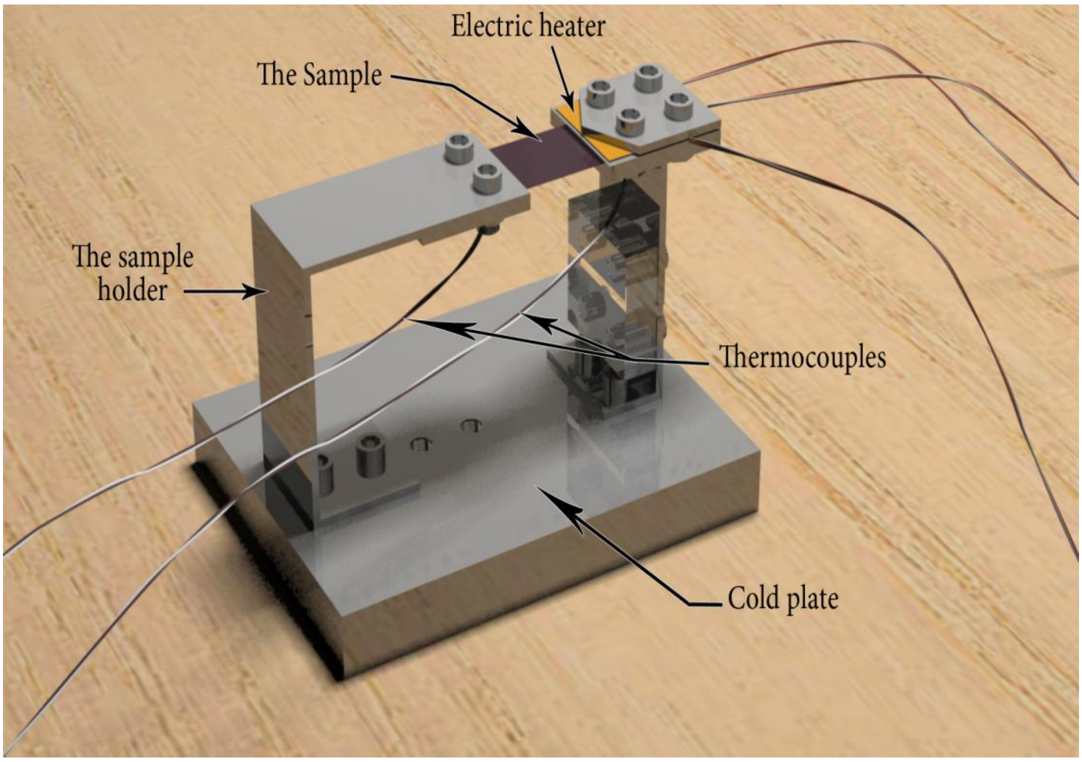

Figure 6.1 Configuration of the sample holder and the experimental set-up to measure the in-plane thermal conductivity of the MEA components.

Silicon rubber electric heaters (SRH-029) are attached to the upper end of the sample holder between the sample and the low thermal conductivity material. The hot plate temperature was about 100 ~ 120 °C and this was because it assisted in providing a suitable power resolution and the temperature was in the same range that occurs in the operating conditions of PEM fuel cells. The sample holder was made of aluminium, which has a high thermal conductivity. A low thermal conductivity material was attached to the heat flow path between the heat source and the heat sink in order to ensure that the magnitude of the sample’s thermal conductance was at least one-tenth of the thermal conductance of the sample holder, See Appendix A for more details on the dimensions of the low thermal conductivity material which has been placed in the setup to achieve this condition. The temperatures at the sides of the sample were measured using two thermocouples (PFA® T-Type). All readings; temperature, pressure, current and voltage were controlled and monitored via a LabVIEW application, See Figure 6.2.

Cold Plate (deg.C) 18.5981

Hot Plate (deg.C) 90.6207

Chamber Vacuum (Torr) 0.021 extrapolated

V heaters (V) 12.4682

I (A) 1.21884

P heaters (W) 15.1967

Vin (V) 15.1574

Data File Name C:\Documents and Settings\user\My Documents\Thermal Conductivity Rig Data\TC.XLS

Data Average Time (s) 3

Write Data Enable

Figure 6.2 The Labview programme interface.

6.2.2 Experimental conditions

The in-plane thermal conductivity was measured for seven GDL samples. The samples were provided by the SGL Technologies Gm bH, Germany. The thicknesses of these samples and their PTFE loading are listed in Table 6.1.

Table 6.1 Manufacturers' specifications for the tested GDLs.

GDL	Thickness (μm)	PTFE loading (wt. %)
10AA	390	0
10BA	400	5
10CA	400	10
10DA	400	20
10EA	374	30
10BC	415	23*
10BE	367	50*

* PTFE loading in the MPL (wt. %)

The effect of the temperature on the in-plane thermal conductivity was investigated in the temperature range 35 °C to 65 °C for the samples investigated in this study and all the measurements were made in a vacuum in order to eliminate convection and therefore minimize the heat transfer from the GDL to the surroundings. Therefore, neglecting radiation, the heat flow from the hot plate to the cold plate can be assumed to be one-directional through the sample via conduction.

The in-plane thermal conductivity of the GDLs investigated was evaluated in two orthogonal directions, namely when the orientation of most fibres was (i) parallel and (ii) normal to the heat flux. Furthermore, the effect of the PTFE loading on the in-plane thermal conductivity of the GDL was determined for five different samples (0, 5, 10, 20, and 30 wt.% PTFE loadings) and the orientation of the fibres was parallel to the heat flux. The effect of the micro porous layer (MPL) on the in-plane thermal conductivity of the GDL was determined for two different samples, namely 10BC and 10 BE, and the thermal conductivity of them was compared with the main material 10BA without a micro porous layer.

The thermal conductivity of the membrane was determined for a Nafion® membrane using Nafion® 115 (Du Pont, USA), which is about 127 μm in thickness, and in the temperature range from 35 °C to 65 °C, which is most likely the mean temperature inside the PEM fuel cells.

The effect of Pt loading in the in-plane thermal conductivities of the catalyst layer was investigated for three samples with different platinum loading, namely 0.41, 0.45 and 0.51 mg·cm^{-2}, which are within the realistic range available for the catalyst loading in PEM fuel cells.

6.2.3 Methodology

The thermal resistance of the holder without the sample, R_o, is measured as follows [59]:

$$R_o = \frac{\Delta T}{IV} \tag{6.1}$$

where ΔT is the temperature drop across the holder, V is the voltage applied to the heater in the circuit, and I is the current applied to the heater.

In the second stage, the GDL sample is attached to the circuit and again the thermal resistance is calculated for the circuit with the sample. Subsequently, the total thermal resistance after attaching the sample is determined as follows:

$$R = \frac{\Delta T}{IV} \tag{6.2}$$

where R is the thermal resistance to the sample and the holder.

Finally, by subtracting the thermal resistance of the holder from the total thermal resistance, the thermal resistance of the sample is determined as follows:

$$\frac{1}{R_S} = \frac{1}{R} - \frac{1}{R_o} \tag{6.3}$$

where R_S is the thermal resistance of the sample [59].

By including the sample dimensions, the length and the cross sectional area, the thermal conductivity of the sample is calculated as follows:

$$R_S = \frac{L}{kA} \tag{6.4}$$

where k is the thermal conductivity of the sample, L is the length of the sample and A is the cross-sectional area of the sample [59].

6.2.4 Validation of the measurement technique

The experimental technique was validated by using a standard copper wire. The thermal conductivity of the copper wire was measured to be about 384.7±6.3 W·m^{-1}·K^{-1}, which was found to be in good agreement with the reported value for the thermal conductivity of copper wire, which is about 386 W·m^{-1}·K^{-1} at room temperature [73].

6.2.5 Uncertainty analysis

The uncertainty in the thermal conductivity measurements may be calculated based on the combined uncertainty in the power measurements [100]. The maximum uncertainty comes from the temperature measurements and it was about 0.5 °C for T-type thermocouples. The uncertainty in the measurements is calculated as follows:

$$\frac{\delta k}{k}=\sqrt{\left(\frac{\delta T_c}{T_c}\right)^2+\left(\frac{\delta I}{I}\right)^2+\left(\frac{\delta V}{V}\right)^2+\left(\frac{\delta T_h}{T_h}\right)^2+\left(\frac{\delta L}{L}\right)^2+\left(\frac{\delta A}{A}\right)^2} \tag{6.5}$$

This value is calculated and reported for every measurement. It is important to note that the uncertainty in the measurements was not more than 6% for all the measurements performed in this investigation.

6.3 Results and Discussions

6.3.1 Effect of the temperature on the in-plane thermal conductivity of the membrane

The thermal conductivity was obtained for dry Nafion® 115 membrane over a range of temperatures 35 – 65 °C. The thermal conductivity is calculated from the slope of the curve for the thermal resistance versus the membrane length in the steady state thermal conductivity technique, see Figure 6.3, as follow:

$$k = \frac{1}{slope} \times \frac{1}{A} \tag{6.6}$$

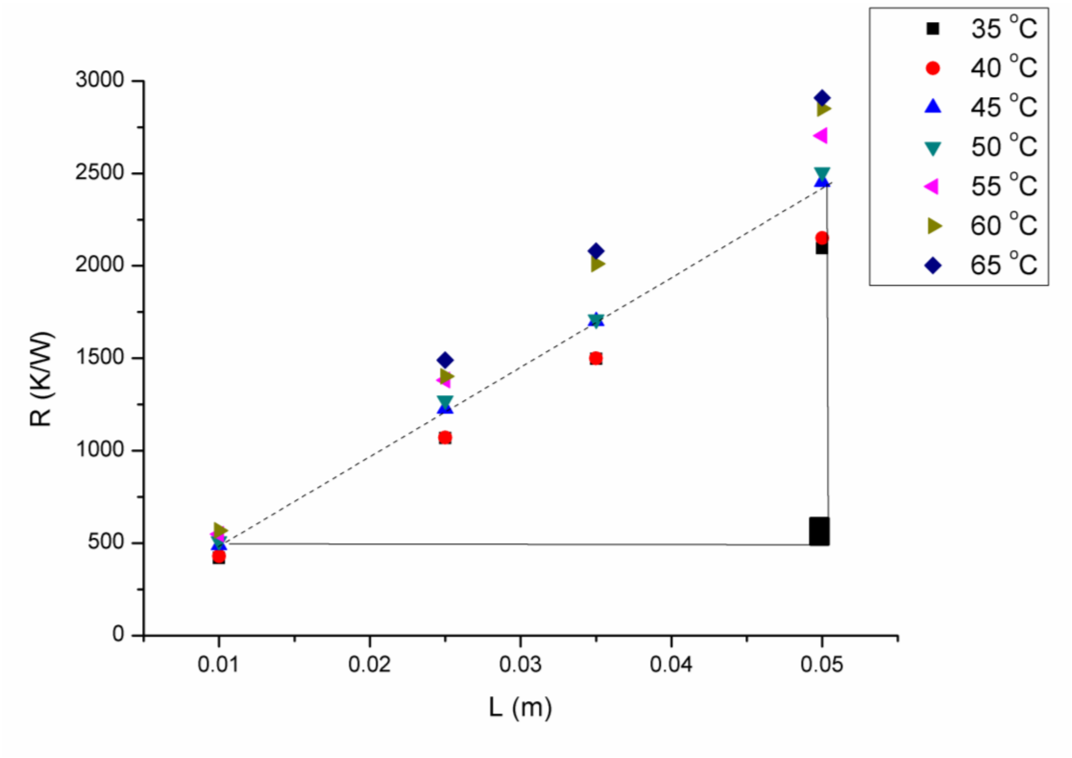

Figure 6.3 Measured thermal resistances of the membrane as a function of the temperature by the conventional steady-state technique.

The thermal conductivities of the membrane which were calculated using the conventional steady-state technique are listed in Table 6.2.

Table 6.2 The thermal conductivity of the membrane as a function of the temperature by the conventional steady-state technique.

The thermal conductivity ($W \cdot m^{-1} \cdot K^{-1}$)						
35 °C	40 °C	45 °C	50 °C	55 °C	60 °C	65 °C
0.188±0.015	0.183±0.015	0.160±0.013	0.158±0.013	0.145±0.012	0.138±0.011	0.135±0.011

However, the thermal conductivity may be calculated directly from the thermal resistance in the parallel thermal conductance technique because the thermal contact resistances have been eliminated through the manipulation shown in Section 6.2.3.

$$k = \frac{L}{R_s A} \tag{6.7}$$

These thermal conductivities of the membrane as a function of the temperature, calculated by the parallel thermal conductance technique, are listed in Table 6.3.

Table 6.3 The thermal conductivity of the membrane as a function of the temperature by the parallel thermal conductance.

L (m)	The thermal conductivity (W·m^{-1}·K^{-1})						
	35 °C	40 °C	45 °C	50 °C	55 °C	60 °C	65 °C
0.01	0.187±0.015	0.183±0.015	0.161±0.013	0.158±0.012	0.144±0.011	0.138±0.011	0.134±0.011
0.025	0.186±0.015	0.184±0.015	0.160±0.013	0.158±0.013	0.145±0.011	0.139±0.011	0.135±0.011
0.035	0.188±0.015	0.184±0.015	0.160±0.013	0.157±0.013	0.144±0.011	0.139±0.011	0.135±0.011
0.05	0.187±0.015	0.183±0.015	0.160±0.013	0.157±0.012	0.145±0.012	0.138±0.011	0.135±0.011

It is clear that the thermal conductivities of the membrane calculated by both methods are in good agreement. However, by using the method of parallel thermal conductance, the thermal conductivity could be calculated immediately from one measurement of the thermal resistance. Therefore, the parallel thermal resistance could be used to measure the thermal resistance of a thin film accurately and in a short time.

As it can be seen in Figure 6.4, the thermal conductivity of the membrane was 0.188±0.015 $W \cdot m^{-1} \cdot K^{-1}$ when the temperature was 35 °C, and as the temperature increases the thermal conductivity of the membrane slowly decreases. The thermal conductivity of the membrane at the maximum reported temperature, i.e. 65 °C, was 0.135±0.011 $W \cdot m^{-1} \cdot K^{-1}$. Basically, the thermal conductivity of the membrane decreases with increasing temperature due to the decrease in the phonon mean free path as a result of increasing the number of phonon at the high temperature for the polymers as Nafion material [101]. This relation is explained by using this equation [102]:

$$k_{mem} = \frac{1}{3} c_{ph} v_{ph} l_{ph} \tag{7.12}$$

where k_{mem} is the thermal conductivity of the membrane, l_{ph} is the phonon mean free path, c_{ph} is the phonon heat capacity and v_{ph} the phonon velocity. In the high temperature c_{ph} and v_{ph} are almost constants, while l_{ph} decreases and consequently the thermal conductivity of the membrane decreases [103, 104], which is considered as an insulating material. It should be noted that these results are in good agreement with the reported thermal conductivities of the Nafion® by Kandelwal and Mench [40], see Figure 6.4.

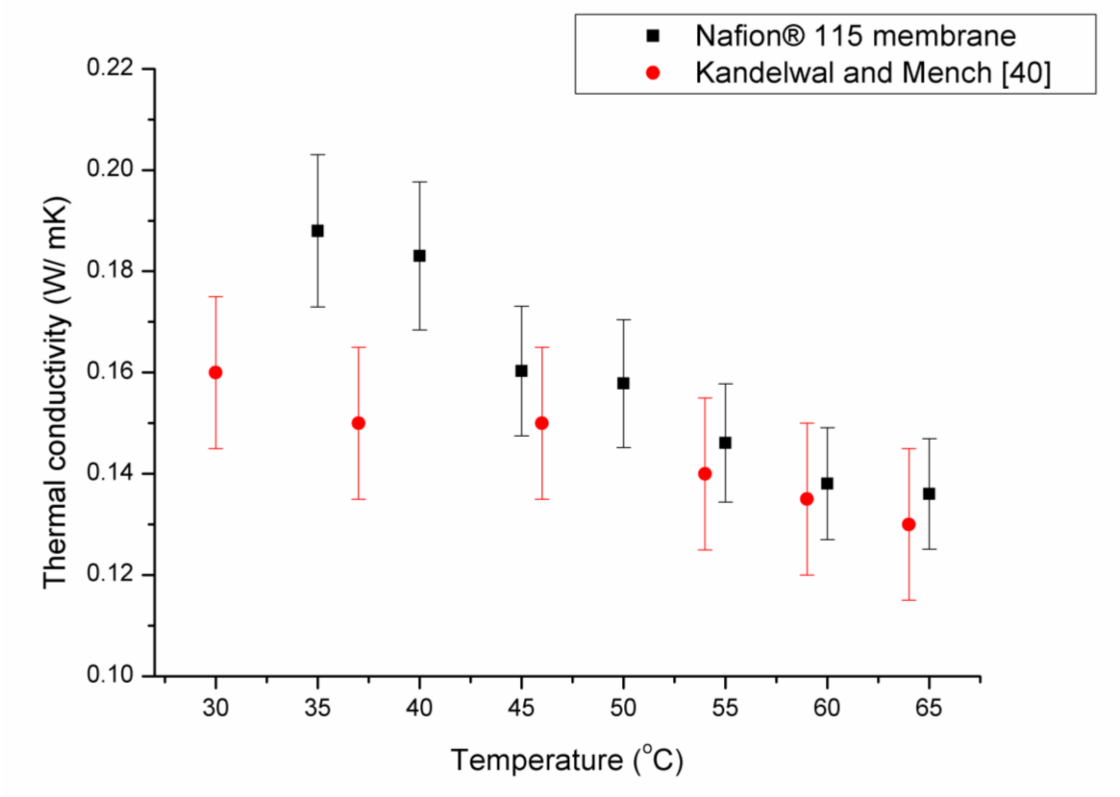

Figure 6.4 Measured thermal conductivities of the membrane as a function of the temperature, including the experimental error bars.

Typically, the membrane is humidified inside the fuel cell. However, it is difficult to measure the thermal conductivity of the humidified membrane because the heat generated in the apparatus used to measure the thermal conductivity will dry out the membrane. In addition, the measurement of the thermal conductivity of the membrane is performed under vacuum conditions and this will also make the membrane dry out from the original water content. Therefore, the effect of water on the thermal conductivity of the membrane was theoretically estimated based on the assumption that the wet membrane is a mixture of water and membrane material. The effective thermal conductivity of the wet membrane can then be calculated by averaging the thermal conductivity of the water, the air and the membrane to their volume fractions [84, 85]:

$$k_{eff} = k_{water} v_{water} + k_{air} v_{air} + k_{mem} \ v_{mem} \tag{6.8}$$

where k_{water}, k_{air} and k_{mem} are the thermal conductivities of the water, air and membrane, respectively. v_{water}, v_{air} and v_{mem} are the volume fractions of the water, air and membrane, respectively.

The volume fractions of water and membrane are calculated considering (i) the linear expansion of membrane when it is soaked with water and the extrapolated of these values at different temperatures, as listed in Table 6.4, and (ii) the porosity of the membrane, which is reported to be 0.28 [105, 106].

Table 6.4 The physical properties of the fully-humidified Nafion® membrane [104].

property	23 °C	100 °C
Thickness expansion (%)	10	14
Linear expansion (%)	10	15

However, it should be noted that the linear expansion of the membrane reported above is most likely to be limited inside the fuel cells and this is due to the presence of the ribs and the sealing gaskets in the fuel cells. Therefore, the thermal conductivity values of the wet membrane reported in Figure 6.5 were the maximum possible ones inside the fuel cell. It was observed that the thermal conductivity of the membrane significantly increases as it becomes wetter. This is due to the fact that the thermal conductivity of the water (k_{water} = 0.66 $W \cdot m^{-1} \cdot K^{-1}$) is more than the thermal conductivity of the membrane (k_{mem} = 0.18 $W \cdot m^{-1} \cdot K^{-1}$). It is also noteworthy that the thermal conductivity of water increases with increasing the temperature [107]. Furthermore, the volume fraction of the water was measured experimentally by weighing a piece of membrane before and after being soaked with water. The difference in weight was assumed to be due to the addition of liquid water and subsequently converted to a volume fraction for water.

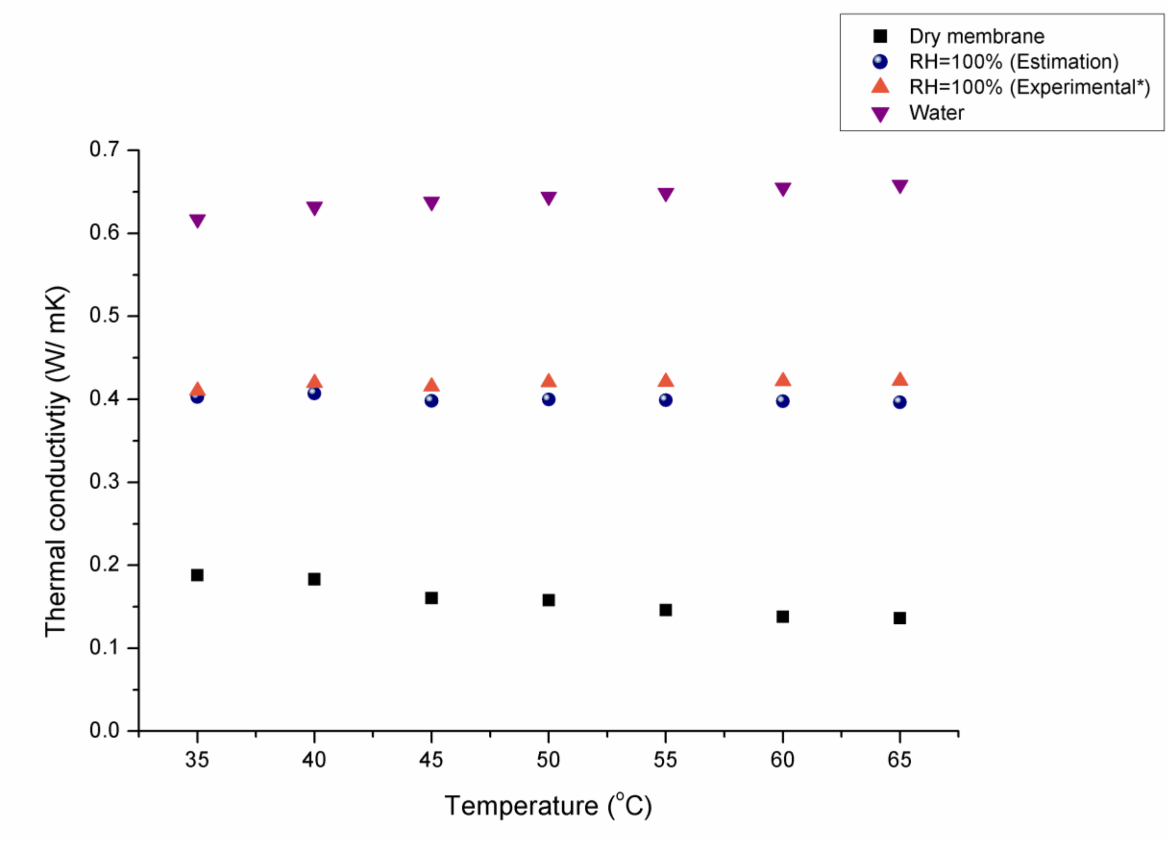

Figure 6.5 Estimated thermal conductivity of dry and fully-humidified Nafion® membrane as a function of the temperature.

* The experimental estimation of the volume fraction of the water.

As can be seen from Figure 6.5, the thermal conductivity of the wet membrane that has been calculated based on the experimental estimation of the volume fraction of the water was in good agreement with that obtained based on the reported values for the linear expansion and porosity of the membrane. The dry membrane results give the lower bound for the thermal conductivity of the membrane, and the results of the membrane with 100% RH give the upper bound for the thermal conductivity of the membrane. In conclusion, Equation (6.8) should give a good estimate of the range of possible values for the thermal conductivity of a membrane within a fuel cell.

6.3.2 Effect of the temperature on the in-plane thermal conductivity of the GDL

Figure 6.6 shows the thermal resistances of the GDLs as a function of the sample length for various temperatures. It was observed that the thermal resistance of the GDL increased as the temperature increases at normal operating temperatures that occur inside a PEM fuel cell. This is due to the presence of the binder whose thermal conductivities decrease with increasing temperature [108]. It was difficult to compare the in-plane thermal conductivity of the SGL GDL with that reported in the literature because they did not use the same type of GDL. However, the effect of temperature on the in-plane thermal conductivity of the GDL reported in this chapter was in line with that reported by Zamel et al. [109].

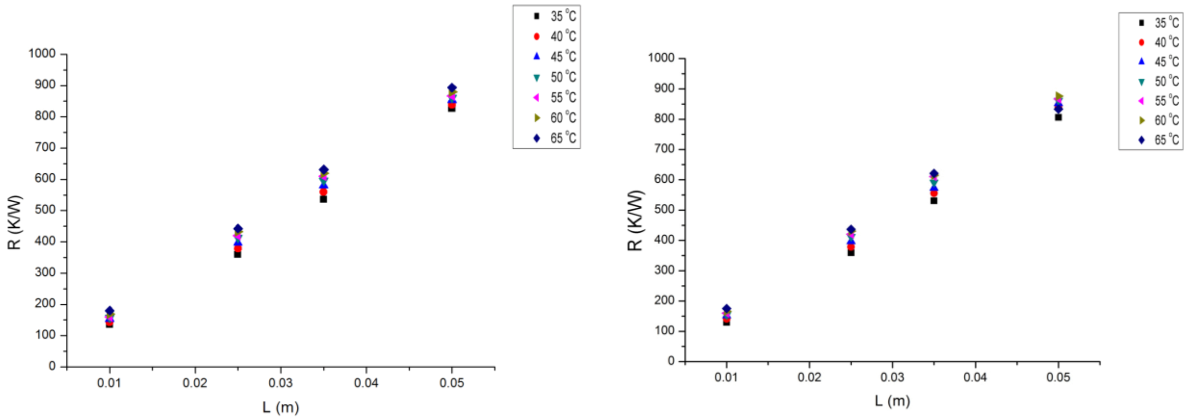

(a) SGL 10AA (b) SGL 10BA

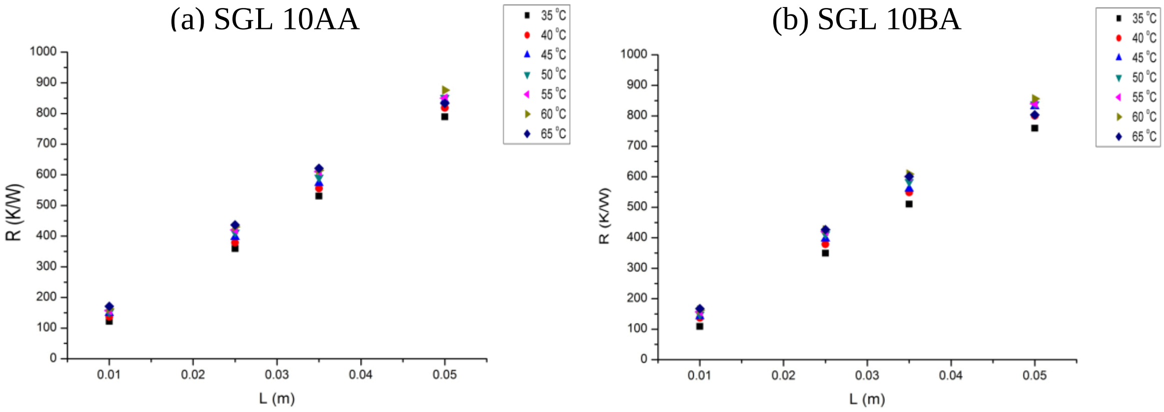

(c) SGL 10CA (d) SGL 10DA

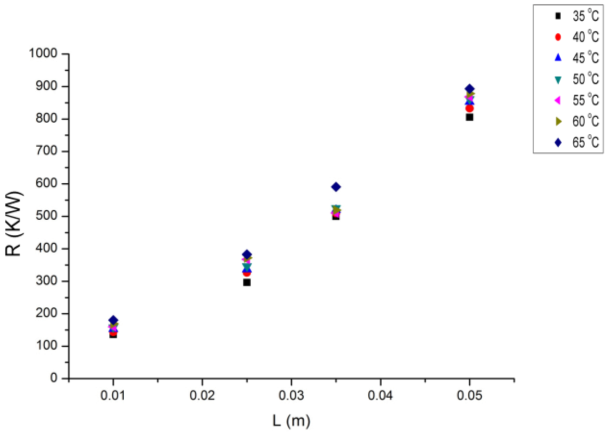

(e) SGL 10EA

Figure 6.6 Measured thermal resistances of the GDLs as a function of the temperature for (a) SGL 10AA, (b) SGL 10BA, (c) SGL 10CA, (d) SGL 10DA, and (e) SGL 10EA.

6.3.3 Effect of the fibre direction on the in-plane thermal conductivity of the GDL

Due to the fibrous nature of the material used in GDLs, the thermal conductivity of the GDL is normally anisotropic. In order to illustrate this phenomenon, the thermal conductivity of 10AA which is cut in two perpendicular directions, namely where the fibres are parallel and normal to the heat flux, as seen in Figure 6.7, were investigated. As mentioned in Section 6.2.2, the measurements were made for two sets of samples. The orientation of the fibres was parallel to heat flux in the first set and normal to heat flux in the second set. The thermal conductivity was found to be rather sensitive to the fibre direction, as shown in Figure 6.8.

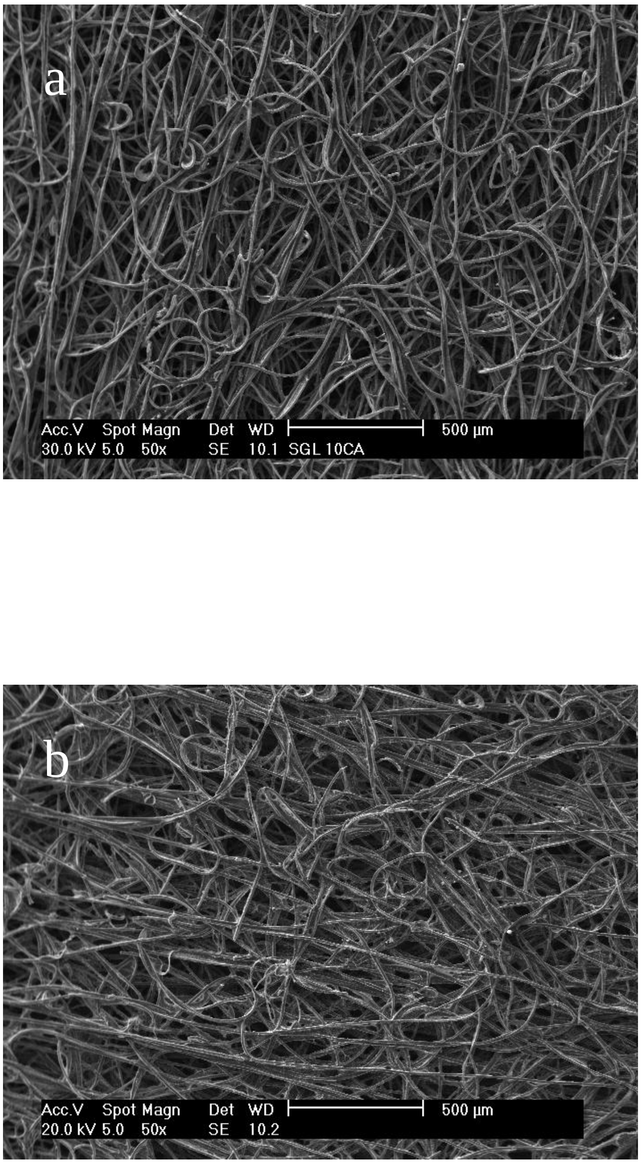

Figure 6.7 SEM images of the surface of two fibre directions of the GDL, namely (a) 0°, and (b) 90°.

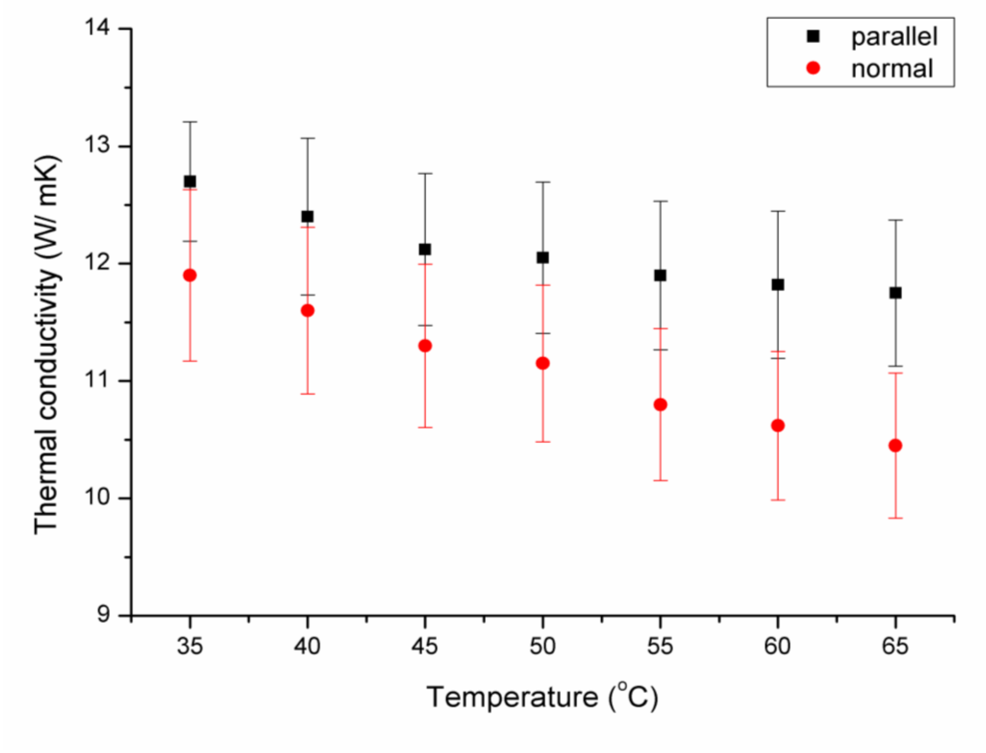

Figure 6.8 Thermal conductivity of the 10 AA GDL measured in two orthogonal in-plane directions, along with the experimental error bars.

The in-plane thermal conductivity of the GDL was higher when the fibre orientation was parallel to the heat flux because the heat is transported more easily along the fibres than perpendicular to the fibres. The in-plane thermal conductivity of the SGL 10AA was determined to be 12.67±0.17 and 11.9±0.16 W·m^{-1}·K^{-1} at a mean temperature of 35 °C when the orientation of the fibre is parallel to the heat flux and normal to the heat flux, respectively. A similar ordering of thermal conductivities as a function of orientation were found for all the GDL samples under investigation.

6.3.4 Effect of the PTFE on the in-plane thermal conductivity of the GDLs

Polytetrafluoroethylene (PTFE) is a high molecular-weight fluorocarbon polymer which is usually known as Teflon. PTFE is a white solid thermoplastic at room temperature with a density of about 2.2 $g \cdot cm^{-3}$. The PTFE melts at a temperature of 327 °C and it is an insulating material with a thermal conductivity of approximately 0.25 $W \cdot m^{-1} \cdot K^{-1}$ [110]. For fuel cells applications, the gas diffusion layers are usually treated with PTFE because of its hydrophobic properties. Therefore it minimises wetting of the GDL fibres during fuel cell operation, and hence minimises problems of blocking gas transport. The SGL samples which have been investigated in this chapter have various PTFE loadings and the thicknesses of these samples are approximately 400 µm, as listed previously in Table 6.1.

The thermal conductivity of carbon is more than two orders of magnitude higher than that of the thermal conductivity of the PTFE. Therefore, the PTFE insulates the carbon fibres from each other as it is clear from the SEM images, see Figure 6.9. This will decrease the through-plane thermal conductivity of the gas diffusion layers since the heat transfer is from fibre to fibre in the through-plane direction. However, the contact resistance does not play a significant role in the through-plane direction as the fibres are under compression and the fibres will always be in contact.

On the other hand, most of the heat is transferred along the fibres in the in-plane direction and adding the PTFE decreases the contact resistance between the fibres and this increases the thermal conductivity in the in-plane direction and this effect was in a manner similar to that reported by Sadeghi et al. [99]. The in-plane thermal conductivity of the GDL is listed in Table 6.5 at different mean temperature. The measurements made that illustrate this are shown in Figure 6.10. Furthermore, the temperature gradient decreases as the PTFE loading increases. Moreover, the contact resistance between the fibres reduces, which increases the thermal conductivity of the GDL. The overall thermal conductivity of the GDL increases as the PTFE loading increases and replaces the air, which has a thermal conductivity of (k_{air} = 0.02 $W\cdot m^{-1}\cdot K^{-1}$) [111], while the PTFE has a higher thermal conductivity (k_{PTFE} = 0.25 W·m^{-1}·K^{-1}) [110].

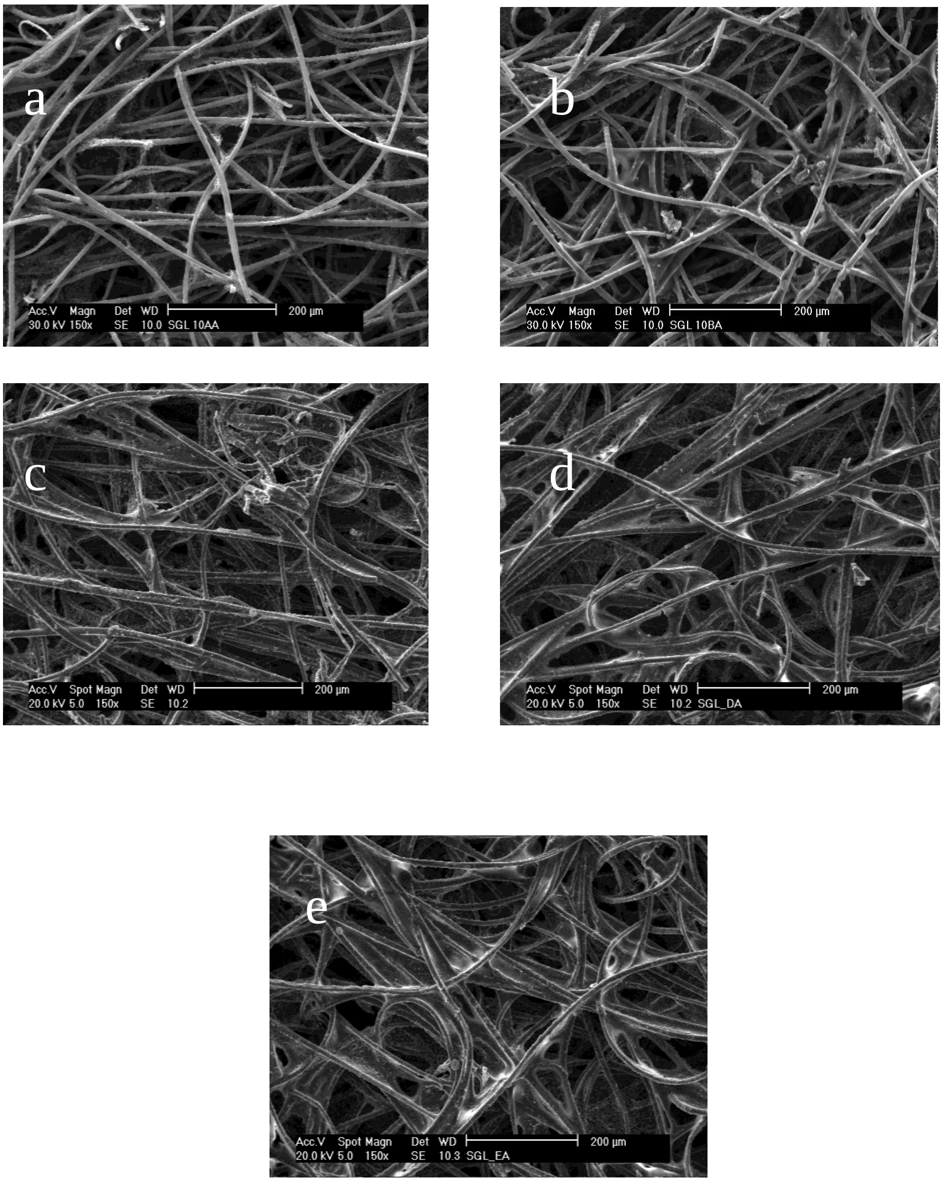

Figure 6.9 SEM images for the surface of PTFE-loading GDLs, (a) SGL 10AA, (b) SGL 10BA, (c) SGL 10CA, (d) SGL 10DA, and (e) SGL 10EA.

Table 6.5 List of the in-plane thermal conductivities of the PTFE-loaded GDLs.

GDL Sample	Temperature (^oC)	The thermal in-plane conductivity ($W \cdot m^{-1} \cdot K^{-1}$)
10AA	35	12.6 ± 0.76
	45	12.2 ± 0.73
	55	12.0 ± 0.72
	65	11.7 ± 0.7
10BA	35	13.2 ± 0.79
	45	12.8 ± 0.76
	55	12.1 ± 0.73
	65	11.8 ± 0.70
10CA	35	15.3 ± 0.91
	45	14.6 ± 0.87
	55	13.8 ± 0.83
	65	12.9 ± 0.77
10DA	35	16.2 ± 0.97
	45	15.6 ± 0.93
	55	15.2 ± 0.90
	65	14.2 ± 0.85
10EA	35	17.3 ± 1.03
	45	16.4 ± 0.98
	55	15.6 ± 0.93
	65	14.8 ± 0.88

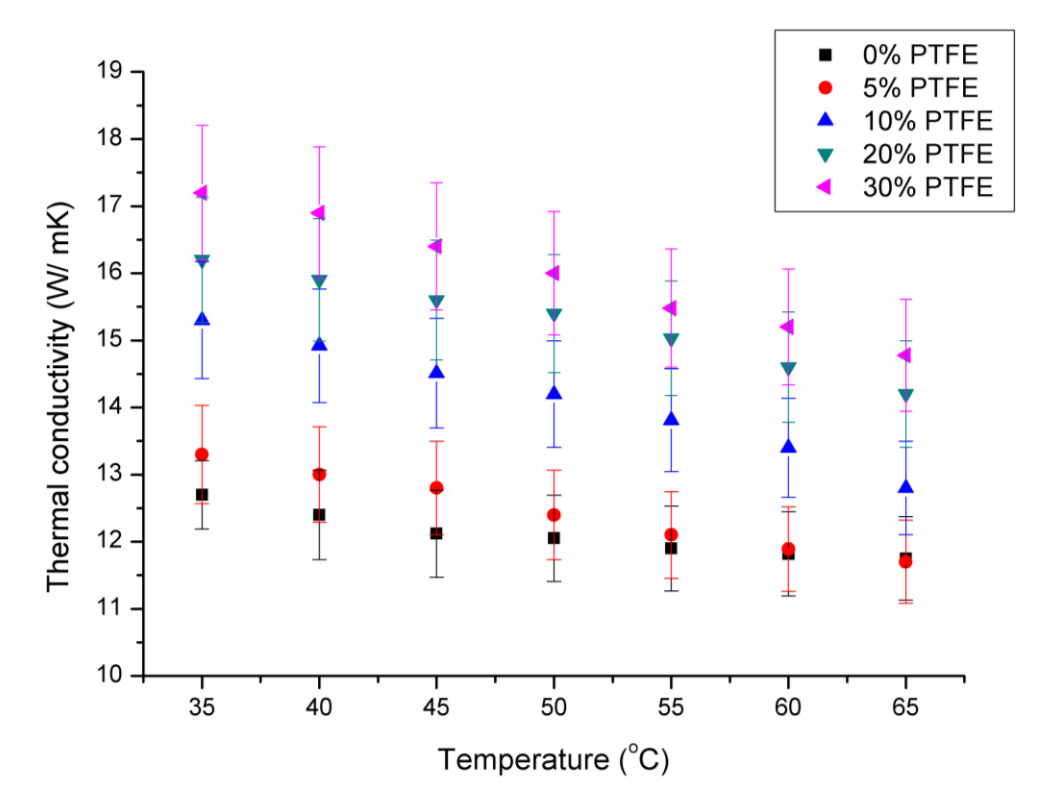

Figure 6.10 Measured thermal conductivities of PTFE-treated GDLs as a function of the temperature, including the experimental error bars.

6.3.5 Effect of the MPL on the in-plane thermal conductivity of the GDL

The micro porous layer (MPL) in the gas diffusion layer consists of a mix of hydrophobic agents with a layer of black powder carbon nanoparticles. This layer is added to the fuel cell between the gas diffusion layer and the catalyst layer in order to enhance the water management and to decrease the contact resistance between the gas diffusion layer and the catalyst layer [44]. The measured thermal resistances of the MPL treated GDL is illustrated in Figure 6.11.

The thermal contact resistance of the GDL samples decreases when the MPL is added to the GDL. This is not surprising as one of the main aims of adding MPL to the GDL in the fuel cell is to improve the contact between the GDL and the catalyst layer, as can be seen in Figure 6.11.

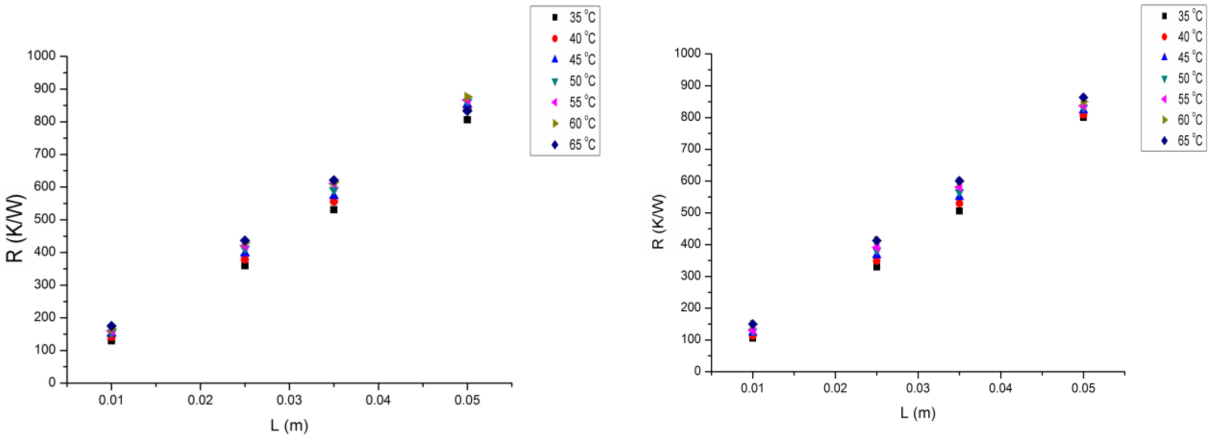

(a) SGL 10BA

(b) SGL 10BC

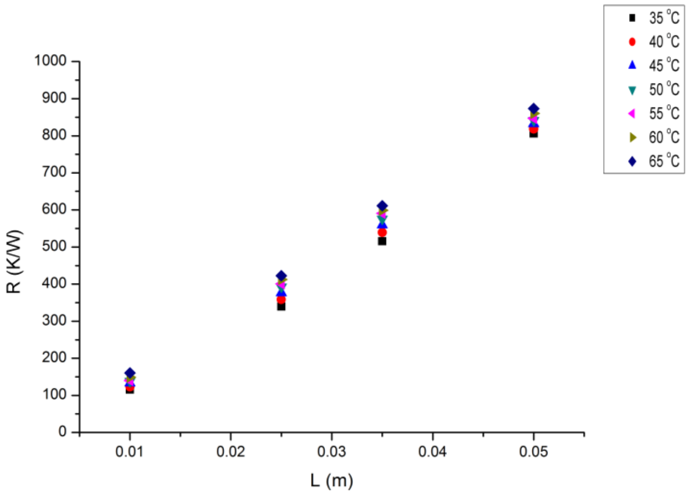

(c) SGL 10BE

Figure 6.11 Measured thermal resistance for the tested GDLs (a) SGL 10BA, (b) SGL 10BC, and (c) SGL 10BE.

Scanning electron microscope (SEM) has been used to image the surface of the GDL, as shown in Figure 6.12. The sample which has the highest porosity and the largest pores was the 10 BA which was without an MPL. In addition, it is clear from the SEM images that the samples which have an MPL have a lower porosity than the samples without the MPL. However, it should be stressed that the mercury porosimetry and the method of stand porosimetry (MSP) are required to measure the three-dimensional microstructure of the pores and to obtain a full view for the pore sizes [112].

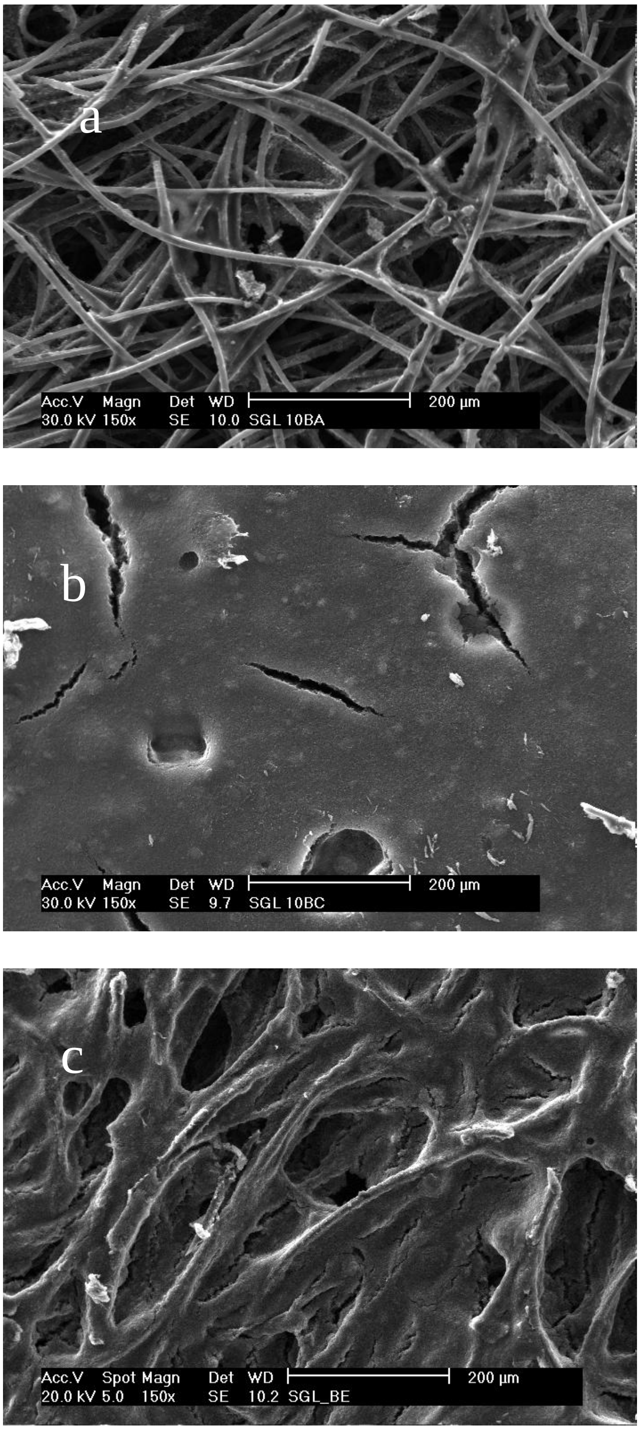

Figure 6.12 SEM images for the surface of the GDLs (a) SGL 10BA, (b) SGL 10BC, and (c) SGL 10BE [113].

Furthermore, 10 BA which is the untreated GDL has a lower thermal conductivity than the treated GDL, the values of all these thermal conductivity at different mean temperature are listed in Table 6.6.

Figure 6.13 illustrated that the 10BE has a lower thermal conductivity than that of 10BC. The main reason for this is that the MPL of 10BE has a higher amount of PTFE (50%) and a lower amount of carbon powder. Furthermore, the thermal conductivity of the PTFE, 0.25 $W \cdot m^{-1} \cdot K^{-1}$, is much lower than the thermal conductivity of carbon, 120 $W \cdot m^{-1} \cdot K^{-1}$, and 10 BC has a lower amount of PTFE (30%) and a higher amount of carbon powder which increased the overall thermal conductivity of 10BC.

Table 6.6 List of the in-plane thermal conductivities of the MPL-coated the GDLs.

GDL Sample	Temperature (^oC)	The thermal conductivity ($W\cdot m^{-1}\cdot K^{-1}$)
10BA	35	13.2 ± 0.79
	45	12.8 ± 0.76
	55	12.1 ± 0.73
	65	11.8 ± 0.70
10BC	35	17.6 ± 1.05
	45	16.9 ± 1.01
	55	16.3 ± 0.97
	65	15.5 ± 0.93
10BE	35	16.9 ± 1.01
	45	16.2 ± 0.98
	55	15.4 ± 0.92
	65	14.8 ± 0.88

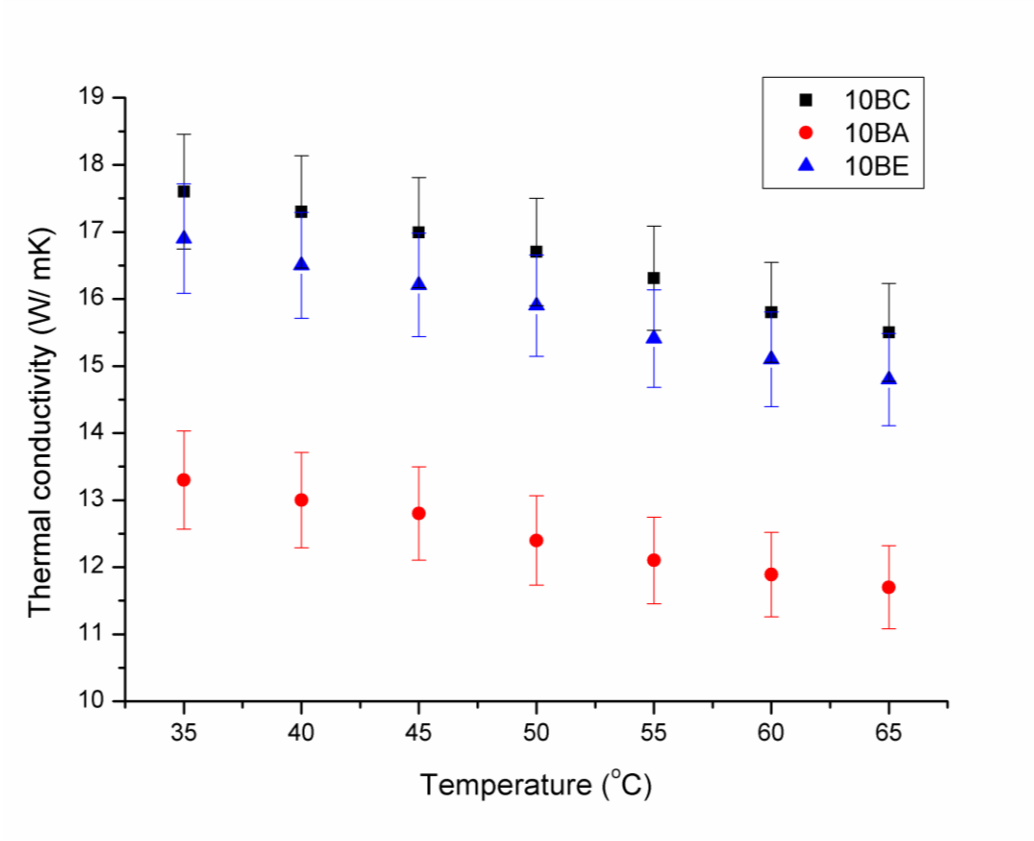

Figure 6.13 Measured thermal conductivities of the investigated GDLs (10BA, 10BC and 10BE) as a function of the temperature along with the experimental error bars.

6.3.6 Effect of the temperature on the in-plane thermal conductivity of the catalyst layer

The catalyst layer is a mixture of carbon powder and platinum particles. The catalyst layers in the PEM fuel cell are in direct contact with both the membrane and the GDL layers. These five layers are compressed together to form the membrane electrode assembly (MEA).

The thermal conductivity of an in-house fabricated 10BA GDL-based MEA is measured in order to determine the thermal conductivity of the catalyst layer which is reported to be between 0.2-1.5 $W\cdot m^{-1}\cdot K^{-1}$ [40,114]. The thickness of the catalyst layer was estimated to be 3×10^{-5} m, the thickness of the membrane was 1.27×10^{-4} m and the thickness of the GDL was 4×10^{-4} m. The platinum loadings was about 0.4 $mg\cdot cm^{-2}$ which corresponds to 60 % Pt/C.

The thermal conductivity of the catalyst layer was estimated by making use of the measured conductivity of the entire MEA and previously-measured conductivities for the membrane and the GDLs:

$$k_{MEA} = 2(v_{GDL}k_{GDL}) + v_{mem}k_{mem} + 2(v_{cl}k_{cl}) \tag{6.9}$$

where k_{MEA} is the thermal conductivity of the membrane electrode assembly. k_{GDL}, k_{cl} and k_{mem} are the thermal conductivities of GDL, catalyst layer and membrane, respectively. v_{GDL}, v_{cl} and v_{mem} are the volume fractions of GDL, catalyst layer and membrane, respectively [84, 85].

Figure 6.14 shows the thermal conductivity of the catalyst layer as a function of the temperature. It was observed that the thermal conductivity of the catalyst is almost independent of the temperature and it was 0.291±0.018 $W \cdot m^{-1} \cdot K^{-1}$. This value is in a good agreement with the reported value of the thermal conductivity of the catalyst layer by Kandelwal and Mench [40], namely 0.27±0.05 $W \cdot m^{-1} \cdot K^{-1}$, as they used the same method by estimating the thermal conductivity of the catalyst from the thermal conductivity of the MEA and they have not taken into account the effect of the temperature on the thermal conductivity of the catalyst layer.

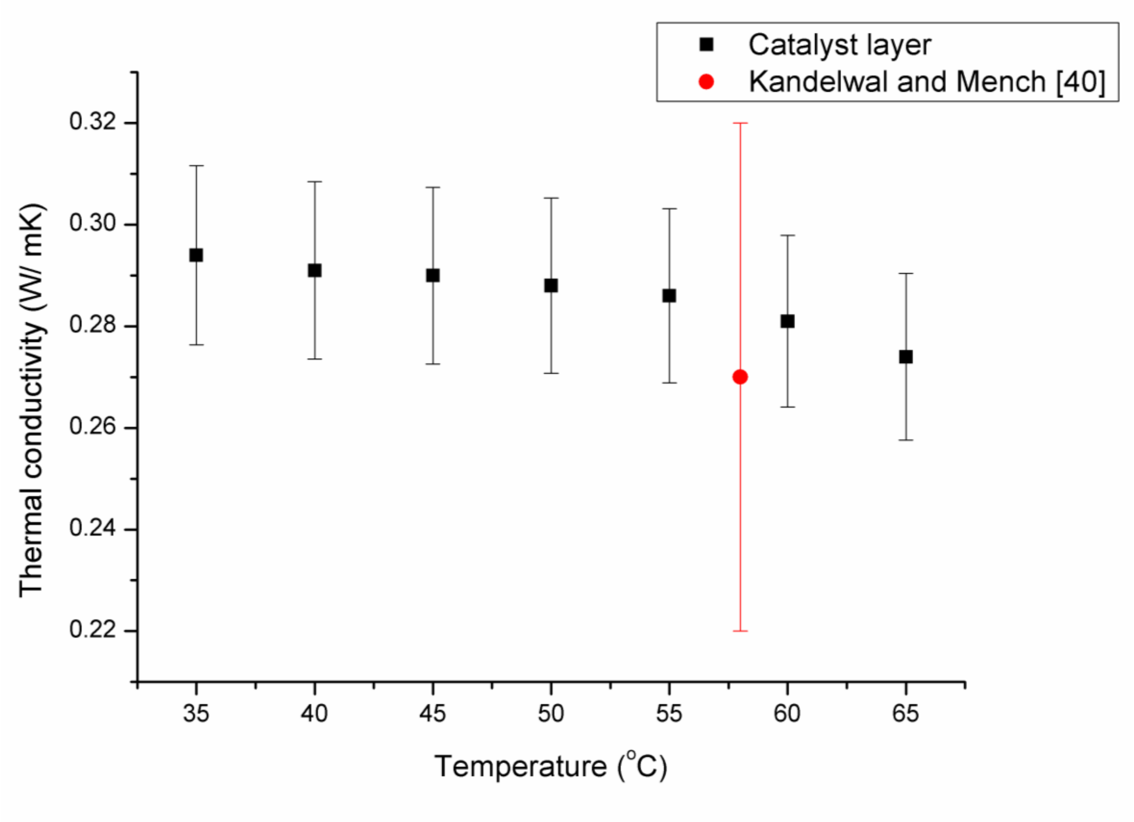

Figure 6.14 Measured thermal conductivities of the catalyst in the MEA as a function of the temperature along with the experimental error bars.

However, there is a big assumption here as the contact resistances between the GDL and the catalyst layer and between the membrane and the catalyst layer were ignored. Furthermore, the effect of the compression the MEA on the thermal conductivity was ignored as the thermal conductivities of the GDL and the membrane inside the MEA were assumed to be the same as those of the 'bare' GDL and membrane. Therefore, the thermal conductivity of the catalyst layer was measured again after applying the catalyst to 3 samples of 10 BA GDL, see Appendix B for more details on applying the catalyst ink on the GDL. The resulting platinum loadings for the catalysed samples were 0.41, 0.45 and 0.51 mg·cm^{-2}. The thickness and the weight of the samples were measured both before and after applying the catalyst in order to determine the thickness of the catalyst and calculate the volume fractions of the GDL and the catalyst. In addition, the thermal conductivities of these three GDL samples were measured before and after applying the catalyst. By using the parallel model to measure the thermal conductivity of the catalyst as illustrated in Figure 6.15, the thermal conductivity of the catalysed GDL can be expressed as follows:

$$k_{total} = v_{GDL} k_{GDL} + v_{cl} k_{cl} \tag{6.10}$$

where k_{total} is the thermal conductivity of the GDL after spraying the catalyst ink on it.

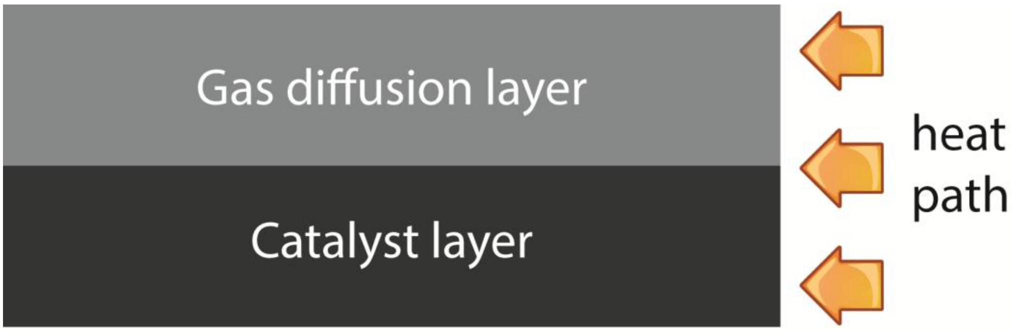

Figure 6.15 Calculating the thermal conductivity of the catalyst using the parallel model.

The thermal resistances of the catalyst is measured for these three samples in order to accurately measure the thermal resistances of the catalyst layer and investigate the effect of Pt loadings on the thermal resistance of the catalyst layer, with the results summarised in Figure 6.16. It is clear from the figure that the thermal resistance increases slightly with increasing Pt loading. This is due to the addition of platinum which has a thermal conductivity of 71.6 $W \cdot m^{-1} \cdot K^{-1}$ in this range of temperatures [115]. Moreover, the thermal conductivity of the catalyst is found to be insensitive to the temperature. The maximum thermal conductivity of the catalyst layer with a platinum loading of 0.41 mg·cm^{-2} is 0.338 ± 0.020 W·m^{-1}·K^{-1} when the temperature is 35 °C, and the minimum thermal conductivity of this catalyst layer is 0.317± 0.019 W·m^{-1}·K^{-1} when the temperature is 65 °C.

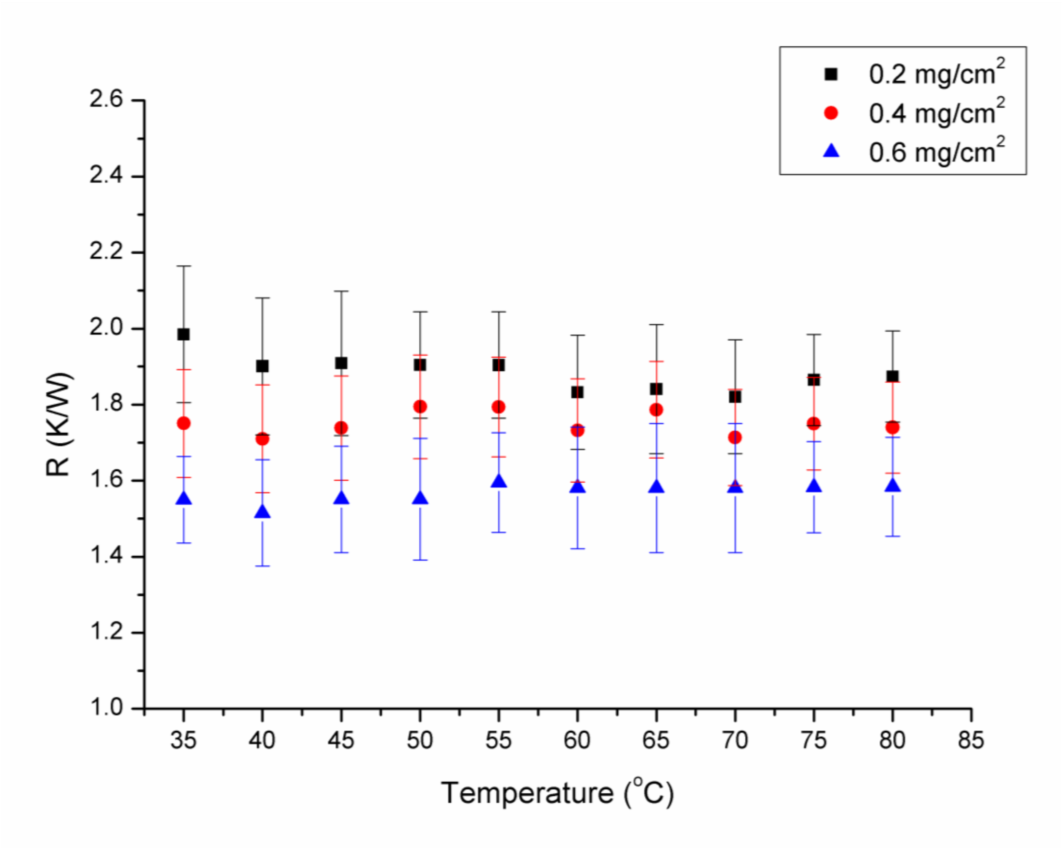

Figure 6.16 Measured thermal resistances of the catalyst layers as a function of the temperature along with the experimental error bars.

6.4 Conclusions

The parallel thermal conductance technique has been employed to measure the thermal conductivity of the GDL as a function of the temperature, fibre direction, PTFE loading and MPL coating. Also, the thermal conductivities of the membrane and the catalyst layer have been experimentally estimated. The main conclusions of these measurements are as follows:

- The thermal conductivity of the membrane decreases when the temperature increases. The thermal conductivity of the Nafion® 115 membrane was found to be 0.188±0.015 $W\cdot m^{-1}\cdot K^{-1}$ and 0.135±0.011 $W\cdot m^{-1}\cdot K^{-1}$ when the temperature was 35 °C and 65 °C, respectively.

- The in-plane thermal conductivity of the GDL decreases as the temperature increases from 35 °C to 65 °C. This decrease is due to the fact that the GDL consists of a polymeric resin and/or PTFE whose thermal conductivities decrease with increasing temperature. The in-plane thermal conductivity of the GDL increases slightly with PTFE loading. This is due to the fact that the PTFE is replacing air, which has a lower thermal conductivity than that of the PTFE. Moreover, the thermal contact resistance between the fibres reduce when adding PTFE between the fibres and this assists in the transfer of heat along the fibres, thus increasing the in-plane thermal conductivity of the GDL. The in-plane thermal conductivity of the GDL is higher when the fibres are oriented parallel to the heat flux as this provides a direct and easy way for the heat to be transferred along the fibre. It is found that the in-plane thermal conductivity of the GDL is higher in the samples which contain MPLs and this is due to the fact that the MPLs used are rich in carbon which is a highly conductive material compared to the material of the non-coated GDL. Therefore, the overall thermal conductivity of the coated GDL increases.

- The in-plane thermal conductivity of the catalyst layer was found to be insensitive to the temperature and increases with Pt loading.

The performance of the PEM fuel cell improves with increasing the thermal conductivity of the components of the MEA and this is due to better heat dissipation. Therefore, these measurements can be used to provide a basis for better designs for the PEM fuel cells and thus enhance their performance. Furthermore, these parameters could be used in PEM fuel cells models to predict a more accurate temperature distribution in the fuel cell and this will assists in the thermal management of the PEM fuel cell.

Chapter 7

Measurement of the Through-plane Thermal Conductivity and the Contact Resistance of the Components of the Membrane Electrode Assembly in Proton Exchange Membrane Fuel Cells

7.1 Introduction

As mentioned in section 5.3.2, many researchers use a steady state method to measure the thermal conductivity of gas diffusion layers (GDLs) in the through-plane direction [44, 65]. In particular, Vie et al. [80] were the first research group who attempted to measure the thermal conductivity of the fuel cell components. In their study, many thermocouples have been inserted in the fuel cell and the temperature gradient is measured at different locations. The thermocouples were inserted between the gas diffusion layers, the catalyst layers and the membrane. The thermal conductivity of the E-Tek ELAT GDL and the catalyst layer was about 0.2±0.1 $W \cdot m^{-1} \cdot K^{-1}$. However, these measurements were not accurate due to the high uncertainty on the locations of the thermocouples and due to the fact that the thermocouples blocked some of the active area of the fuel cell. Khandelwal and Mench [40] reported that the through-plane thermal conductivity of SIGRACET to be 0.22±0.04 $W \cdot m^{-1} \cdot K^{-1}$, whereas Toray reported to be 1.8±0.27 W/(m.K). Ramousse et al. [41] reported the through-plane thermal conductivity of the GDL under different pressures, obtaining values of about 0.2 and 0.27 $W\cdot m^{-1}\cdot K^{-1}$under pressures of 4.6 and 13.9 bar, respectively. In addition, they estimated the thermal conductivity of a typical GDL to be lower than the thermal conductivity of pure carbon samples but they did not take into account the effect of the compaction pressure on the thickness of the sample [112]. Nitta et al. [116] measured the thermal conductivity of SGL 10BA GDL and the thermal contact resistance between the GDL and the graphite rods. It was found that the values of the GDL thermal conductivity obtained were almost 4 times larger than those found in the literature and it depends on the compression pressure on the sample. They reported the measured through-plane thermal conductivity of the GDL to be about 1.8±0.11 $W\cdot m^{-1}\cdot K^{-1}$. Karimi et al. [42] determined the through-plane thermal conductivity of SpectraCarb GDL experimentally. The contact resistance between the GDL and the aluminium apparatus surface was studied as a function of compression and PTFE content at a mean temperature of 70 °C.

In this chapter, an experimental setup, based on the steady-state method, is developed to measure the through-plane thermal conductivity of the components in the membrane electrode assembly (MEA) at different operating temperatures. The thermal conductivities of the GDLs are investigated as a function of the

PTFE loading, temperature and compression pressure. In addition, for the present study to be comprehensive, the through-plane thermal conductivities of Nafion® membranes and catalyst layers are measured and reported as a function of the temperature.

7.2 Materials and Procedures

7.2.1 Test apparatus

An experimental apparatus has been developed to measure the thermal conductivity of the various components of the MEA under steady state conditions. Therefore, the formula employed to estimate the thermal conductivity is the Fourier law [59]:

$$q_s = k_s A_s \frac{\Delta T}{L_S} \tag{7.1}$$

where A_s is the cross-sectional area of the sample, L_S is the length of the sample, k_S is the thermal conductivity of the sample, and ΔT is the temperature drop across the sample.

The test apparatus is shown in Figure 7.1. It consists of, from top to bottom, (i) a dial gauge indicator to measure the reduction in the thickness of the sample under compression, (ii) a low thermal conductivity material, See Appendix C for more details on the dimensions of the low thermal conductivity material which has been placed in the setup, and a load cell which records the compression pressure on the sample, (iii) the upper steel flux meter, which contains 3 thermocouples, (iv) the tested sample, and (v) the lower steel flux meter which also contains 3 thermocouples whose temperature gradient is maintained low and constant using a cooling system, see Section 7.2.3 for more details.

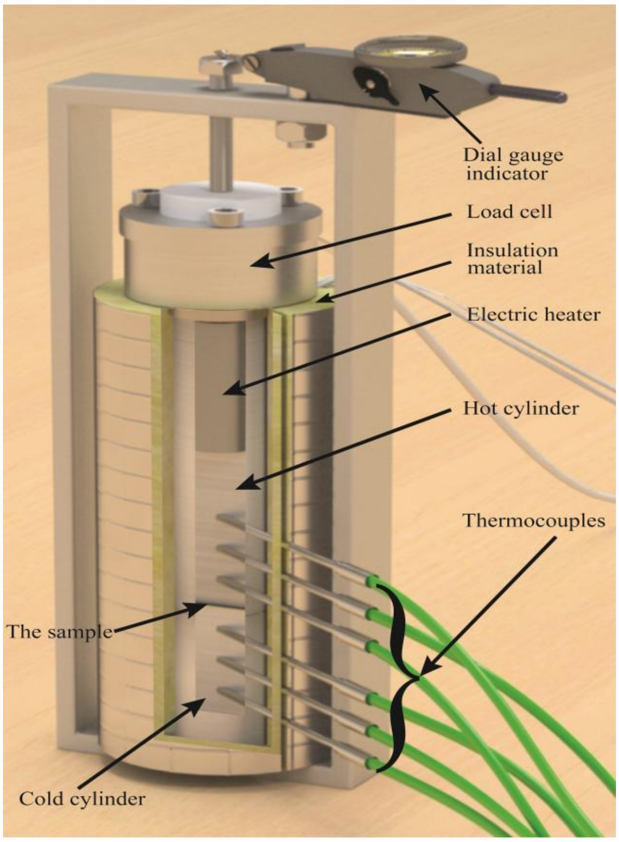

Figure 7.1 Configuration of the experimental set-up to measure the through-plane thermal conductivity of the MEA components.

7.2.2 Materials

The through-plane thermal conductivity of the GDL is determined for the same seven different SGL samples (10AA, 10BA, 10CA, 10DA, 10EA) whose PTFE loading are 0, 5, 10, 20 and 30%, respectively. These samples are listed previously in Table 6.1. In addition, the through-plane thermal conductivity of a 115 Nafion® 115 membrane

(Du Pont, USA), which is about 127 μm thick, is also measured and reported. Furthermore, the through-plane thermal conductivity of the catalyst is evaluated with three different platinum (Pt) loadings, namely 0.2, 0.4 and 0.6 $mg{\cdot}cm^{-2}$ in order to investigate the effect of this loading on the through-plane thermal conductivity of the catalyst layer.

7.2.3 Experimental conditions

All measurements were performed under vacuum conditions in order to eliminate the heat transfer by convection. Moreover, the fixtures and the samples were well insulated by using Rockwool insulation to minimise the heat loss in the radial direction and mitigate heat transfer by radiation. The effect of the temperature on the through-plane thermal conductivity of all the components in the MEA was investigated in the temperature range 35-80 °C, which is the most likely operating temperature range of PEM fuel cells [117]. In addition, the effect of the compression pressure was investigated for the compression range 1-20 bar, in which the normally-used compressive pressure on PEM fuel cells lies [118]. The lower steel cylinder was maintained cold by using EXT-440 Koolance's and CHC-122 cooling block through which the cooling fluid flows. All the thermocouple readings, the current, the voltage in the circuit and the pressure readings, were controlled and monitored by a LabVIEW application, see Figure 7.2.

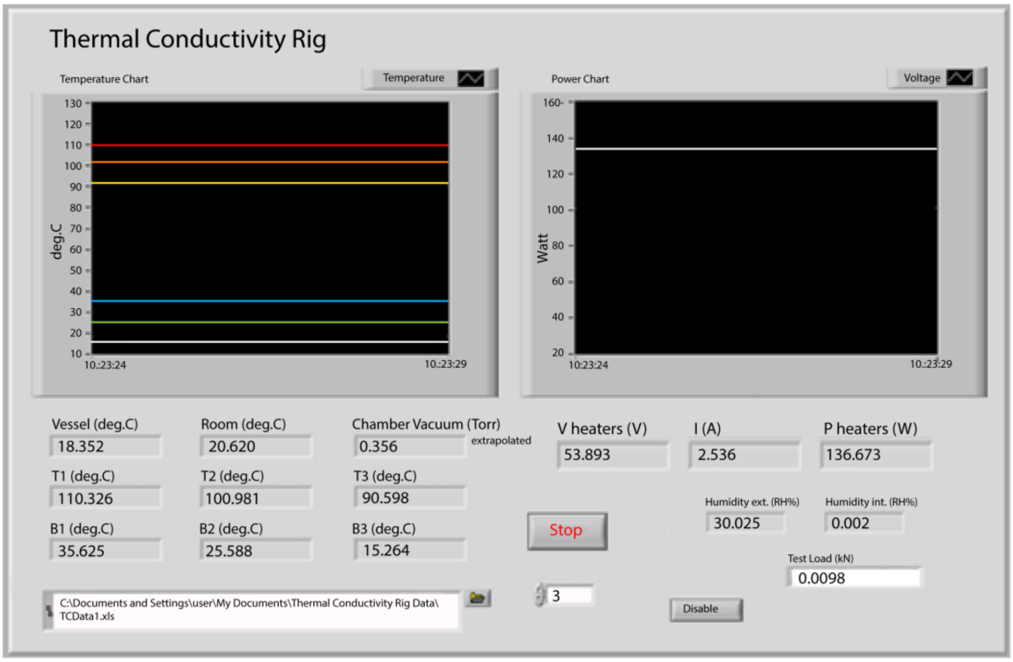

Vessel (deg.C) 18.352
Room (deg.C) 20.620
Chamber Vacuum (Torr) 0.356 extrapolated
V heaters (V) 53.893
I (A) 2.536
P heaters (W) 136.673
T1 (deg.C) 110.326
T2 (deg.C) 100.981
T3 (deg.C) 90.598
B1 (deg.C) 35.625
B2 (deg.C) 25.588
B3 (deg.C) 15.264
Humidity ext. (RH%) 30.025
Humidity int. (RH%) 0.002
Test Load (kN) 0.0098
C:\Documents and Settings\user\My Documents\Thermal Conductivity Rig Data\TCData1.xls
3

Figure 7.2 The interface of the LabView programme.

It is important to note that every measurement in this study was repeated at least twice in order to check for repeatability. If the results were not repeatable then further measurements were made until repeatable results were obtained.

7.2.4 Methodology

The axial heat flux through the tested samples was estimated by averaging the heat fluxes through upper and lower flux meters by using the following equations:

$$q_{up} = k_m \frac{T_1 - T_3}{L_1 - L_3} \quad (7.2)$$

$$q_{low} = k_m \frac{T_4 - T_6}{L_4 - L_6} \quad (7.3)$$

$$q_s = \frac{q_{up} + q_{low}}{2} \quad (7.4)$$

where q_s is the heat flux through the sample, q_{up} is the heat flux through the upper flux-meter, q_{low} is the heat flux through the lower flux-meter, k_m is the thermal conductivity of the standard material, and T_1, T_2, T_3, T_4,T_5, and T_6 are the temperatures measured by the first, second, third, fourth, fifth and the sixth thermocouples, respectively.

The temperature drop ΔT across the test sample is obtained by ‘joining’ the temperature gradients of the lower and upper fixtures, as shown in Figure 7.3.

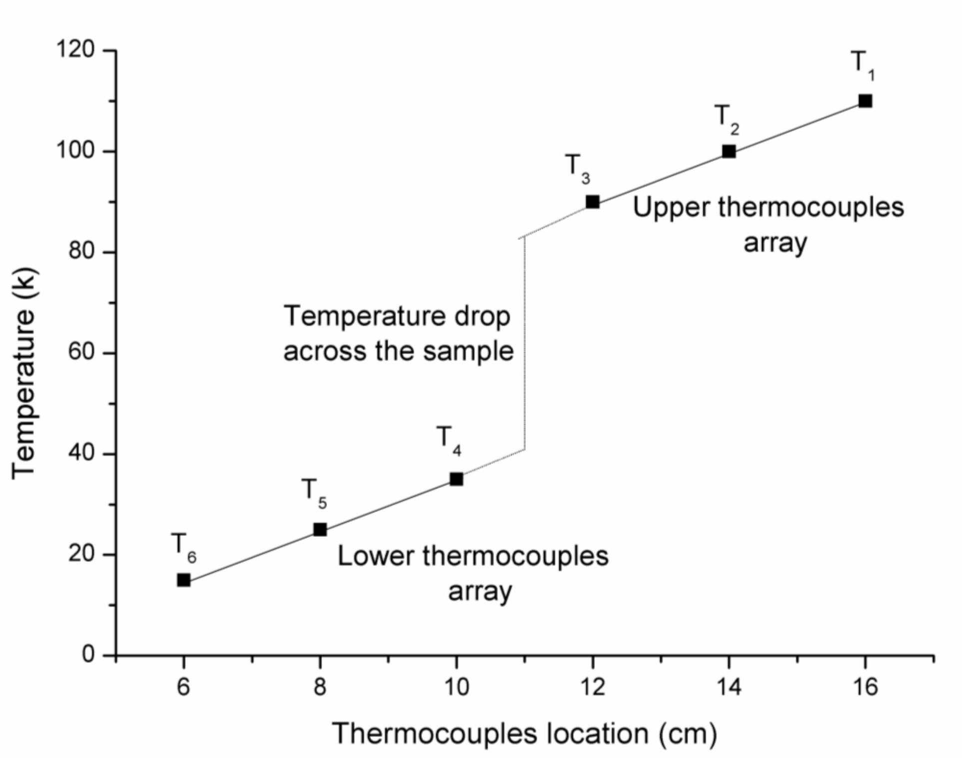

Figure 7.3 A typical steady state temperature profile through the fixture.

The total resistance, RTotal, to the heat flow, which is the sum of ‘bulk’ thermal resistance and the contact resistance [59], can be expressed using the Fourier equation as follows:

$$R_{Total} = \frac{\Delta T}{q_s} = 2R_{H-sample} + R_{th} \tag{7.5}$$

where R_{th} is the sample thermal resistance, $R_{H\text{-}sample}$ is the contact resistance between the sample and the holder, ΔT is the temperature drop across the sample, and q_s is the heat transferred through the sample which is given by equation (4). The thermal contact resistance is calculated from the total resistance for a single GDL as follows:

$$R_{total} = R_{sample} + 2R_{H-sample} \tag{7.6}$$

Since it is not feasible to estimate the contact resistance between the sample and the holder using a single sample with a given thickness, we need either to change the thickness of the sample used or use a stack of samples. However, it is significantly difficult to vary the thickness of the sample as typically the GDL is not available in different thicknesses. Alternatively, the thickness is varied by making stacks of different numbers of individual GDL samples and assuming that the contact resistance between the samples are the same [83]. However, this introduces a new variable, which is the contact resistance between individual samples. So, the total contact resistance for a stack of GDL samples is calculates as follows:

$$R_{total,n} = nR_{sample} + (n-1)R_{sample-sample} + 2R_{H-sample} \tag{7.7}$$

In the current study, a stack of five GDL samples is used to vary the thickness of the tested specimens. This means that there will be five equations with three unknowns in order to ensure that the assumption that the contact resistance between the samples are the same.

The thermal resistance offered by the sample is given by:

$$R_{total,1} = R_{sample} + 2R_{H-sample} \tag{7.8}$$

The thermal resistance offered by the sample is given by:

$$R_{th} = \frac{L_s}{k_s A_s} \tag{7.9}$$

where L_S is the length of the sample, k_S is the thermal conductivity, and A_S is the heat transfer area [59]. For a given compression, the contact resistance between the GDL sample and the holder surface is assumed to be insensitive to the number of the samples involved in the stack. Then, the thermal conductivity of the sample k_S is calculated from the slope of the curve of the total thermal resistance as a function of GDL thickness:

$$k_s = \frac{1}{slope} \times \frac{1}{A_s} \tag{7.10}$$

7.2.5 Validation of the measurement technique

The experimental technique was validated by using a standard thin film material. The thermal conductivity of a stack of 27±2.5 *μm* aluminum foils was measured to be about 236.3 ± 4.2 W·m^{-1}·K^{-1}, which was found to be in good agreement with the reported value for the thermal conductivity of aluminum foils, which is about 235 W·m^{-1}·K^{-1} at room temperature [15].

7.2.6 Uncertainty analysis

The uncertainty in the thermal conductivity values can be estimated based on the combined uncertainties in the dimensions of the sample, and the temperature drop across the sample [100] as follows:

$$\frac{\delta k}{k} = \sqrt{\left(\frac{\delta T_c}{T_c}\right)^2 + \left(\frac{\delta T_h}{T_h}\right)^2 + \left(\frac{\delta L}{L}\right)^2 + \left(\frac{\delta A}{A}\right)^2} \tag{7.11}$$

where T_c and T_h are the temperature of the cold and hot plates, respectively. L is the length of the sample and A is the sample cross sectional area.

The uncertainty in the through-plane thermal conductivity value is calculated and reported for all the measurements and it was not more than 8% in this study.

7.3 Results and Discussions

7.3.1 Effect of the temperature on the through-plane thermal conductivity of the membrane

As seen in Figure 7.4, the through-plane thermal conductivity of the membrane is in good agreement with the in-plane thermal conductivity of the membrane, which has been previously measured [76], and this is because of the homogenous nature of the membrane. The maximum through-plane thermal conductivity of the membrane was 0.193±0.02 $W\cdot m^{-1}\cdot K^{-1}$ when the temperature was 35 °C, and as the temperature increases then the thermal conductivity of the membrane decreases. For example, the minimum through-plane thermal conductivity of the membrane was 0.132±0.02 $W\cdot m^{-1}\cdot K^{-1}$ when the temperature was 80 °C.

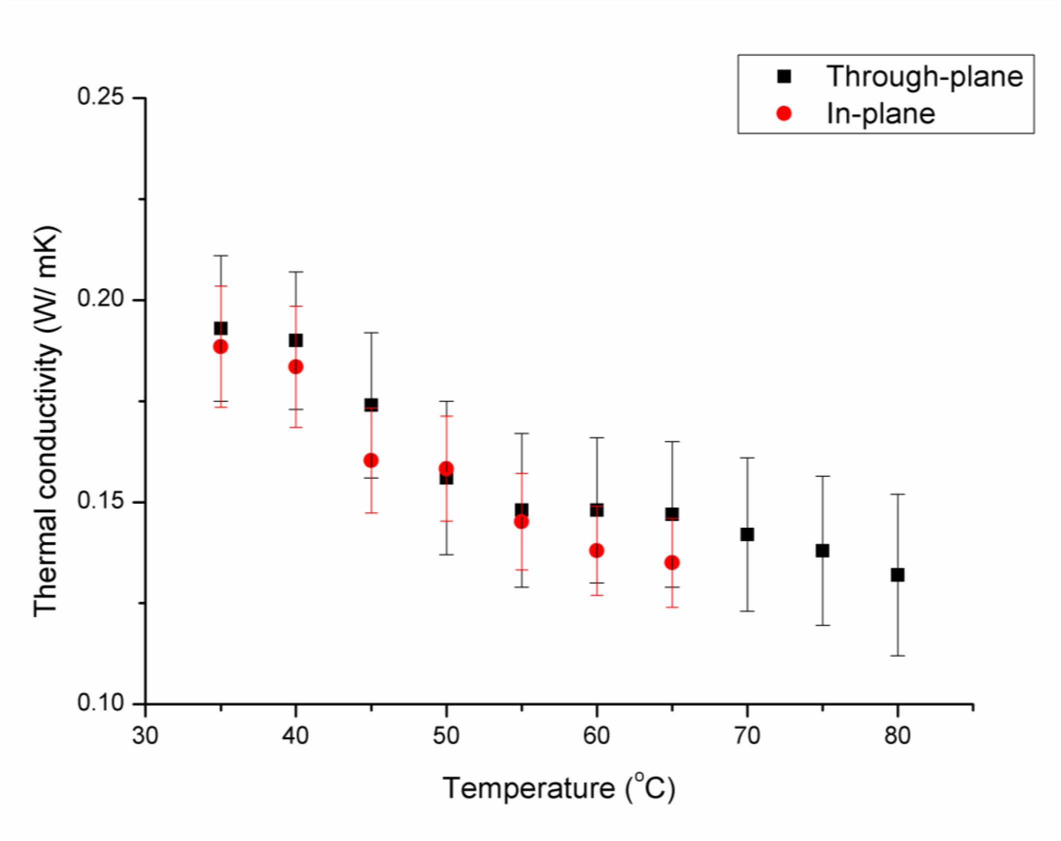

Figure 7.4 Measured in- and through-plane thermal conductivities of the membrane as a function of the temperature along with the experimental error bars.

This decrease in the thermal conductivity of the membrane is due to the increase in the thermal resistance of the membrane with temperature, as shown in Figure 7.5. This decrease with increasing temperature is due to the decrease in the phonon mean free path for the material of the Nafion® membranes [103].

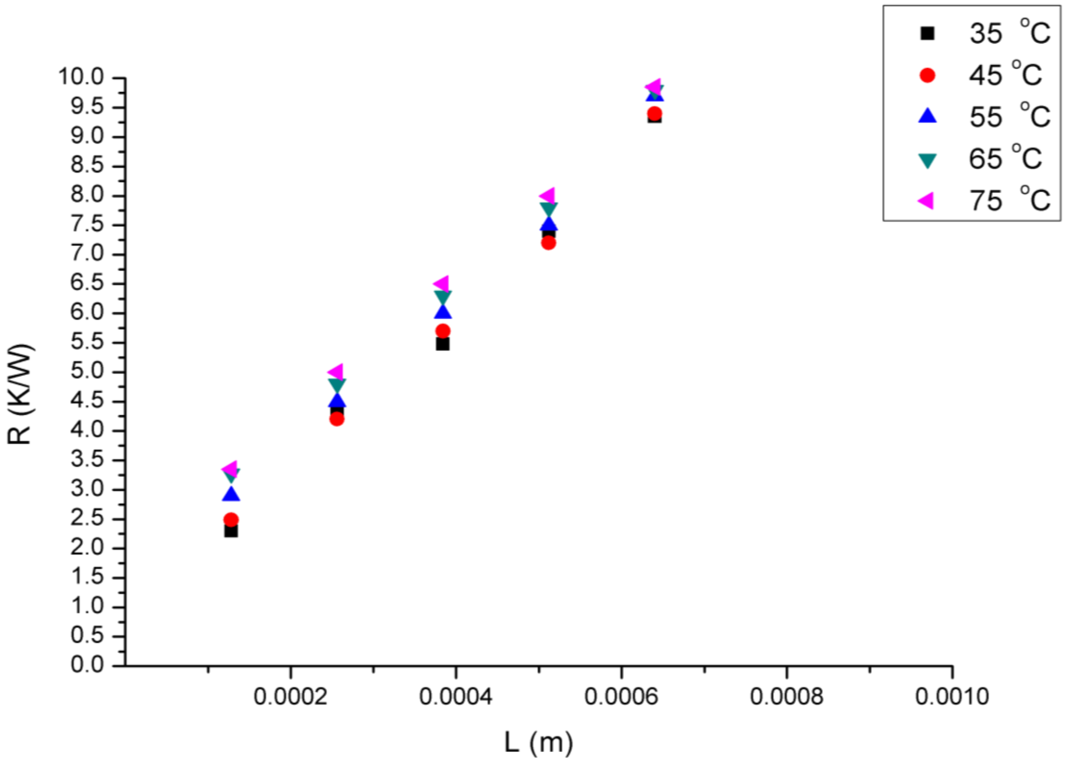

Figure 7.5 Measured thermal resistance of the membrane as a function of the temperature.

7.3.2 Effect of the temperature on the through-plane thermal conductivity of the GDL

Due to the presence of the PTFE binder and the polymeric resin, whose thermal conductivities decrease with increasing temperature, the total thermal resistance of the GDL was found to increase with increasing temperature and subsequently the thermal conductivity decreases as the temperature increases [108]. This effect is clearly shown in Figure 7.6. However, the through-plane thermal conductivity of GDL is significantly lower than its in-plane thermal conductivity [76].

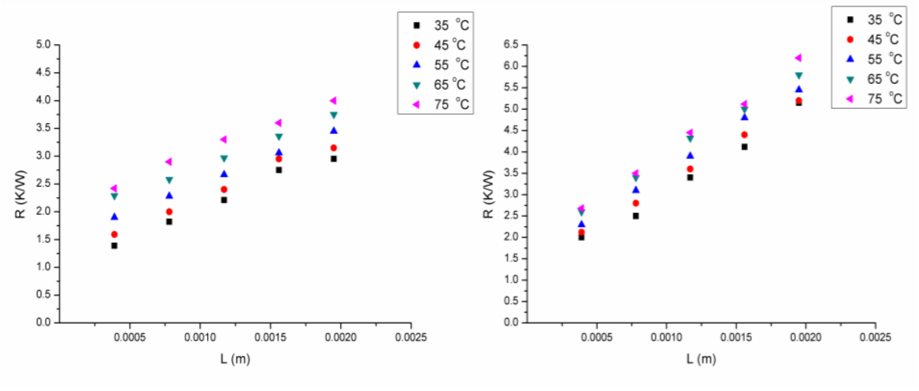

(a) SGL 10AA (b) SGL 10BA

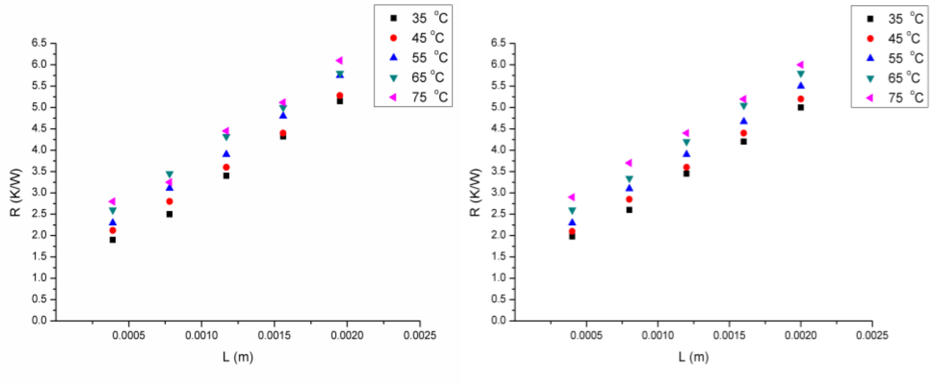

(c) SGL 10CA (d) SGL 10DA

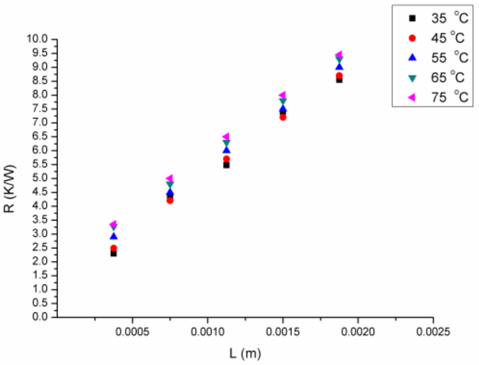

(e) SGL 10EA

Figure 7.6 Measured thermal resistances of the GDLs as a function of the temperature for (a) SGL 10AA, (b) SGL 10BA, (c) SGL 10CA, (d) SGL 10DA, and (e) SGL 10EA.

7.3.3 Effect of the PTFE loading on the through-plane thermal conductivity of the GDLs

Since the heat transfer is from fibre to fibre in the through-plane direction, the addition of PTFE decreases the through-plane thermal conductivity of the gas diffusion layer because of the low thermal conductivity of the PTFE, which is about 0.25 $W \cdot m^{-1} \cdot K^{-1}$ [109,110].

As illustrated in Figure 7.7, overall, the thermal conductivity of the GDL significantly decreases after PTFE-treatment. The GDL, without PTFE, has the highest through-plane thermal conductivity and its thermal conductivity is about 50% higher than that of the PTFE-treated GDLs. However, the real relation between adding PTFE and the through-plane thermal conductivity of the GDL is not clear as there was no significant difference in the through-plane thermal conductivity of the GDL after adding 5, 10, 20, and 30% PTFE to the GDL. This point certainly requires further investigation. The through-plane thermal conductivities of the PTFE treated GDL at different mean temperature are listed in Table 7.1.

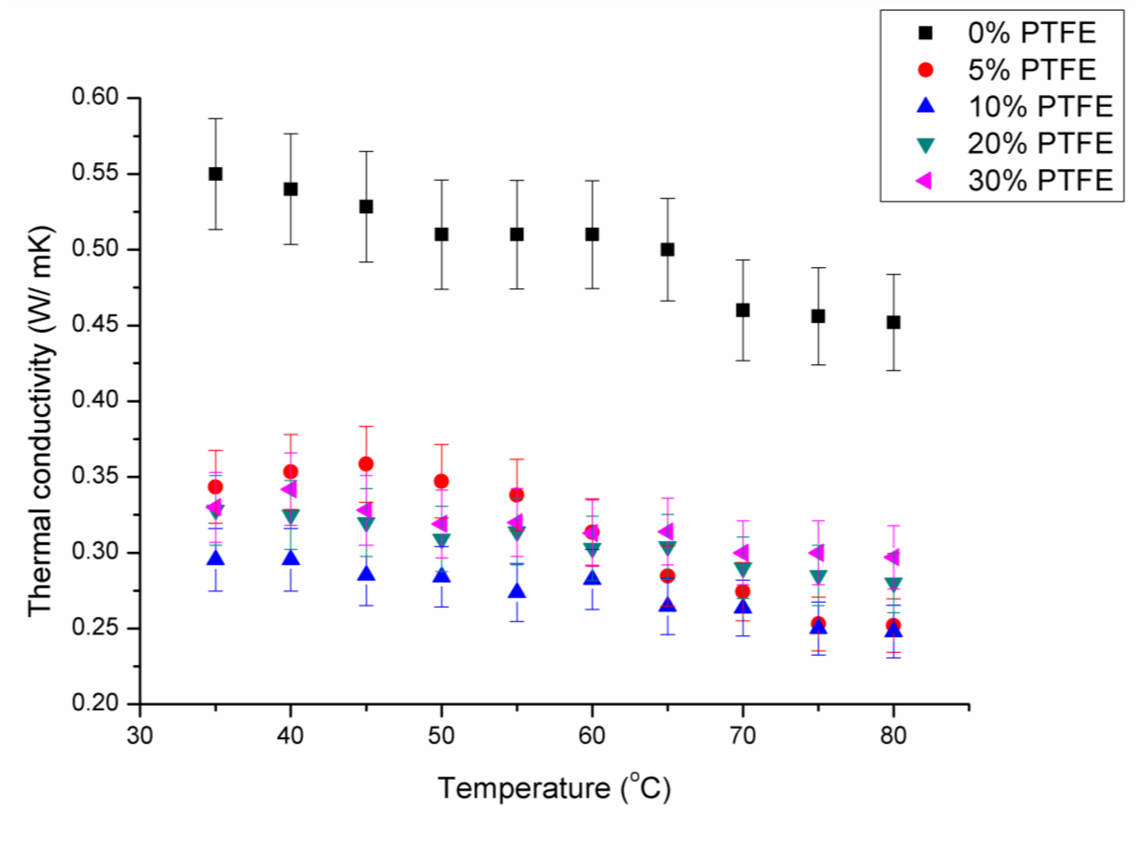

Figure 7.7 Measured thermal conductivity of the GDLs as a function of the temperature and PTFE loading along with the experimental error bars.

Table 7.1 List of the through-plane thermal conductivities of the PTFE-loaded GDLs.

GDL Sample	Temperature (^0C)	The thermal in-plane conductivity ($W \cdot m^{-1} \cdot K^{-1}$)
10AA	35	0.55 ± 0.036
	45	0.53 ± 0.035
	55	0.51 ± 0.036
	65	0.50 ± 0.034
10BA	35	0.34 ± 0.024
	45	0.36 ± 0.025
	55	0.34 ± 0.021
	65	0.28 ± 0.020
10CA	35	0.29 ± 0.020
	45	0.29 ± 0.019
	55	0.27 ± 0.019
	65	0.26 ± 0.021
10DA	35	0.33 ± 0.022
	45	0.32 ± 0.022
	55	0.32 ± 0.022
	65	0.31 ± 0.021
10EA	35	0.33 ± 0.023
	45	0.32 ± 0.023
	55	0.32 ± 0.022
	65	0.31 ± 0.022

7.3.4 Effect of compression pressure on the through-plane thermal conductivity of the GDL

In PEM fuel cells, the GDL is deforming under the ribs and the thickness of the GDL under the ribs is less than its thickness under the channel. The GDL thickness is greatly affected by the external compression, which affects the transport properties, the contact resistance and the thermal and electrical conductivities of the GDL and these subsequently affect the temperature and the water management in PEM fuel cells [119]. Therefore, the effect of the compression on the thermal conductivity of the GDL is needed to be taken into account. The effect of compression pressure on the reduction in the thickness of the GDL is shown in Figure 7.8.

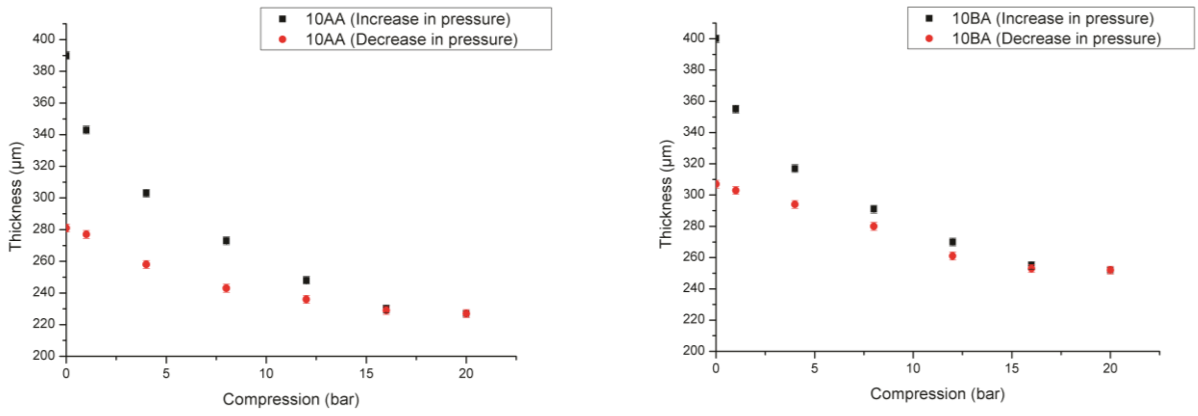

(a) SGL 10AA

(b) SGL 10BA

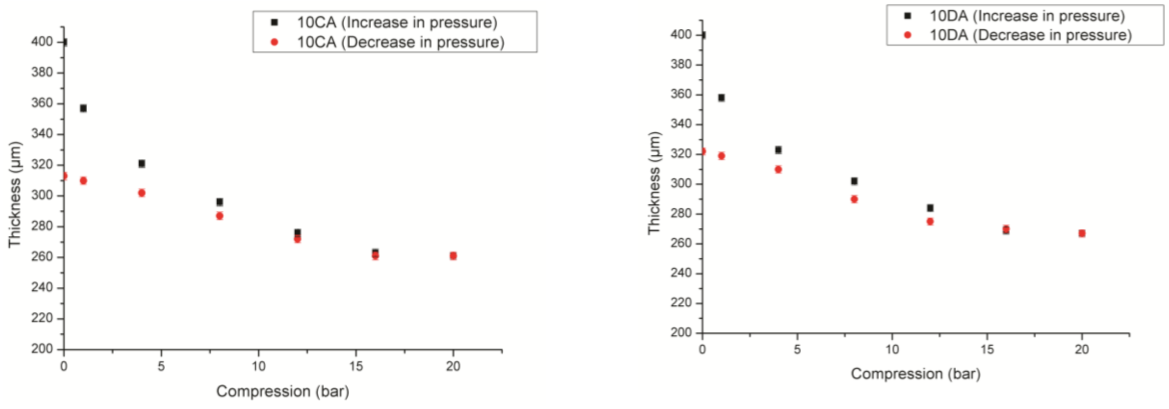

(c) SGL 10CA

(d) SGL 10DA

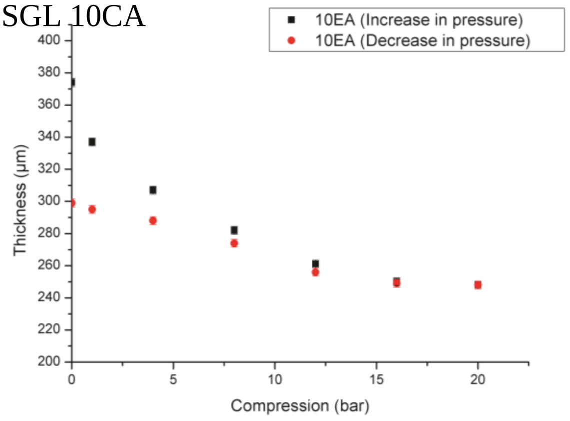

(e) SGL 10EA

Figure 7.8 Hysteresis in the thickness of the GDL under the external compression for (a) SGL 10AA, (b) SGL 10BA, (c) SGL 10CA, (d) SGL 10DA, and (e) SGL 10EA.

The reduction in the thickness is initially very high when applying the compression pressure. Then, the variation in thickness is almost negligible after increasing the pressure which indicates that the deformation of the GDL has ‘saturated’. Note that there is an hysteresis effect in the compression curves which signals that there has been a permanent deformation in the compressed GDL sample [120]. In Figure 7.9, the effect of the applied load on the thermal resistance has been investigated. It is clear that the thermal resistance values of the treated GDLs are higher than that of the untreated GDL. This is due to the increase in the contact resistance between the fibres of the GDL after adding the PTFE [121].

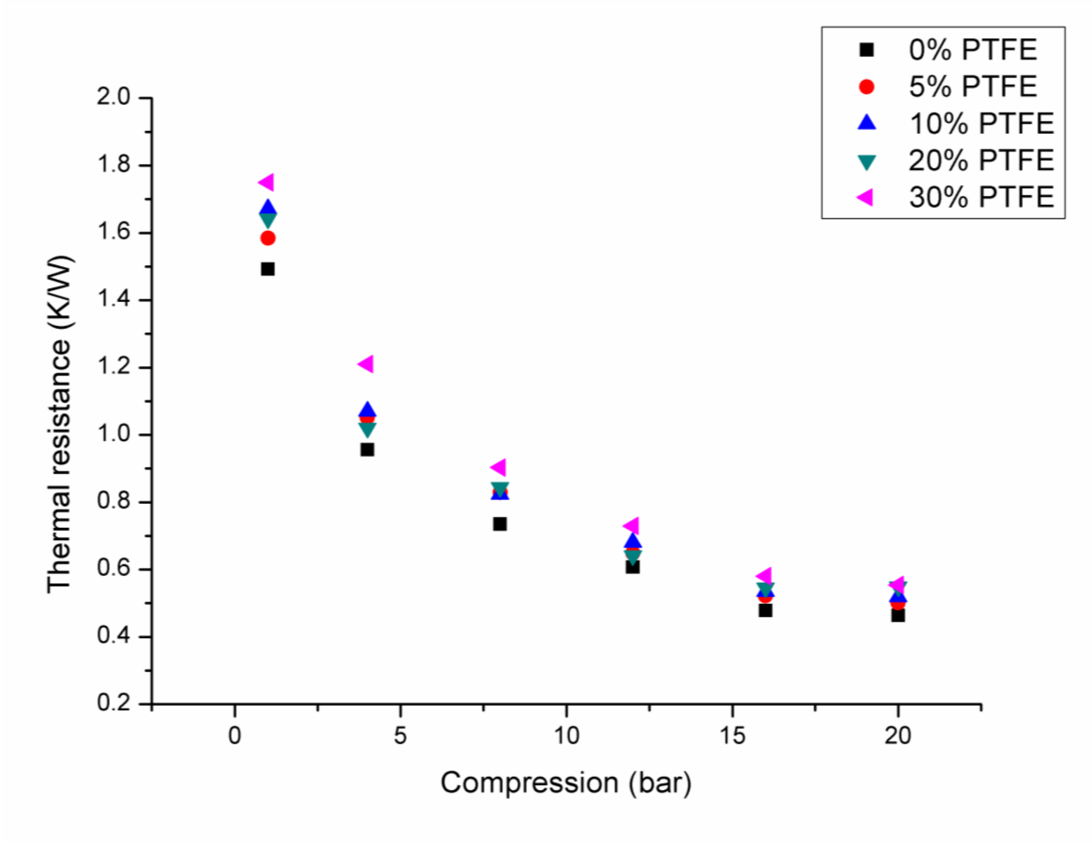

Figure 7.9 Measured thermal resistance of the GDLs at different compression loads.

The through-plane thermal conductivity of the GDL increases when the compression pressure increases, as shown in Figure 7.10. This is as a result of the larger contact area and consequently this provides more heat paths and thus the higher thermal conductivity [122].T he values of the through-plane thermal conductivity of the GDL under different compression pressure are listed in Table 7.2.

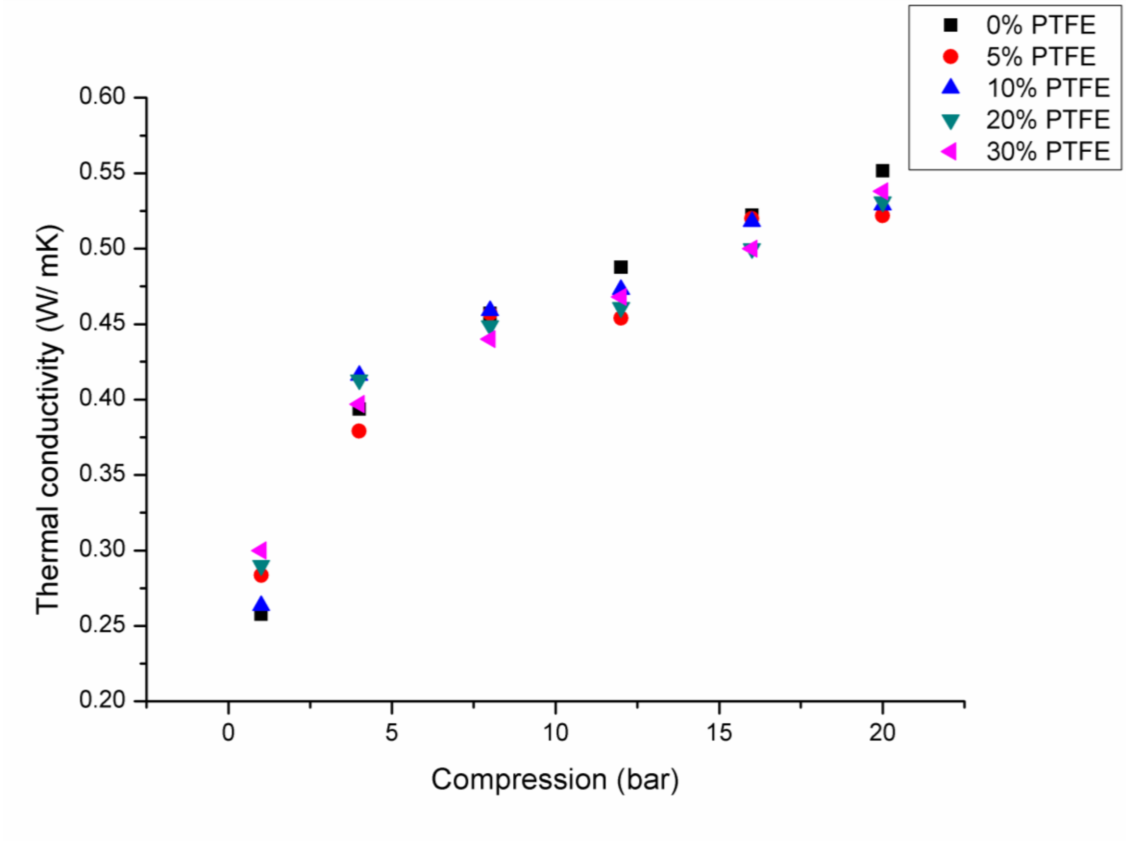

Figure 7.10 Measured thermal conductivity of the GDLs at different compression loads.

Table 7.2 List of the through-plane thermal conductivities of the PTFE-loaded GDLs with different compression.

GDL Sample	Compression (bar)	The thermal through-plane conductivity (W·m^{-1}·K^{-1})
10AA	4	0.39 ± 0.026
	8	0.46 ± 0.037
	12	0.49 ± 0.032
	16	0.52 ± 0.036
10BA	4	0.37 ± 0.025
	8	0.46 ± 0.034
	12	0.45 ± 0.031
	16	0.52 ± 0.030
10CA	4	0.41 ± 0.031
	8	0.46 ± 0.036
	12	0.47 ± 0.033
	16	0.51 ± 0.034
10DA	4	0.41 ± 0.034
	8	0.45 ± 0.033
	12	0.46 ± 0.032
	16	0.51 ± 0.031
10EA	4	0.39 ± 0.028
	8	0.44 ± 0.031
	12	0.46 ± 0.032
	16	0.51 ± 0.036

7.3.5 Effect of the MPL coating on the through-plane thermal conductivity of the GDL

In order to enhance the water and thermal management in the PEM fuel cells, a micro porous layer (MPL) is added to the gas diffusion layer. This layer consists of a carbon black powder and hydrophobic agent [112].

The thermal contact resistance of the GDL samples decreases when the MPL is added to the GDL. This is not surprising as one of the main aims of adding MPL to the GDL in the fuel cell is to improve the contact between the GDL and the catalyst layer, see Figure 7.11.

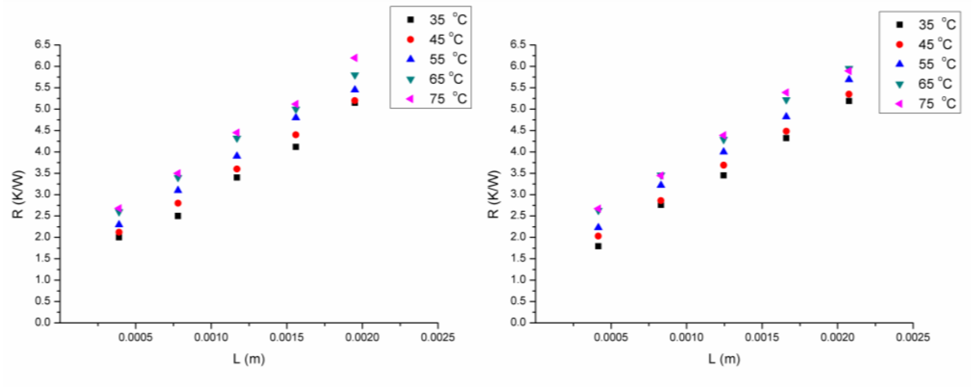

(a) SGL 10BA (b) SGL 10BC

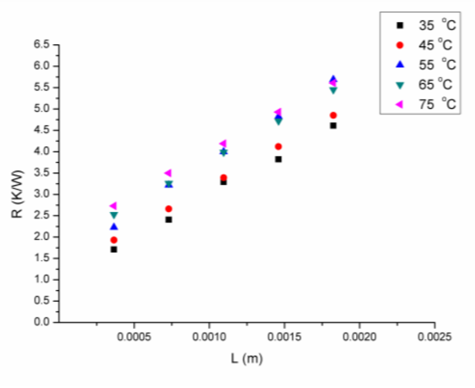

(c) SGL 10BE

Figure 7.11 Measured thermal resistance for the tested GDLs (a) SGL 10BA, (b) SGL 10BC, and (c) SGL 10BE.

Furthermore, it is clear from Figure 7.12 that the untreated 10BA has a lower thermal conductivity than that of 10BC and 10BE, which are MPL coated GDLs. The main reason for this is that the MPL is rich in carbon powder which is considered as a high thermal conductivity material compared to the thermal conductivity of the untreated GDL.

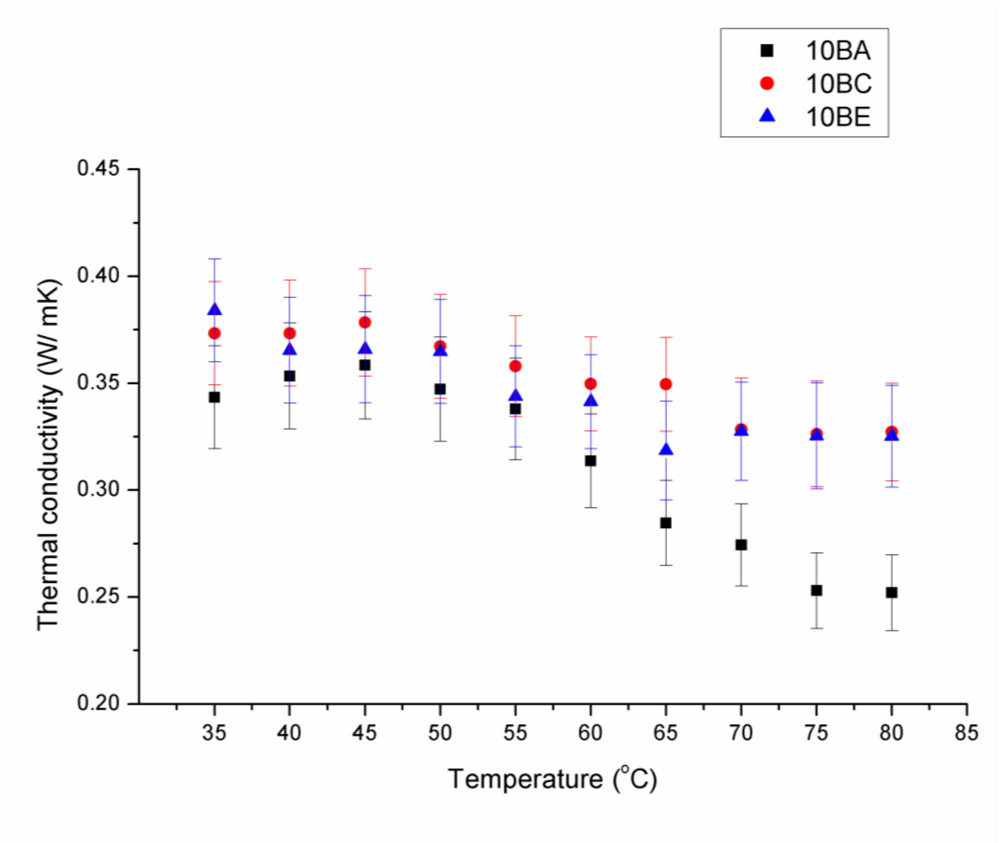

Figure 7.12 Measured thermal conductivity for the MPL GDLs along with the experimental error bars.

The through-plane thermal conductivities of the MPL treated GDL at different mean temperature are listed in Table 7.3.

Table 7.3 List of through-plane thermal conductivities of the MPL-coated the GDLs.

GDL Sample	Temperature (^{0}C)	The thermal conductivity (W·m^{-1}·K^{-1})
10BA	35	0.34 ± 0.024
	45	0.36 ± 0.025
	55	0.34 ± 0.021
	65	0.28 ± 0.020
10BC	35	0.37 ± 0.024
	45	0.38 ± 0.025
	55	0.36 ± 0.023
	65	0.45 ± 0.022
10BE	35	0.38 ± 0.024
	45	0.36 ± 0.025
	55	0.34 ± 0.023
	65	0.32 ± 0.022

7.3.6 Effect of the temperature on the through-plane thermal conductivity of the catalyst layer

The through-plane thermal conductivity of the catalyst layer was investigated by manually spraying the Pt ink onto some 10BA GDL samples and then measure the through-plane thermal conductivity of the samples before and after adding the catalyst layer. Since the layers are lumped in series, the series model [84, 85] illustrated in Figure 13 was used to calculate the thermal conductivity of the catalyst, as follows:

$$k_{total} = \frac{1}{\frac{v_{cl}}{k_{cl}} + \frac{v_{GDL}}{k_{GDL}}} \tag{7.13}$$

where k_{total} is the thermal conductivity of the catalysed GDL. k_{GDL} and k_{cl} are the thermal conductivities of the GDL and catalyst layer, respectively. v_{GDL} and v_{cl} are the volume fractions of the GDL and catalyst layer, respectively.

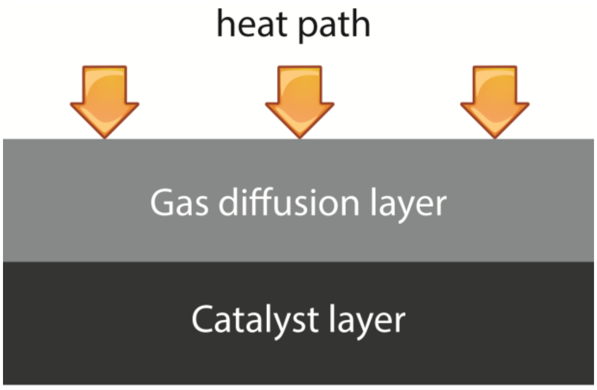

Figure 7.13 Calculating the thermal conductivity of the catalyst using the series model.

As shown in Figure 7.14, the through-plane thermal conductivity of the catalyst layer, with 0.4 mg·cm^{-2} platinum loading, was found to be comparable with the in-plane thermal conductivity of the catalyst layer which has been previously measured and reported in [76]. This indicates that the catalyst layer is a homogenous material. Furthermore, the through-plane thermal conductivity of the catalyst layer was almost insensitive to the temperature. The maximum through-plane thermal conductivity of the catalyst layer is 0.345 ± 0.02 W·m^{-1}·K^{-1} when the temperature is 35 °C, and the minimum through-plane thermal conductivity of this catalyst layer is 0.334 ± 0.02 W·m^{-1}·K^{-1} when the temperature is 80 °C.

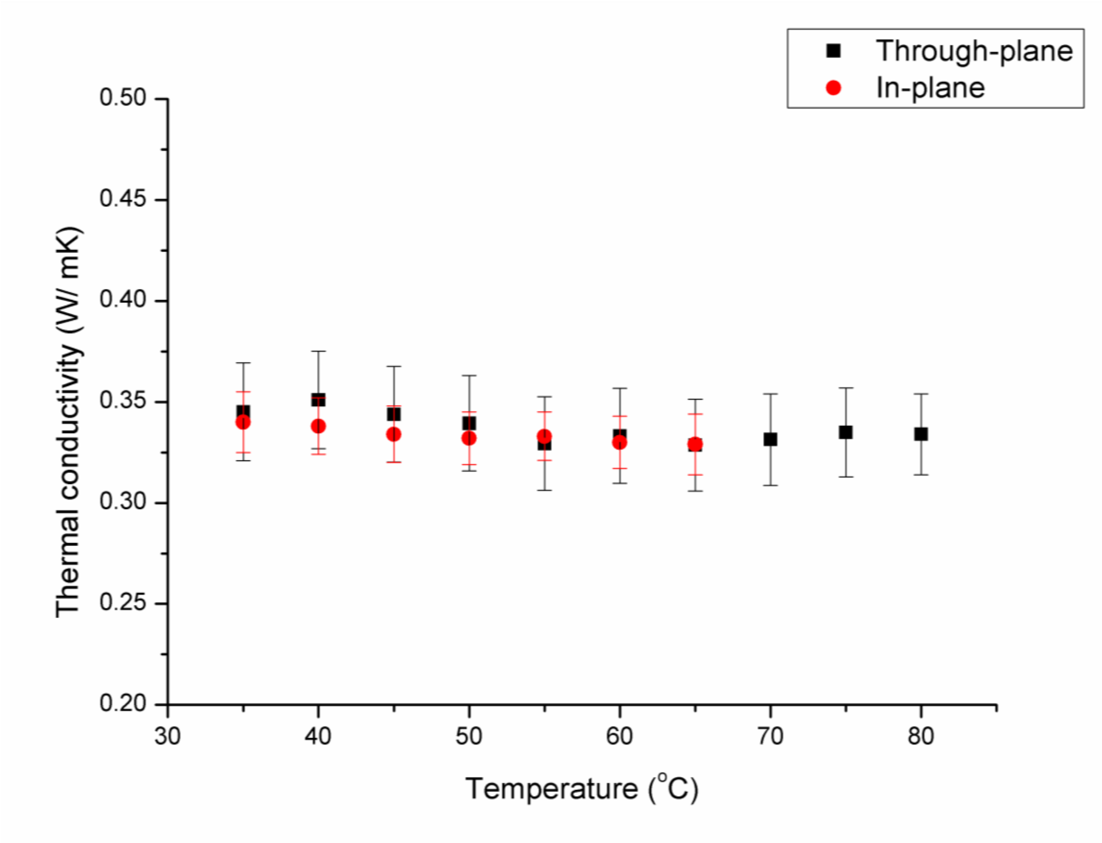

Figure 7.14 Measured thermal conductivity of the catalyst layers as a function of the temperature along with the experimental error bars (the platinum loading for this case is 0.4 mg·cm^{-2}).

In order to investigate the effects of the Pt loading on the through-plane thermal resistance of the catalyst layer, the catalyst layers with three different Pt loadings (0.2, 0.4, 0.6) mg·cm^{-2} were prepared and the through-plane thermal resistance of them were compared, see Figure 7.15.

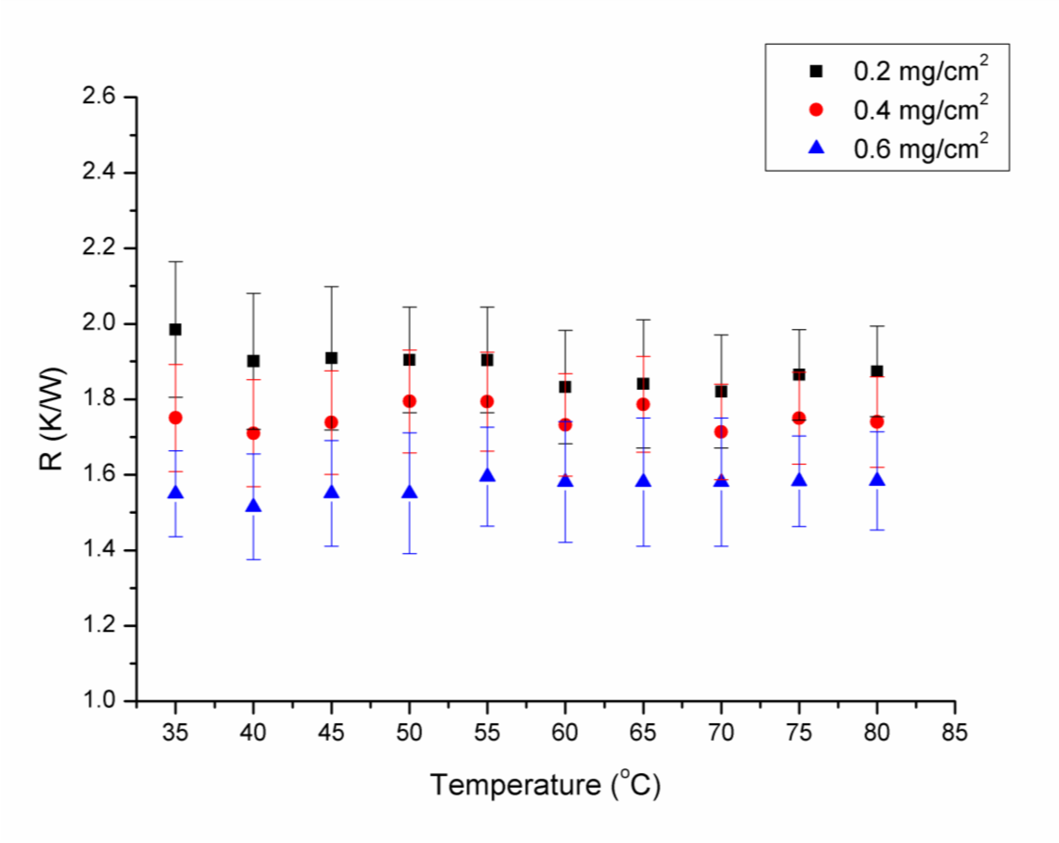

Figure 7.15 Measured thermal resistances of the catalyst layers as a function of the Pt loading along with the experimental error bars.

The through-plane thermal resistance of the catalyst layer was found to decrease with Pt loading. This is mainly because of the thickness of the catalyst layer. As the platinum loading increases, the thickness of the catalyst layer increases. This leads to a better contact between the catalyst layer and the holder of the sample. Therefore, the reduction in the total resistance as a result of increasing the platinum loading is more to do with the contact resistance and not with the thermal conductivity which must ideally remain constant.

7.4 Conclusions

In this study, an experimental technique has been developed to determine the through-plane thermal conductivity and the contact resistance of the components in the MEA. The main conclusions of these measurements are as follows:

- The through-plane thermal conductivity of the membrane was found to be comparable with the in-plane thermal conductivity and it decreases with increasing the temperature. The through-plane thermal conductivity of the membrane was found to be 0.193 ± 0.018 $W \cdot m^{-1} \cdot K^{-1}$ and 0.132 ± 0.02 $W \cdot m^{-1} \cdot K^{-1}$ when the temperature was 35 °C and 80 °C, respectively.

- The through-plane thermal conductivity of the GDL was found to be significantly lower than its in-plane thermal conductivity. The through-plane thermal conductivity of the GDL decreases with increasing the temperature and increases with increasing compression pressure.

- The through-plane thermal conductivity of the catalyst layer is comparable to its in-plane thermal conductivity and it was found to be almost insensitive to the temperature and the thermal resistance of the catalyst layer decreases slowly with Pt loading due to the increase in the thickness of the catalyst layer and the contact resistance. The through-plane thermal resistance of the catalyst layer, when the temperature was 35 °C, was found to be 1.985 ± 0.18 $K \cdot W^{-1}$and 1.553 ± 0.13 $K \cdot W^{-1}$ when the Pt loading was 0.2 and 0.6 $mg \cdot cm^{-2}$, respectively.

The through-plane thermal conductivity of the MEA components provides some of the necessary parameters which will enhance the predictions of the profiles of temperature and water saturation in PEM fuel cells.

Chapter 8
Conclusions and Possible Future Work

8.1 Introduction

In this thesis, a numerical study has been performed in order to investigate the effect of the anisotropic thermal conductivity of the components of the membrane electrode assembly (MEA), namely the gas diffusion layer, the catalyst layer and the membrane, on the performance of proton exchange membrane (PEM) fuel cells. In addition, the sensitivity of the temperature distribution and the water saturation in the PEM fuel cells to the thermal conductivity of the components of the MEA has been highlighted based on the application of the computational fluid dynamics (CFD) technique. The commercial Fluent® software was used to simulate the PEM fuel cells in all the cases presented in this study, and the results obtained have been validated with those obtained experimentally using an in-house PEM fuel cell. In addition, the experimental techniques were developed to measure the thermal conductivity of the components of PEM fuel cells in both directions, namely the in-plane and the through-plane directions, in order to provide comprehensive results on the thermal conductivity of the components in PEM fuel cells.

The novel aspects of this thesis are summarised in the following section of this chapter; this is followed by all the main conclusions from the modelling and the experimental works performed, and the suggestions on possible future work are illustrated in the last section of this chapter.

8.2 Novel Aspects of the Project

The research which has been carried out in this thesis has provided unique contributions in the following fields:

- A numerical investigation on the effect of the inhomogeneous thermal conductivity of the gas diffusion layer (GDL) has been performed. This shows that the inhomogeneous thermal conductivity of the GDL cannot be neglected due to the sensitivity of the PEM fuel cell performance to the thermal conductivity of the GDL. In addition, increases in the thermal conductivity of the GDL decreases the maximum temperature in the GDL which, in turn, leads to a more uniform temperature within the MEA, and more water to be humidified on the membrane.
- An investigation into the effects of a high electrical and thermal conductivity metal-based GDL with a uniform porous distribution and an optimized pore size instead of

the conventional GDL on the performance of PEM fuel cells. This alternative metallic-based GDL maximizes the performance of the PEM fuel cells and assists in achieving a uniform temperature distribution across the GDL.

- The experimental techniques for measuring the thermal conductivity and the contact resistance have been developed to measure the thermal conductivity of the components in PEM fuel cells in the two main directions, namely the in-plane and the through-plane directions. These techniques could be used to measure the thermal conductivity and the contact resistance of any micro scale material and take into account many parameters, such as the effect of compression pressure, temperature, fibre direction, MPL coatings, and PTFE loadings. This provides a comprehensive study on the thermal conductivity of the components in PEM fuel cells which provides some of the necessary parameters that may be used in CFD models to better understand the thermal and water management in PEM fuel cells, which is one of the main issues when operating the PEM fuel cells.

8.3 General Conclusions

In order to have a comprehensive study on the thermal conductivity of the components of the PEM fuel cells, this study provides the experimental measurements and the numerical investigations on the effect of the thermal conductivity of MEA components on the performance of PEM fuel cells and the main conclusions are as follows:

8.3.1 Modelling conclusions

The sensitivity of the PEM fuel cells' performance to the thermal conductivities of the membrane, GDL and catalyst layers is reported in Chapters 2 to 4. A 3-D multiphase model was developed in the Fluent® software to investigate the effect of the anisotropic thermal conductivity of the GDL, the thermal conductivity of the catalyst layer, the thermal conductivity of the membrane and the metallic-based GDL. All the results were experimentally validated with an in-house PEM fuel cell. The main conclusions are as follows:

- It has been found that the power density of PEM fuel cells increases due to the decrease in the electrical resistance in the fuel cell when the thermal conductivity of the GDL increases in both directions, namely the in-plane and the through-plane directions. Moreover, increasing the thermal conductivity of the GDL results in a more uniform temperature distribution and decreases the temperature gradient in the membrane electrode assembly due to the dissipation of heat from the MEA. Additionally, this leads to an increase in the liquid water saturation as the maximum temperature decreases and this assists in humidifying more liquid water in the membrane.

- The performance of PEM fuel cells increases significantly in PEM fuel cells operating with copper-based and aluminium-based GDLs compared with that operating with a conventional GDL. This is because of the high thermal and electrical conductivity of the metallic GDL compared to the conventional GDL. In addition, using the metallic GDL increases the liquid water saturation and decreases the temperature gradient which enhances the performance of PEM fuel cells.
- The temperature gradient decreases when the thermal conductivities of the membrane or the catalyst layer increase due to the dissipation of the heat from the MEA and this leads to a more uniform temperature in the membrane and more water saturation.

In general, it can be concluded that the performance of PEM fuel cells improves significantly with a better heat dissipation from the membrane and a more uniform temperature across the MEA which leads to more water saturation in the membrane. This could be achieved by increasing the thermal conductivity of the membrane electrode assembly components. The results of these numerical investigations into the effect of the thermal conductivity of the MEA indicate that it is extremely important to accurately determine the thermal conductivity of the GDL, the catalyst layer and the membrane.

8.3.2 Experimental conclusions

There are many experimental methods which may be used to measure thermal conductivity (see Chapter 5). However, due to the structure of the materials which are used in the PEM fuel cells and the micro scale length of the fuel cell components, two experimental techniques have been developed in Chapters 6 and 7 based on the steady state method to measure the thermal conductivity of the components in the PEM fuel cells. The thermal conductivity is measured in two directions, namely the in-plane direction with two orthogonal directions and the through-plane direction in the temperature range 35-80°C and in the compression range 0-20 bar, since these are the most likely average temperature and compression that occur in PEM fuel cells. The main conclusions from the experimental study are as follows:

- The parallel thermal conductance technique was designed, as shown in Chapter 6, to determine the in-plane thermal conductivity of the components in PEM fuel cells, namely the gas diffusion layer, the catalyst layer and the membrane. The results of this experimental investigation indicate that the in-plane thermal conductivity of the membrane and the GDL decreases when the mean temperature increases. This is because of the presence of the binders and the polymeric resins, and the fact that their thermal conductivity increases with increasing temperature. Furthermore, the addition of PTFE, which has a higher thermal conductivity than air, assists the heat transfer along the fibre direction, which increases the overall thermal conductivity of the GDL. In addition, the MPL treated GDLs have a higher in-plane thermal conductivity than the untreated GDLs. This is mainly because the MPL is rich in carbon powder which has a higher thermal conductivity compared to the GDL. Also, the in-plane thermal conductivity was higher when the fibres were oriented parallel to the heat flux than when the fibres were oriented normal to the heat flux in all the samples used in this investigation. This is because when the fibres are oriented parallel to the heat flux this provides a direct way for the heat to be transferred along the fibres. The in-plane thermal conductivity of the catalyst layer was found to be insensitive to the temperature and the in-plane thermal resistance of the catalyst layer increased with increasing Pt loading. This is due to the increase in the contact resistance of the catalyst layer as a result of increasing the thickness of the catalyst. .

- In Chapter 7 an experimental technique, based on the steady state method, has been developed to determine the through-plane thermal conductivity and the contact resistance of the components in the MEA. The results obtained show that the through-plane thermal conductivity of the GDL is at least one order of magnitude lower than the in-plane thermal conductivity of the GDL, and that this is due to the fibrous nature of the GDL. However, there was no significant difference between the in-plane and the through-plane thermal conductivities of the membrane and the catalyst layer, and this indicates that they are homogeneous materials. The measurements show that the through-plane thermal conductivity of the GDL decreases with increasing temperature and increases with increasing compression pressure. Similar to that found for the in-plane thermal conductivity of the catalyst layer, the through-plane thermal conductivity of the catalyst layer is found to be insensitive to the temperature and the through-plane thermal resistance of the catalyst layer increases with increasing Pt loading.

In conclusion, the obtained experimental results for measuring the in-plane and the through-plane thermal conductivity of the MEA components provides some of the necessary parameters which will enhance the future prediction of the heat distribution and the water saturation. Also, it will assist in the thermal management of PEM fuel cells and this is one of the essential issues that needs resolving in order to improve the fuel cell performance and lifetime.

8.4 Possible Future Work

This study highlights the effect of using metallic GDLs in PEM fuel cells. However, it will be of great interest if the metallic GDL could be investigated in more detail. More research is required on many parameters that occur in metallic GDLs and there is a need for further investigations, e.g., the effects of the porous diameter and the thickness of the metallic GDL on the performance of PEM fuel cells, as well as the distance between the pores (see Figure 8.1) or possibly to model the metallic GDL with a different range of metals, which may be coated with a low resistance material to achieve a novel design with an alternative material for the gas diffusion layer.

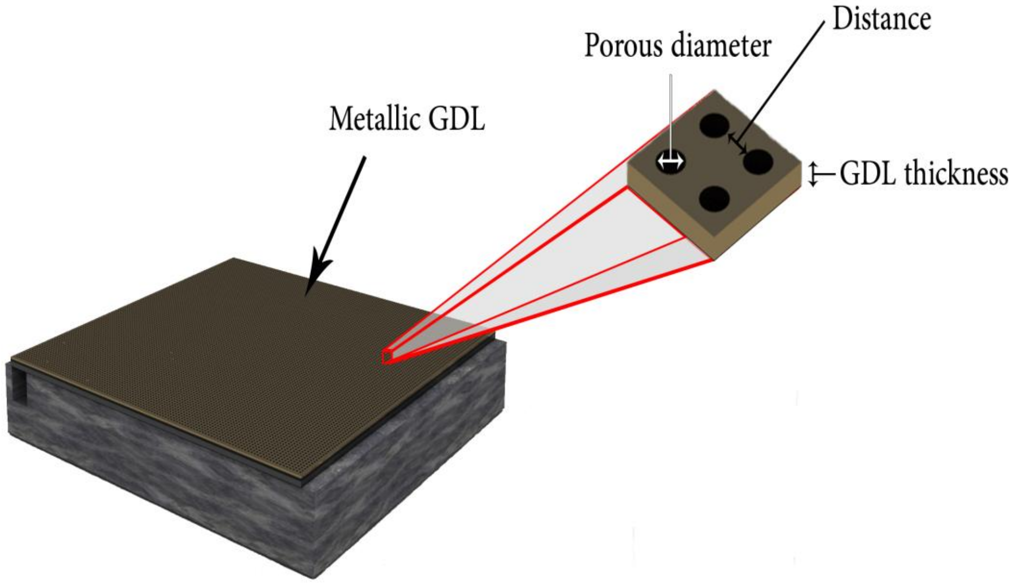

Figure 8.1 Some of the parameters that need further investigations in metallic GDLs.

One of the main limitations of this investigation is the very high computational expense, which is necessary in order to build the geometry and generate the mesh for every pore in the GDL. It is also worth completing this investigation by performing an experimental validation for an in-house PEM fuel cell with a metallic GDL.

In addition, investigating the effect of the anisotropic compression of the GDL on the performance of PEM fuel cell would be illuminating. Although the compression pressure under the channel regions is not the same as the compression pressure under the current collector regions, for simplicity and to save computational time and memory the GDL is usually assumed to be isotropic in the through-plane direction. However, there is a real need for modelling the GDL taking into consideration the anisotropic permeability, thermal conductivity and electrical conductivity in the through-plane direction, as illustrated in Figure 8.2. In addition, Section 7.4 indicates that there is a deformation on the carbon fibre GDL thickness under compression. The thickness of the GDL under the channels is about 400 µm and it is decreased to about 320 and 260 µm where the compression under the current collectors is about 4 and 16 bar, respectively.

It would be interesting to compare the differences between the effect of an isotropic compression of the GDL and the anisotropic compression of the GDL on the performance of PEM fuel cells. This could lead to accurate predictions for the thermal distribution in PEM fuel cells and provide more validation with experimental data from PEM fuel cells.

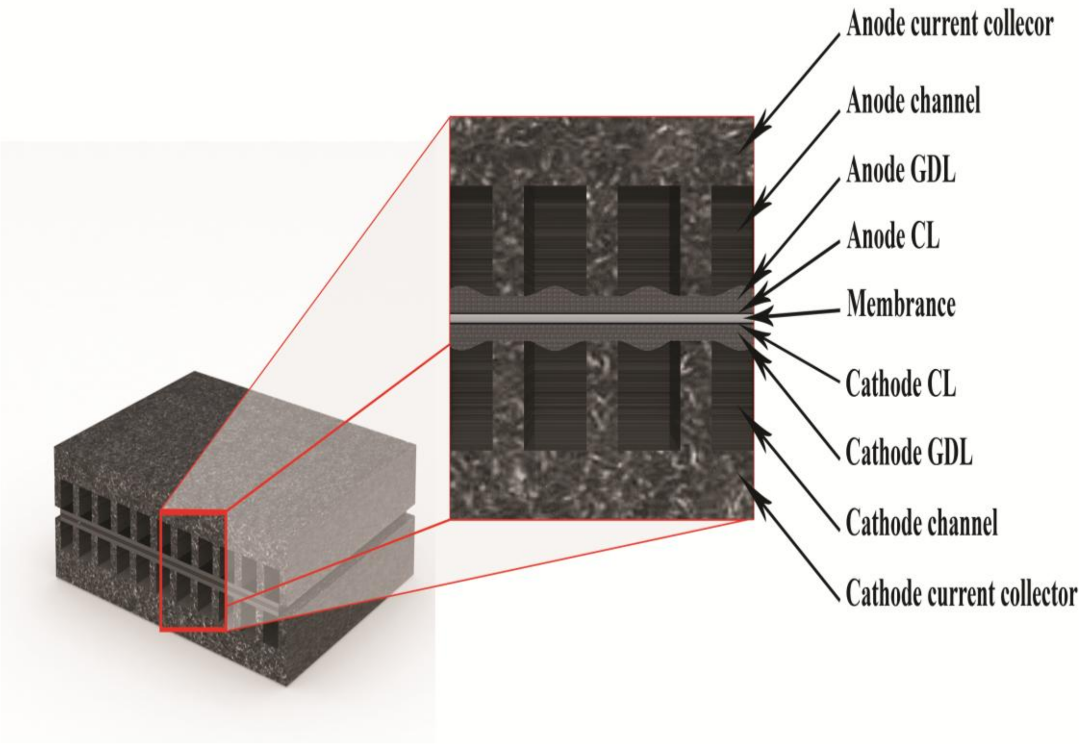

Figure 8.2 Inhomogeneous compression of gas diffusion layer (GDL) in PEM fuel cells.

On the other hand, the effect of compression on the in-plane thermal conductivity of the GDL needs to be investigated experimentally due to the presence of the sealing gasket in the practical fuel cells [119] (see Figure 8.3) even though this compression in the in-plane direction is far less than that in the through-plane direction.

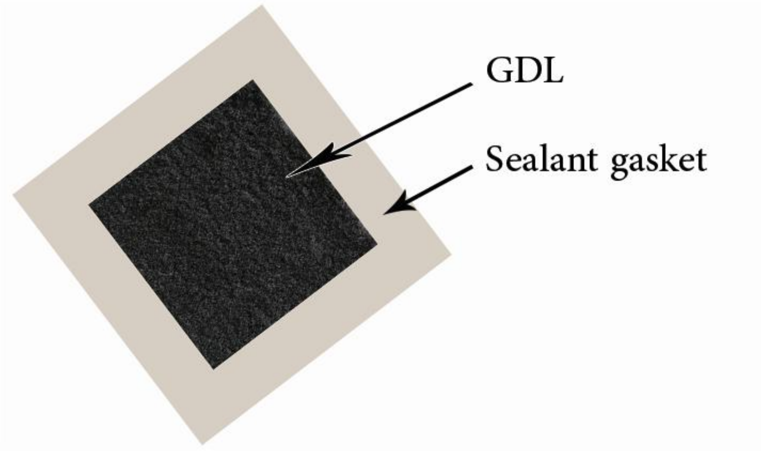

Figure 8.3 The compression of the GDL in the in-plane direction by the sealing gasket

Bibliography

1. Barclay, F. J., Fuel cells, engines, and hydrogen, John Wiley & Sons, 2006. Chapter 1: p. 29-308.

2. Srinivasan, S., Fuel cells: from fundamentals to applications. Springer, 2006. Chapter 8: p. 375-436.

3. Busby, R. L., Hydrogen and Fuel Cells: A Comprehensive Guide, First ed, PennWell, 2005. Chapter 1: p. 3-21.

4. Hoogers, G., Fuel cell technology handbook, CRC Press, 2003. Chapter 2: p. 21-236.

5. Blomen, L. J., M. J. and Mugerwa M. N., Fuel cell systems. Plenum Press, 1993.Chapter 1: p. 19-33.

6. Barbir, F., PEM Fuel Cells: Theory and Practice. Elsevier Science & Technology, 2011. Chapter 1: p. 1-16.

7. O'Hayre, R. P., Fuel cell fundamentals. 2006: John Wiley & Sons. Chapter 1: p. 3-25.

8. Srinivasan, S., Fuel cells: from fundamentals to applications. 2006: Springer. Chapter 4: p. 189-232.

9. Larmine, J. and A. Dicks, Fuel Cell Systems Explained, Second ed, Chichester (UK): John Wiley & Sons, 2003. Chapter 1: p. 1-24.

10. Busby, R. L., Hydrogen and Fuel Cells: A Comprehensive Guide, First ed. PennWell, 2005. Chapter 4: p. 140-148.

11. Srinivasan, S., Fuel cells: from fundamentals to applications. Springer, 2006.Chapter 5: p. 235-262.

12. Blomen L. J., M. J. and Mugerwa M. N., Fuel cell systems. Plenum Press, 1993. Chapter 2: p. 37-69.

13. Larmine, J. and A. Dicks, Fuel Cell Systems Explained, Second ed., Chichester (UK), John Wiley & Sons, 2003. Chapter 4: p. 67-118.

14. Larmine, J. and A. Dicks, Fuel Cell Systems Explained, Second ed, Chichester (UK), John Wiley & Sons, 2003. Chapter 5: p. 121-138.

15. Larmine, J. and A. Dicks, Fuel Cell Systems Explained, Second ed., Chichester (UK), John Wiley & Sons, 2003. Chapter 7: p. 163-226.

16. Carrette, L., K. A. Friedrich, and U. Stimming, Fuel cells: Principles, types, fuels, and applications. Chemphyschem, 2000. Chapter 4: p. 162-193.

17. Hoogers, G., Fuel cell technology handbook. CRC Press, 2003. Chapter 1: p. 2-20.

18. O'Hayre, R. P., Fuel cell fundamentals, John Wiley & Sons, 2006. Chapter 5: p. 162-194.

19. Larmine, J. and A. Dicks, Fuel Cell Systems Explained, Second ed., Chichester (UK), John Wiley & Sons, 2003. Chapter 3: p. 45-66.

20. O'Hayre, R. P., Fuel cell fundamentals, John Wiley & Sons, 2006. Chapter 4: p. 111-156.

21. Mehta, V. and J.S. Cooper, Review and analysis of PEM fuel cell design and manufacturing. Journal of Power Sources, 2003. 114: p. 32-53.

22. Barbir, F., PEM Fuel Cells: Theory and Practice. Elsevier Science & Technology, 2011. Chapter 4: p. 73-112.

23. Litster, S. and G. McLean, PEM fuel cell electrodes. Journal of Power Sources, 2004. 130: p. 61-76.

24. Basu, S., Recent trends in fuel cell science and technology. Springer, 2006. Chapter 4: p. 117-127.

25. Ju, H., Investigation of the effects of the anisotropy of gas-diffusion layers on heat and water transport in polymer electrolyte fuel cells. Journal of Power Sources, 2009. 191(2): p. 259-268.

26. Barbir, F., PEM Fuel Cells: Theory and Practice. Elsevier Science & Technology, 2011. Chapter 6: p. 147-204.

27. Tawfik, H., Y. Hung, and D. Mahajan, Metal bipolar plates for PEM fuel cell-A review, Journal of Power Sources, 2007. 163: p. 755-767.

28. Misran, E., W.R.W. Daud, and E.H. Majlan. Review on serpentine flow field design for PEM fuel cell system, 13th ICPE International Conference on Precision Engineering, Singapore: Trans Tech Publications Ltd, July 28- 30, 2010.

29. Vargas, J. V. C., J. C. Ordonez, and A. Bejan, Constructal flow structure for a PEM fuel cell. International Journal of Heat and Mass Transfer, 2004. 47: p. 4177-93.

30. Srinivasan, S., Fuel cells: from fundamentals to applications, Springer, 2006. Chapter 9: p. 441-569.

31. Litster, S., Buie C. R., Fabian T., Eaton J. K., J. Santiago G., Active water management for PEM fuel cells. Journal of the Electrochemical Society, 2007. 154: p. 1049-58.

32. Srinivasan, S., Fuel cells: from fundamentals to applications, Springer, 2006. Chapter 4: p. 189-232.

33. Basu S., Recent trends in fuel cell science and technology. Springer, 2006. Chapter 5: p. 129-135.

34. Hung, A.-J., Yu C.-C., Chen Y.-H., Sung L.-Y., Cost analysis of proton exchange membrane fuel cell systems. AIChE Journal, 2008. 54: p. 1798-1810.

35. Bar-On, I., R. Kirchain, and R. Roth, Technical cost analysis for PEM fuel cells. Journal of Power Sources, 2002. 109: p. 71-75.

36. Wen, L., K. Ruth, and G. Rusch, Membrane durability in PEM fuel cells. Journal of New Materials for Electrochemical Systems, 2001. 4: p. 227-232.

37. Cuni, A., Weber, M., Steinberger-Wilckens, R., Hydrogen production sources part I: Distribution issues, 2008. p. 27-29.

38. Srinivasulu, G.N., T. Subrahmanyam, and V.D. Rao, Parametric sensitivity analysis of PEM fuel cell electrochemical Model. 2011. 36: p. 14838-14844.

39. O'Hayre, R.P., Fuel cell fundamentals, John Wiley & Sons, 2006. Chapter 6: p. 195-222.

40. Khandelwal, M. and Mench M., Direct measurement of through-plane thermal conductivity and contact resistance in fuel cell materials, Journal of Power Sources, 2006. 161: p. 1106-1115.

41. Ramousse, J., Lottin O., Didierjean S., Maillet D., Heat sources in proton exchange membrane (PEM) fuel cells, Journal of Power Sources, 2009. 192: p. 435-441.

42. Karimi, G., Li X. and Teertstra P., Measurement of through-plane effective thermal conductivity and contact resistance in PEM fuel cell diffusion media, Electrochimica Acta, 2010. 55: p. 1619-1625.

43. Pharoah, J. G. and Burheim O. S., On the temperature distribution in polymer electrolyte fuel cells. Journal of Power Sources, 2010.195: p. 5235-5245.

44. Zamel, N., Li x., Shen J., Wiegmann A., Becker J., Estimating effective thermal conductivity in carbon paper diffusion media. Chemical Engineering Science, 2010. 65: p. 3994-4006.

45. Burlatsky, S., Atrazhev V., Gummalla M., Liu F., The impact of thermal conductivity and diffusion rates on water vapor transport through gas diffusion layers. Journal of Power Sources, 2009. 190: p. 485-492.

46. He, G., Yamazaki Y. and Abudula A., A three-dimensional analysis of the effect of anisotropic gas diffusion layer (GDL)

thermal conductivity on the heat transfer and two-phase behavior in a proton exchange membrane fuel cell (PEMFC). Journal of Power Sources, 2010. 195: p. 1551-1560.

47. Ma, L., Inghham D. B., Pourkashanian M., Review of the computational fluid dynamics modeling of fuel cells, Journal of Fuel Cell Science and Technology, 2005. 2: p. 246-257.

48. Patankar, S. V., Numerical heat transfer and fluid flow, Taylor & Francis,1980. p. 120-132.

49. Mazumder, S. and J.V. Cole, Rigorous, 3-D mathematical modeling of PEM fuel cells - II. Model predictions with liquid water transport. Journal of the Electrochemical Society, 2003. 150(11): p. 1510-1517.

50. Ismail, M. S., Hughes K. J., Ma L., Inghama D. B., Pourkashaniana M., Effects of anisotropic permeability and electrical conductivity of gas diffusion layers on the performance of proton exchange membrane fuel cells, Applied Energy, 2012.95: p. 50-63.,

51. Bernardi, D. M. and M. W. Verbrugge, A Mathematical Model of the Solid Polymer Electrolyte Fuel Cell. Journal of the Electrochemical Society, 1992.139(9): p. 2477-2491.

52. P.M. Wilde, M.M., M. Murata, and N. Berg, Structural and Physical Properties of GDL and GDL/BPP Combinations and their Influence on PEMFC Performance, Fuel Cells, 2004. 4(3): p. 180-184.

53. Ismail M. S., Damjanovicb T., Inghama D. B., Ma L., Pourkashaniana M., Effect of polytetrafluoroethylene-treatment and microporous layer-coating on the in-plane permeability of gas diffusion layers used in proton exchange membrane fuel cells, Journal of Power Sources, 2010. 195(19): p. 6619-6628.

54. Ismail, M. S., Damjanovicb T., Inghama D. B., Pourkashaniana M., Westwood A., Effect of polytetrafluoroethylene-treatment and microporous layer-coating on the electrical conductivity of gas diffusion layers used in proton exchange membrane fuel cells, Journal of Power Sources, 2010. 195(9): p. 2700-2708.

55. Kim, G.-S., Sui, P. C., Shah, A. A., Djilali, Ned, Reduced-dimensional models for straight-channel proton exchange membrane fuel cells, Journal of Power Sources. 195 (10): p. 3240-3249.

56. Cheng, C., H. Lin, and G J. Lai, Numerical prediction of the effect of catalyst layer Nafion loading on the performance of PEM fuel cells. Journal of Power Sources, 2007. 164(2): p. 730-741.

57. ANSAYS Fluent, Fuel cell modules manual, Lebanon, New Hampshire, USA, Fluent Inc, 2010. p. 4-14.

58. Versteeg, H. K. and W. Malalasekera, An introduction to computational fluid dynamics: the finite volume method, Pearson Education Ltd, 2007. Chapter 2, p. 10-39.

59. Tritt, T. M., Thermal conductivity: theory, properties, and applications, Kluwer Academic, Plenum Publishers, 2004. Chapter 2, p. 21-88.

60. Meng H., Numerical studies of liquid water behaviors in PEM fuel cell cathode considering transport across different porous layers. International Journal of Hydrogen Energy, 2010. 35: p. 5569-5579.

61. Gostick, T., Ioannidis A., Pritzker D., and Fowler W., Impact of liquid water on reactant mass transfer in PEM fuel cell electrodes. Journal of the Electrochemical Society, 2010. 157: p. 563-571.

62. Cindrella, L., Kannana A.M., Lina J.F., Saminathana K., Hoc Y., Lind C.W., Wertze. J., Gas diffusion layer for proton exchange membrane fuel cells-A review. Journal of Power Sources, 2009. 194(1): p. 146-160.

63. Arvay, A., Yli-Rantalac E., Liua C.-H., Pengb X.-H., Koskic P., Cindrellad L., Kauranenc P., Wildee P.M., Kannan A.M. , Characterization techniques for gas diffusion layers for proton exchange membrane fuel cells – A review, Journal of Power Sources, 2012. 213: p. 317-337.

64. Brett DL, Brandon NP. Review of Materials and Characterization Methods for Polymer Electrolyte Fuel Cell

Flow-Field Plates. J. Fuel Cell Sci. Technol. 2006.4(1): p. 29-44.

65. Park, S., J.-W. Lee, and B.N. Popov, A review of gas diffusion layer in PEM fuel cells: Materials and designs, International Journal of Hydrogen Energy, 2012. 37(7): p. 5850-5865.

66. Shao, Z.G., Zhu F.Y., Lin W.F., Christensen P.A., Zhang H.M., Yi B.L., Preparation and characterization of new anodes based on Ti mesh for direct methanol fuel cells, Journal of the Electrochemical Society, 2006.153: p. 1575-1583.

67. Shao, Z. G., Lin W. F., Zhu F.Y., Christensen P.A., Zhang HM, Yi BL. A tubular direct methanol fuel cell with Ti mesh anode, Journal of Power Sources, 2006.160: p. 1003-1008.

68. Oedegaard, A., Hebling C., Schmitz A, Moller-Holst S,Tunold R. , Influence of diffusion layer properties on low temperature DMFC, Journal of Power Sources, 2004. 127: p. 187-196.

69. Yu E. H., Scott K. Direct methanol alkaline fuel cell with catalysed metal mesh anodes. Electrochemistry Communications, 2004. 6: p. 361-365.

70. Liu, P., Yin G. P., Lai Q. Z., Gold-plated Ni mesh as the gas diffusion medium for air-breathing direct methanol fuel cell. International Journal of Energy Research, 2009. 33: p. 1-7.

71. Chen R, Zhao T. S. A novel electrode architecture for passive direct methanol fuel cells, Electrochemistry Communications 2007. 9: p. 718-724.

72. Zhang, F.-Y., S. G. Advani, and A. K. Prasad, Performance of a metallic gas diffusion layer for PEM fuel cells. Journal of Power Sources, 2008. 176(1): p. 293-298.

73. Joseph, G., K.J.A. Kundig, and I.C. Association, Copper: Its Trade, Manufacture, Use, and Environmental Status, Asm International, 1999. Chapter 2, p. 45-115.

74. Hatch, J.E., Aluminum: Properties and Physical Metallurgy. American Society for Metals,1984. Chapter 1, p. 2-24.

75. Berman, R., Thermal conduction in solids, Clarendon Press, 1976. Chapter 9, p. 104-115.

76. Alhazmi N., Ingham D. B, Ismail M. S, Hughes K. J., Ma L., Pourkashanian M., The in-plane thermal conductivity and the contact resistance of the components of the membrane electrode assembly in proton exchange membrane fuel cells, Journal of Power Sources, 2013. 241(0): p. 136-145.

77. Matsuura, T., M. Kato, and M. Hori, Study on metallic bipolar plate for proton exchange membrane fuel cell. Journal of Power Sources, 2006. 161(1): p. 74-78.

78. Antunes A., Cristina M., Oliveirab L., Ettb G., Ettb V., Corrosion of metal bipolar plates for PEM fuel cells: A review. International Journal of Hydrogen Energy, 2010. 35(8): p. 3632-3647.

79. Peker, M. F., Ö. N. Cora, and M. Koç, Investigations on the variation of corrosion and contact resistance characteristics of metallic bipolar plates manufactured under long-run conditions. International Journal of Hydrogen Energy, 2011. 36(23): p. 15427-15436.

80. Vie, P. J. S., and Kjelstrup S., Thermal conductivities from temperature profiles in the polymer electrolyte fuel cell. Electrochimica Acta, 2004. 49: p. 1069-1077.

81. Maggio, G., V. Recupero, and C. Mantegazza, Modelling of temperature distribution in a solid polymer electrolyte fuel cell stack. Journal of Power Sources, 1996. 62(2): p. 167-174.

82. Yan, W.-M., Chenb F., Wub H.-Y., Soongc C.-Y., Chud H.-S., Analysis of thermal and water management with temperature-dependent diffusion effects in membrane of proton exchange membrane fuel cells, Journal of Power Sources, 2004. 129(2): p. 127-137.

83. Burheim, O., Vie P. J. S., Pharoah J. G., and Kjelstrup S., Ex situ measurements of through-plane thermal conductivities in a polymer electrolyte fuel cell,Journal of Power Sources, 2010. 195: p. 249-256.

84. Sahimi M., Flow and Transport in Porous Media and Fractured Rock, Wiley, 2012. Chapter 7, p. 179-211.

85. Dagan G., Flow and transport in porous formations. Springer-Verlag, 1989. Chapter 2, p. 45-151.

86. Carson, J. K., Lovatt, S. J., Tanner, D. J., and Cleland, A. C., Thermal conductivity bounds for isotropic, porous materials, International Journal of Heat and Mass Transfer, 2005. 48: p. 2150-2158.

87. Jagjiwanram, R. S., Effective thermal conductivity of highly porous two-phase systems, Applied Thermal Engineering, 2004. 24: p. 2727-2735.

88. Wang, J., Carson, J. K., North, M. F., and Cleland, D. J., A new approach to modelling the effective thermal conductivity of heterogeneous materials, International Journal of Heat and Mass Transfer, 2006. 49: p. 3075-3083.

89. Wang, J., Carson, J. K., North, M. F., and Cleland, D. J., A new structural model of effective thermal conductivity for heterogeneous materials with co-continuous phases, International Journal of Heat and Mass Transfer, 2008. 51: p. 2389-2397.

90. Sadeghi, E., Bahrami, M., and Djilali, N., Analytic determination of the effective thermal conductivity of PEM fuel cell gas diffusion layers, Journal of Power Sources, 2008. 179: p. 200-208.

91. Delan, A., Rennau, M., Schulz, S. E., and Gessner, T., Thermal conductivity of ultra low-k dielectrics, Microelectronic Engineering, 2003. 70: p. 280-284.

92. Burzo, M. G., Komarov, P. L., and Raad, P. E., Optimized thermo-reflectance system for measuring the thermal properties of thin-films and their interfaces, Semiconductor Thermal Measurement and Management Symposium, Twenty-Second Annual IEEE, 2006. p. 87-94.

93. Flynn, D. R., Zarr, R. R., Hahn, M. M., and Healy, W. M., Insulation Materials: Testing and Applications: 4th volume, ASTM International, West Conshohocken, 2002. p. 98-115.

94. Zawilski, B. M. L., Roy T., Tritt T. M., Description of the parallel thermal conductance technique for the measurement of the thermal conductivity of small diameter samples. Review of Scientific Instruments, 2001. 72: p.1770-1774.

95. Teertstra, P., Karimi G. , and Li X., Measurement of in-plane effective thermal conductivity in PEM fuel cell diffusion media. Electrochimica Acta, 2011. 56: p. 1670-1675.

96. Tang, X., Aaron, K., He, J. and Tritt, T. M., Determination of in-plane thermal conductivity of Nax Co2O4 single crystals via a parallel thermal conductance (PTC) technique. Phys. Status Solidi A, 2008. 205: p.1152–1156.

97. Berning, T., Lu D.M. , and Djilali N., Three-dimensional computational analysis of transport phenomena in a PEM fuel cell, Journal of Power Sources, 2002. 106: p. 284–294

98. Hamour, M., Garnier J. P., Grandidier J. C., Ouibrahim A., Martermianov S., Thermal-conductivity characterization of gas diffusion layer in proton exchange membrane fuel cells and electrolyzers under mechanical loading. International Journal of Thermophysics, 2011. 32: p. 1025-1037.

99. Sadeghi, E., Djilali N., and Bahrami M., A novel approach to determine the in-plane thermal conductivity of gas diffusion layers in proton exchange membrane fuel cells. Journal of Power Sources, 2011. 196: p. 3565-3571.

100. Moffat, R. J., Describing the uncertainties in experimental results. Experimental Thermal and Fluid Science, 1988. 1: p. 3-17.

101. Choy, C. L., Wong, Y. W., Yang, G. W., Kanamoto, T., Elastic modulus and thermal conductivity of ultradrawn polyethylene. Journal of Polymer Science Part B: Polymer Physics, 1999. 37(23): p. 3359-3367.

102. Song, L., Y. Chen, and J. W. Evans, Measurements of the Thermal Conductivity of Polyethylene oxide Lithium Salt Electrolytes. Journal of the Electrochemical Society, 1997. 144(11): p. 3797-3800.

103. Mauritz, K. A., Moore R. B., State of understanding of Nafion, Chem.Rev., 2004. 104: p.4535-4585.

104. Nafion product sheet, Dupont, USA, http://www.fuelcellmarkets.com/content/images/articles/nae101.pdf [cited 2014 /2].

105. Um, S., C. Y. Wang, and K.S. Chen, Computational Fluid Dynamics Modeling of Proton Exchange Membrane Fuel Cells. Journal of the Electrochemical Society, 2000. 147: p. 4485-4493.

106. Gurau, V., H. Liu, and S. Kakaç, Two-dimensional model for proton exchange membrane fuel cells. AIChE Journal, 1998. 44: p. 2410-2422.

107. Ramires, M. L. V., Nieto C., Nagasaka Y., Nagashaima A., Assael M., Wakeham W., Standard Reference Data for the Thermal Conductivity of Water. Journal of Physical and Chemical Reference Data,1995. 24: p.1377-1381.

108. Price D. M. and Jarratt M., Thermal conductivity of PTFE and PTFE composites. Thermochimica Acta, 2002. p. 231-236.

109. Zamel N., Litovsky E., Shakhshir S., Li X., Kleiman J., Measurement of the through-plane thermal conductivity of carbon paper diffusion media for the temperature range from -50 to +120 c. International Journal of Hydrogen Energy, 2011. 36: p. 12618-12625.

110. Blumm J., Meyer M. and Strasser C., (2010) Characterization of PTFE Using Advanced Thermal Analysis Techniques. International Journal of Thermophysics 31: p. 1919-1927.

111. Stephan, K. and A. Laesecke, The Thermal Conductivity of Fluid Air. Journal of Physical and Chemical Reference Data, 1985, 14: p. 227-234.

112. Ramousse, J., Lottin O., Didierjean S., Maillet D., Estimation of the effective thermal conductivity of carbon felts used as PEMFC Gas Diffusion Layers, International Journal of Thermal Sciences, 2008. 47: p. 1-6.

113. Ismail, M. S., Inghama D. B. , Ma L., Pourkashaniana M., Effect of PTFE loading of gas diffusion layers on the performance of proton exchange membrane fuel cells running at high efficiency operating conditions, International Journal of Energy Research, 2012. 37 (13): p. 1592-1599.

114. Rowe, A. and Li X., Mathematical modeling of proton exchange membrane fuel cells. Journal of Power Sources, 2001. 102: p. 82-96.

115. Bhatta, R. P., Annamalai S. , Mohr R. K., Brandys M., Pegg I. L., High temperature thermal conductivity of platinum microwire by 3 omega method, Review of Scientific Instruments, 2010. 81: p. 1149040 -1149045.

116. Nitta, I., O. Himanen, and M. Mikkola, Thermal conductivity and contact resistance of compressed gas diffusion layer of PEM fuel cell. Fuel Cells, 2008. 8: p. 111-119.

117. Karvonen, S., T. Hottinen, J. Ihonen, and H. Uusalo, Modeling of Polymer Electrolyte Membrane Fuel Cell Stack End Plates. Journal of Fuel Cell Science and Technology, 2008. 5 (4): p. 410091-410099.

118. Burheim, O. S., Pharoah, J. G. , Lampert, H. , Vie, P. J. S. , Kjelstrup, S. , Through-plane thermal conductivity of PEMFC porous transport layers, Journal of fuel cell science and technology , 2011. 8: p. 363-373.

119. Escribano, S., Blachot, J., Ethve J., Morin A., Mosdale R., Characterization of PEMFCs gas diffusion layers properties, Journal of Power Sources, 2006. 156(1): p. 8-13.

120. Sadeghi, E., N. Djilali, and M. Bahrami, Effective thermal conductivity and thermal contact resistance of gas diffusion layers in proton exchange membrane fuel cells. Part 2: Hysteresis effect under cyclic compressive load. Journal of Power Sources, 2010. 195: p. 8104-8109.54.

121. Nitta, I., O. Himanen, and M. Mikkola, Contact resistance between gas diffusion layer and catalyst layer of PEM fuel cell. Electrochemistry Communications, 2008. 10(1): p. 47-51.

122. Sadeghi, E., N. Djilali, and M. Bahrami, Effective thermal conductivity and thermal contact resistance of gas diffusion layers in proton exchange membrane fuel cells. Part 1: Effect of compressive load, Journal of Power Sources, 2011. 196: p. 246-254.

Appendix A
Calculating the Minimum Dimensions for the Low Thermal Conductivity Material in the In-plane Set-up

One of the important conditions in the set-up for measuring the thermal conductivity in the in-plane direction was that a low thermal conductivity material should be placed between the heat source and the heat sink. This is so that the sample thermal conductance is at least 10% higher than the thermal conductance of the holder.

$$C_S = \frac{k_S \times A}{L} \tag{A.1}$$

$$C_S = \frac{20 \times A}{L} \tag{A.2}$$

Where C_S is the thermal conductance of the sample, A is the sample cross-sectional area and L is the sample length. The maximum thermal conductivity of the sample is 20, as estimated from the parallel model in Chapter 5.

$$C_S = \frac{20 \times 0.01 \times 400 \times 10^{-6}}{1 \times 10^{-2}} \tag{A.3}$$

$$C_S = 8^{-3}\ (W/K) \tag{A.4}$$

The condition is:

$$C_S \geq \frac{C_{holder}}{10} \tag{A.5}$$

The maximum thermal conductance of the sample holder is:

$$C_{holder} = 10 \times C_S \tag{A.6}$$

$$C_{holder} = 0.08\ (W/K) \tag{A.7}$$

$$C_{holder} = \frac{k \times A}{L} \tag{A.8}$$

$$0.08 = \frac{0.2 \times 0.01 \times 0.01}{L} \tag{A.9}$$

Where 0.2 $W{\cdot}m^{-1}{\cdot}k^{-1}$ is the thermal conductivity of the polymer material. So the length of the material should be more than:

$$L = 2.5 \times 10^{-4} m \tag{A.10}$$

So the length of the polymer material which is placed between the heat source and the heat sink should be more than 250 μm.

The length of the material has been chosen to be 1 cm.

Appendix B
Spraying the Catalyst Ink Technique

B.1 The catalyst ink

The mixed electrode is prepared by mixing the 40 mg/cm^2 Pt/C particles with a solvent of methanol and PTFE solution. Then, this mixture is mixed together ultrasonically for about 60 minutes.

B.2 Spraying catalyst ink

Spraying the catalyst ink is one of most popular methods for fabrication of the catalyst layer. In this method, the catalyst ink is sprayed on the carbon fibre GDL by using the airbrush, which is spraying the catalyst ink (as shown in Figure B.1) using pressurized steam nitrogen at a temperature range of 80-120°C, which assists in evaporating the solvent. The coated GDL is then left for 2-4 hours until the catalyst is dry.

Figure B.1 Spraying the catalyst by using the airbrush.

Appendix C
Calculating the Minimum Dimensions for the Low Thermal Conductivity Material in the Through-plane Set-up

In the set-up for measuring the thermal conductivity in the through-plane direction the low thermal conductivity material should be placed between the heat source and the heat sink. This is so that the sample thermal conductance is at least 10% higher than the thermal conductance of the holder.

$$C_S = \frac{0.2 \times A}{L} \tag{C.1}$$

Where C_S is the thermal conductance of the sample, A is the sample cross-sectional area and L is the sample length. The minimum thermal conductivity of the GDL is 0.2, as mentioned in Chapter 5.

$$C_S = \frac{0.2 \times (0.01)^2 \times (\pi / 4)}{400 \times 10^{-6}} \tag{C.2}$$

$$C_S = 0.039\ (W/K) \tag{C.3}$$

$$C_S \geq \frac{C_{holder}}{10} \tag{C.4}$$

The maximum thermal conductance of the sample holder is:

$$C_{holder} = 10 \times C_S \tag{C.5}$$

$$C_{holder} = 0.39\ (W/K) \tag{C.6}$$

$$C_{holder} = \frac{k \times A}{L} \tag{C.7}$$

$$0.39 = \frac{0.2 \times (0.01)^2 \times (\pi / 4)}{L} \tag{C.8}$$

So the length of the polymer material should be more than:

$$L = 3.06 \times 10^{-5} m \tag{C.9}$$

So the length of the polymer material which is placed between the heat source and the heat sink should be more than 30.6 μm.

The length of the cylinder material has been chosen to be 1 cm.